ANALYSIS OF THE MOLECULAR MECHANISM OF AUTOPHAGOSOME FORMATION IN YEAST AND ZEBRAFISH MODELS

by

Congcong He

A dissertation submitted in partial fulfillment
of the requirements for the degree of
Doctor of Philosophy
(Molecular, Cellular and Developmental Biology)
in The University of Michigan
2009

Doctoral Committee:

Professor Daniel J. Klionsky, Chair
Associate Professor Kenneth M. Cadigan
Assistant Professor John Kim
Assistant Professor Yanzhuang Wang

DEDICATION

To My Parents, Grandparents, and Weibin

ACKNOWLEDGEMENTS

I am very much indebted to my graduate mentor, Dr. Daniel J. Klionsky, who gave me invaluable teaching and guidance throughout my doctoral training. I have learned and benefited a lot from his research insights, scientific enthusiasm, critical thinking and extraordinary studiousness. I would also like to thank my thesis committee members, Dr. Kenneth Cadigan, Dr. John Kim and Dr. Yanzhuang Wang, for their helpful inputs and persistent encouragements to my research.

My research projects are carried out with the collaborative efforts of many past and current members of the Klionsky lab. I would like to thank them all for their generous assistance and discussion in the past four years. I am especially grateful to have Wei-Lien Yen, Dr. Ju Huang, Dr. Heesun Cheong and Dr. Clinton Bartholomew as passionate friends.

I owe my great thanks to Dr. Amy Chang and Dr. John Schiefelbein for enlightening me in experimental design during my rotations. I would also like to thank Dr. David Ginsburg and Dr. Friedhelm Hildebrandt for providing zebrafish facilities, equipment and experimental reagents.

Special thanks are due to my parents and grandparents for their everlasting love and care and for always being there for me spiritually. I am also very thankful to my fiancé and a faithful and inspiring friend, Dr. Weibin Zhou, for his love and support, and for sharing thoughts and ideas with me both in science and in life.

I also would like to appreciate the help from the staff members in the International Center and the MCDB Department at the University of Michigan, for making my study and life in Ann Arbor a rich and wonderful experience.

Final thanks go to the Rackham Graduate School at the University of Michigan, for supporting me financially with the Rackham Predoctoral Fellowship.

Chapter 1 is a manuscript prepared for *Annual Review of Genetics*, 2009, Volume 43, Congcong He and Daniel J. Klionsky. Regulation mechanisms and signaling pathways of autophagy, with minor modifications.

Chapter 2 is reprinted from *Journal of Cell Biology*, Volume 175, Congcong He, Hui Song, Tomohiro Yorimitsu, Iryna Monastyrska, Wei-Lien Yen, Julie E. Legakis and Daniel J. Klionsky. Recruitment of Atg9 to the preautophagosomal structure by Atg11 is essential for selective autophagy in budding yeast, pg. 925-35, Copyright (2006), with minor modifications. Hui Song contributed Fig. 2.1A, 2.2B, 2.2C and 2.2E. Dr. Tomohiro Yorimitsu performed experiments in Fig. 2.3C. Dr. Iryna Monastyrska contributed Fig. 2.8. Wei-Lien Yen and I equally contributed Fig. 2.2D. Dr. Julie E. Legakis provided two yeast strains (JLY87 and JLY88) for yeast two-hybrid analysis. I contributed the rest of the data and wrote the paper.

Chapter 3 is reprinted from *Molecular Biology of the Cell*, Volume 19, Congcong He, Misuzu Baba, Yang Cao and Daniel J. Klionsky. Self-interaction is critical for Atg9 transport and function at the phagophore assembly site during autophagy, pg. 5506-16, Copyright (2008), with minor modifications. Dr. Misuzu Baba performed experiments in

Fig. 3.6. Dr. Yang Cao contributed Table 3.2. I contributed the rest of the data and wrote the paper.

Chapter 4 is reprinted from *Autophagy*, Volume 5, Congcong He, Clinton Bartholomew, Weibin Zhou and Daniel J. Klionsky. Assaying autophagic activity in transgenic GFP-Lc3 and GFP-Gabarap zebrafish embryos, in press, Copyright (2009), with minor modifications. Dr. Weibin Zhou and I generated the transgenic fish lines together. I contributed Fig. 4.1, 4.2, 4.3, 4.4, 4.S1 and 4.S2. Dr. Clinton Bartholomew wrote the Introduction and Discussion, and I wrote the rest of the paper. Dr. Bartholomew and I equally contributed Fig. 4.5, 4.6 and 4.7.

Part of Chapter 5 is adapted from *Autophagy*, Volume 3, Congcong He and Daniel J. Klionsky. Atg9 trafficking in autophagy-related pathways, pg. 271-74, Copyright (2007); and Volume 5, Congcong He, Misuzu Baba and Daniel J. Klionsky. Double duty of Atg9 self-association in autophagosome biogenesis, in press, Copyright (2009). I contributed the figures and wrote the papers.

TABLE OF CONTENTS

LIST OF TABLES

Table

LIST OF FIGURES

Figure

CHAPTER 1

Introduction

Abstract

Autophagy is a process of self-degradation of cellular components, in which double-membrane autophagosomes sequester organelles or portions of cytosol and fuse with lysosomes or vacuoles for breakdown by resident hydrolases. Autophagy is upregulated in response to extra- or intracellular stress and signals, such as starvation, growth factor deprivation, ER stress and pathogen infection. Defective autophagy may play a significant role in human pathologies, including cancer, neurodegeneration and infectious diseases. I present our current knowledge on the key genes composing the autophagy machinery in eukaryotes from yeast to mammalian cells, and the signaling pathways that sense different stress status and induce autophagy for cell survival and homeostasis. I also review the recent advances on the molecular mechanisms that regulate the autophagy machinery at various levels, from transcriptional activation to post-translational protein modification.

Introduction

Cell homeostasis is achieved by balancing biosynthesis and turnover. In eukaryotic cells, the lysosome (or the analogous yeast and plant vacuole) is the primary organelle for degradation, through its wide array of resident acid hydrolases. As an adaptive response in unfavorable conditions such as nutrient deprivation, autophagy mediates a highly regulated "self-eating" process via lysosomes. Double-membrane vesicles, termed autophagosomes, engulf long-lived proteins, damaged organelles and even invasive pathogens, and transport these cargos to the lysosomes. There, the outer-membrane of the autophagosome fuses with the lysosomal membrane and the inner vesicle, together with its cargo, is degraded (Fig. 1.1). The resulting macromolecules can be recycled back to the cytosol for reuse during starvation (235). Malfunction of autophagy contributes to a variety of diseases, including cancer, neurodegeneration, cardiovascular disorders and microbe infection, because efficient sequestration and clearance of unneeded or damaged cellular or non-self components is crucial for cell survival and function.

Autophagosomes have been observed by electron microscopy in mammalian cells since as early as the 1950s (94), whereas the molecular era of autophagy study began little over a decade ago, starting primarily from genetic screens in the budding yeast *Saccharomyces cerevisiae* and the methylotrophic yeasts *Pichia pastoris* and *Hansenula polymorpha*, leading to the identification of 31 autophagy-related (*ATG*) genes. The Atg proteins function at several physiologically continuous steps in autophagy (for instance, induction, cargo recognition and packaging, and vesicle formation and breakdown) and

orchestrate much of the process. Many *ATG* homologs have subsequently been found and characterized in higher eukaryotes, suggesting that autophagy is a highly conserved pathway through evolution. In fungal cells, the site of autophagosome formation is termed the phagophore assembly site (PAS, also known as the preautophagosomal structure). This is the location where the phagophore, the initial sequestering structure, expands and the Atg proteins are recruited. Whereas in mammalian cells autophagosomes emerge from multiple sites, fungi appear to have one distinct PAS adjacent to the vacuole, which allows convenient studies of the mechanisms and dynamic stages of autophagosome biogenesis.

Although bulk cytosol can be randomly turned over through autophagy, in many cases autophagy displays substrate-specificity. For example, two yeast vacuolar proteases, α-mannosidase and the precursor form of aminopeptidase I (Ape1 [prApe1]), are synthesized in the cytoplasm and transported to the vacuole via a selective autophagy pathway, known as the cytoplasm-to-vacuole targeting (Cvt) pathway. The Cvt pathway is mechanistically and genetically similar to bulk autophagy, except that it occurs constitutively in normal growing conditions (97). In addition, damaged or superfluous organelles are selectively targeted for degradation by autophagy. Different terms have been used to describe the selectivity of each process according to the cargo, such as autophagic degradation of mitochondria (mitophagy) (84), ribosomes (ribophagy) (100), peroxisomes (pexophagy) (32) and endoplasmic reticulum (reticulophagy) (8, 209). This chapter provides an overview of recent advances in our understanding of the regulation of different types of autophagy in response to various stimuli or inhibitors, involving

signaling pathways, transcription factors and protein modifiers, as well as functions and interactions of the Atg proteins.

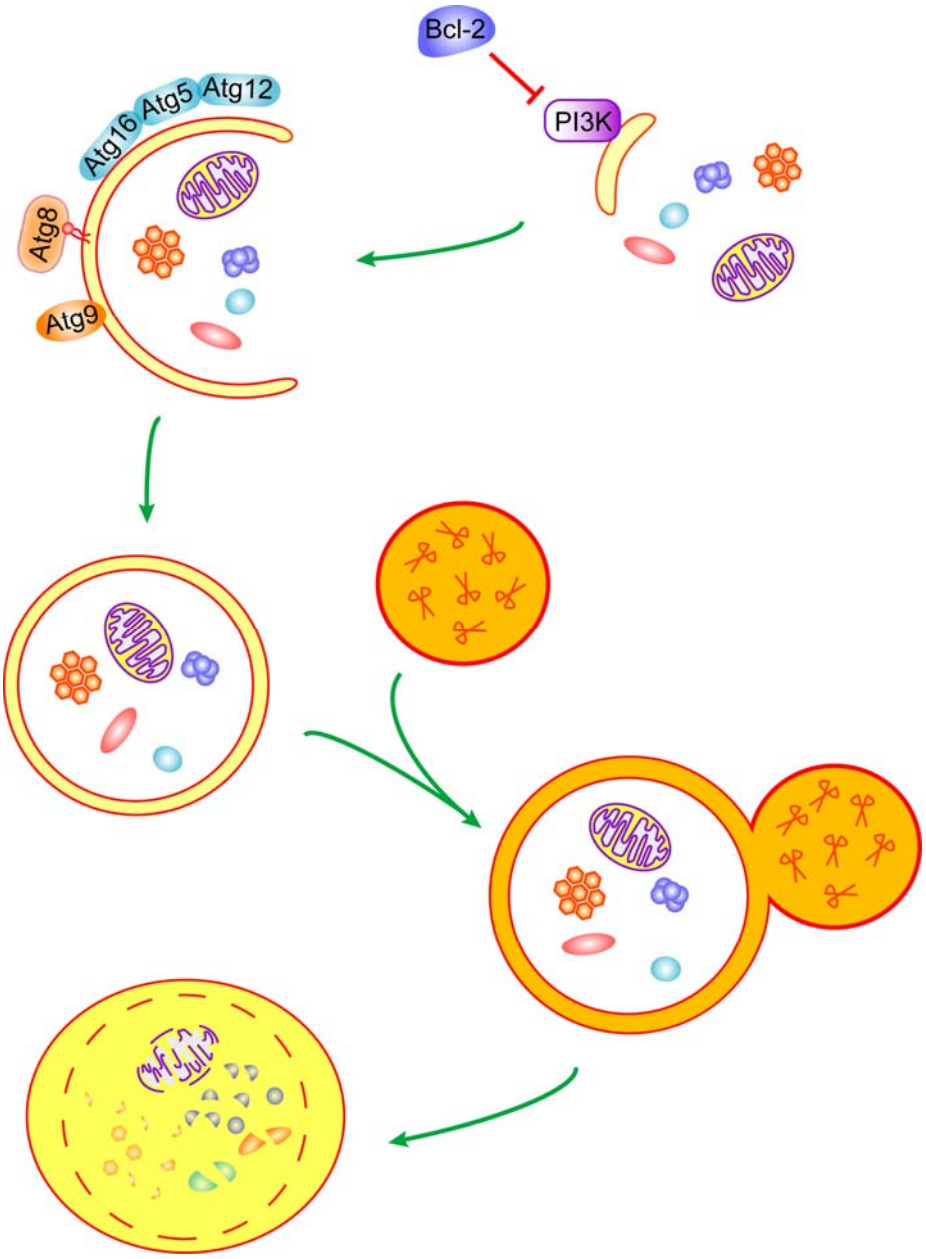

Figure 1.1. A schematic model of autophagy. The class III PI3K complex mediates nucleation of the phagophore membrane, enwrapping cytosolic proteins, protein aggregates and organelles (such as mitochondria). Bcl-2 blocks this step by binding and inhibiting Beclin 1, a component in the PI3K complex. Atg12–Atg5-Atg16 and Atg8–PE conjugates are recruited to and coat on the phagophore, together with the transmembrane protein Atg9, facilitating the phagophore expansion step. Upon vesicle completion, the Atg proteins are dissociated, allowing autophagosome-lysosome fusion and cargo degradation by lysosomal proteases.

Molecular machinery of autophagy

Autophagy-related (Atg) proteins: the core machinery

Induction. Basal-level autophagy is very low under normal conditions; therefore, an efficient mechanism to induce autophagy is crucial for organisms to adapt to stress and extracellular cues. A central inhibitor of autophagy is the serine/threonine protein kinase TOR (Target Of Rapamycin). In yeast and Drosophila, Tor/dTOR integrates input information from multiple upstream signal transduction pathways (discussed below) and negatively regulates another serine/threonine kinase, Atg1, in nutrient-rich conditions (20, 79, 187) (Fig. 1.2B). In yeast, upon Tor inhibition by starvation or rapamycin treatment, the kinase activity of Atg1 is activated and Atg1 binding affinity to Atg13 and Atg17 may also increase (79), which promotes the formation of an Atg1-Atg13-Atg17 scaffold and the recruitment of multiple Atg proteins to the PAS to initiate autophagosome formation (25, 26, 75, 81, 200). Thus, a structural role of the Atg1 kinase complex in protein recruitment is indispensable for autophagy induction. Moreover, it is found that in Drosophila, ATG1 is able to inhibit the phosphorylation and activation of a downstream TOR effector, S6K, during nutrient starvation (104), yet it is not clear how the S6K signaling modulates other autophagy proteins and/or autophagy activity.

There are two mammalian homologs of Atg1, the Unc-51-like kinase 1 (ULK1) and -2 (ULK2), and one homolog of yeast Atg17, FIP200 (the focal adhesion kinase family-interacting protein of 200 kD), which forms a complex with ULKs and mammalian Atg13 and localizes to the phagophore upon starvation (51, 74). Regarding the substrates of the Atg1 kinase during autophagy, it is suggested that mammalian Atg13

and FIP200 are phosphorylated by ULKs (74), and ULKs also autophosphorylates and is conductive to a conformational change and autophagy induction (18). Different from yeast, ULKs-Atg13-FIP200 seem to form a stable complex in mammalian cells. mTOR interacts with, phosphorylates and inactivates ULKs and Atg13 under nutrient-rich conditions. Upon mTOR inhibition by starvation or rapamycin, ULK1 and ULK2 are activated and phosphorylate Atg13 and FIP200, which are essential for autophagy activity (56, 74). These studies raise an interesting hypothesis that Atg13 is phosphorylated by TOR or Atg1/ULKs on different residues, which may exert opposite effects on autophagy induction. Indeed, yeast Atg13 is rapidly dephosphorylated by starvation (79), whereas Atg13 phosphorylation is enhanced during autophagic conditions in Drosophila (20); it is likely that phosphorylation of Atg13 is dependent more on Tor in yeast and more on Atg1 in Drosophila. Atg101, a newly identified protein component in the ULKs-Atg13-FIP200 complex, binds and stabilizes Atg13, which is required for autophagy in mammals (124).

Cargo recognition and selectivity. In selective autophagy, cargos are recognized through interactions with specific receptor proteins. The yeast Cvt pathway delivers prApe1 into the vacuole and generates the mature enzyme Ape1. The cargo prApe1 contains a vacuolar-targeting signal, which can be recognized and bound by the receptor protein Atg19. An adaptor protein, Atg11, binds Atg19 and recruits the Atg19-prApe1 complex to the PAS, where Atg19 interacts with one of the key components in the vesicle-forming machinery, Atg8, for packaging the receptor-cargo complex into Cvt vesicles (analogous to autophagosomes) (188, 191).

In multicellular organisms, an important function of autophagy is the clearance of cytosolic ubiquitinated substrates or aggregate-prone proteins. Recent studies suggest that this degradative process is also selective and mediated through the mammalian protein p62/sequestosome 1 (SQSTM1) (9, 159), or Ref(2)P, the Drosophila homolog of p62 (139). p62 directly binds both poly- or mono-ubiquitin via its ubiquitin-associated (UBA) domain, and the mammalian Atg8 homolog, LC3 (microtubule-associated protein 1 light chain 3) (89, 154), and links the ubiquitinated cargos to the autophagy machinery for autophagic degradation. The structural and functional similarity between a C-terminal motif in mammalian p62 and yeast Atg19 (143) gives rise to an intriguing hypothesis that p62 is an Atg19 analogue in higher eukaryotes and acts as a receptor for ubiquitinated proteins or organelles in selective autophagy. Recent work shows that the P granule proteins, the germ cell determinant in *C. elegans*, are also selectively degraded by autophagy in somatic cells (244). The cargo receptor, SEPA-1 (suppressor of ectopic P granule in autophagy mutants 1), directly interacts with the P granule components and LGG-1, the Atg8 homolog in *C elegans*, and thus functions similarly to Atg19 and p62.

Another selective route of autophagy is pexophagy, and its mechanism has been best studied in the methylotrophic yeast *P. pastoris*. Peroxisome formation is greatly induced by growth on methanol as the sole carbon source; when the medium is replenished with glucose or ethanol, the peroxisomes are no longer needed and are selectively degraded in the vacuole through pexophagy. In *P. pastoris*, PpAtg30 functions as a peroxisome receptor by interacting both with peroxisomal membrane proteins PpPex14 and PpPex3 and with autophagy proteins PpAtg11 and PpAtg17, and therefore links peroxisomes destined for degradation to the PAS (35). A notable feature of the

aforementioned receptor proteins is the high level of pathway-specificity. For example, Atg19 is not required for bulk autophagy or pexophagy and PpAtg30 not involved in the Cvt or bulk autophagy pathways.

Autophagosome formation. Unlike processes of vesicle formation in most endomembrane trafficking systems, double-membrane autophagosomes appear to be assembled at the PAS by addition of new membranes, rather than being generated by budding from the surface of a preexisting organelle or sealing of a single piece of continuous membrane. Thus, formation of the sequestering vesicles is likely the most complex step of autophagy. Multiple Atg proteins are recruited to the phagophore to participate in autophagosome formation, and this step requires the highly regulated coordination of all of these proteins (Fig. 1.1).

The nucleation and assembly of the initial phagophore membrane requires the class III phosphatidylinositol 3-kinase (PtdIns3K) complex, which is composed of the PtdIns3K Vps34 (vacuolar protein sorting 34), a myristoylated serine/threonine kinase Vps15 (p150 in mammalian cells), Atg14 (Barkor or mAtg14 in mammalian cells) and Atg6/Vps30 (Beclin 1 in mammalian cells) (65, 83, 109, 198). The function of Beclin 1 in autophagy is regulated by Bcl-2 (B-cell lymphoma/leukemia-2), an anti-apoptotic protein that inhibits autophagy by binding and sequestering Beclin 1 under nutrient-rich conditions; dissociation of Beclin 1 from Bcl-2 is required for autophagy induction. The PtdIns3K complex produces PI3P (phosphatidylinositol 3-phosphate), and is involved in PAS targeting of a number of yeast Atg proteins that bind PI3P, such as Atg18, Atg20, Atg21 and Atg24 (140, 148, 197). In yeast, Atg20 and Atg24 interact with the Atg1-Atg13-Atg17 complex, and the latter mediates autophagy induction (discussed above);

however, the mammalian homologs of Atg20 and Atg24 are either not identified (Atg20), or not well characterized in autophagy (Atg24). The PtdIns3K complex, in part together with the above Atg proteins, further recruits two interrelated ubiquitin-like (Ubl) conjugation systems, Atg12–Atg5-Atg16 and Atg8–PE (phosphatidylethanolamine), to the phagophore (199, 200), which play an essential role in regulating the membrane elongation and expansion of the forming autophagosome.

The two Ubl proteins, Atg12 and Atg8, undergo conjugation in a similar manner as ubiquitin. Atg12 is activated by Atg7 (E1 activating enzyme), transferred to Atg10 (E2 conjugating enzyme) and attached to an internal lysine of the substrate protein Atg5 covalently. In contrast to ubiquitination, Atg12–Atg5 conjugation is constitutive and irreversible, and no substrate-specific E3 ligase counterpart is required in this process (44). The Atg12–Atg5 conjugate further interacts with a coiled-coil protein Atg16, which links the Atg12–Atg5-Atg16 complex into a tetramer by self-oligomerization and attaches it to the phagophore (125, 127). In the Atg8 conjugation system, Atg8 is first processed by a cysteine protease, Atg4, exposing a C-terminal glycine residue. The same E1 enzyme Atg7 activates Atg8 and transfers it to Atg3 (E2). Atg8 is finally conjugated to the target lipid PE via an amide bond, facilitated by the E3-like Atg12–Atg5 conjugate (39, 50), although Atg12–Atg5 lacks the conserved HECT or RING domains possessed by typical E3 ligases, and is not essential for conjugation to occur. In nutrient-rich conditions, the majority of Atg8 is cytosolic; upon autophagy induction, Atg8 largely exists as the lipid-conjugated form and is localized to both sides of the phagophore (76, 91). It is suggested that Atg8 controls the size of the autophagosome (227), which may

result from its ability to determine membrane curvature. The lipidation of Atg8 and its mammalian homolog LC3 are widely used to monitor autophagy induction.

Various sources including mitochondria, the Golgi complex and the ER are proposed to be the origins of the autophagosomal membrane (72, 168). However, it is not completely clear by what mechanism the additional membranes are delivered to and fused with the growing phagophore. SNAREs (*N*-ethylmaleimide-sensitive factor attachment protein receptors) or small GTPases have not been shown to directly play a role in autophagosome formation. Although the Golgi-resident GTPase Rab33B binds Atg16L (the mammalian Atg16 homolog), the function of this interaction in autophagy is unclear (66). Recent studies demonstrate that self-multimerization of Atg9 may facilitate membrane tethering and/or fusion (52). Atg9 is the only identified integral membrane protein required for autophagosome formation. In yeast, Atg9 localizes to the PAS and peripheral structures and is suggested to cycle between the two sites. Atg11, Atg23 and Atg27 are essential in the anterograde transport of Atg9 to the PAS (19, 54, 105, 232) and the Atg1-Atg13 complex, Atg2, Atg18, and the PtdIns3K complex are involved in its retrograde transport (169). Thus, Atg9 may function as a carrier in supplying membrane, and may also play a role during phagophore expansion through its dynamic self-interaction. Similarly, the mammalian Atg9 (mAtg9) transports from the *trans*-Golgi network (TGN) to late endosomes, which are co-labeled with LC3, when autophagy is induced. In mammalian cells it is the redistribution of mAtg9 from the TGN to late endosomes that is dependent on ULK1 and human Atg13 (18, 239).

Vesicle fusion and autophagosome breakdown. When autophagosome formation is completed, Atg8 attached to the outer membrane is cleaved by Atg4 and

released back to the cytosol (92), allowing fusion with the vacuole/lysosome. However, the retrieval and uncoating mechanisms of other Atg proteins remain to be studied. The autophagosome-lysosome fusion is mediated by the similar machinery in homotypic membrane fusion. In mammalian cells, the fusion event requires the lysosomal membrane protein LAMP2 and the small GTPase Rab7 (68, 205), although the mechanism is less characterized. In yeast, the machinery consists of the Rab family GTPase Ypt7 (the homolog of Rab7), the NSF homolog Sec18, the SNARE proteins Vam3, Vam7, Vti1 and Ykt6, the class C Vps/HOPS complex proteins and two other proteins needed for fusion, Ccz1 and Mon1 (93).

After fusion, degradation of the inner vesicle is dependent on a series of lysosomal/vacuolar acidic hydrolases, including proteinase A and B (encoded by *PEP4* and *PRB1*, respectively) and a lipase Atg15 in yeast (33, 210) and cathepsin B, D (a homolog of proteinase A) and L in mammalian cells (207). The resulting small molecules are transported back to the cytosol for protein synthesis and maintenance of cellular functions under starvation conditions. The identification of Atg22, together with other vacuolar permeases (such as Avt3 and Avt4), as vacuolar amino acid effluxers during yeast autophagy (229), helps the understanding of the mechanisms of nutrient recycling.

Non-Atg components required for autophagy

The secretory and endocytic pathway. Autophagy involves dramatic subcellular membrane remodeling. The role of the secretory pathway in autophagy is largely illuminated by studies in yeast, where a functional ER and Golgi complex are required for autophagy and the Cvt pathway (64, 170). A subset of GTP exchange factors,

including Sec12 and Sec16, and two coatomer subunits of the COPII coat, Sec23 and Sec24, are needed for the biogenesis of autophagosomes but not Cvt vesicles (64); although it is possible that a defect in the Cvt pathway is more subtle due to the relatively reduced need for membrane compared with nonselective autophagy. Nonetheless, there may be some aspects of vesicle formation that are unique to either autophagy or the Cvt pathway. For example, the SNARE-Sec complex containing the tSNARE Tlg2, the vSNARE Tlg1 and the Sec1 homolog Vps45, the Vps-fifty-three (VFT) complex and the sorting nexins Atg20 and Atg24 are required solely for Cvt vesicle formation (1, 140, 171). In addition, Trs85, a component in the TRAPP (transport protein particle) complexes, which mediate ER-to-Golgi and intra-Golgi trafficking, is essential for both nonselective autophagy and selective autophagic processes such as the Cvt pathway and pexophagy (123, 137). Although the underlying mechanism is not well characterized, it is likely that the early secretory mutants affect the membrane flow or correct sorting of some Atg proteins, such as Atg9 transport to the PAS.

Although completed autophagosomes can directly fuse with lysosomes, when cells are overloaded with aggregate-prone proteins, fusion of autophagosomes with the endocytic compartments is essential to facilitate efficient autophagic removal of these proteins. In Drosophila and mammalian cells, the ESCRT (endosomal sorting complexes required for transport) machinery and multivesicular body (MVB)-localized Rab11 play an important role in the fusion of MVBs with completed autophagosomes, and the Drosophila endosomal PtdIns3P 5-kinase Fab1 is involved in fusion of the resulting amphisomes with lysosomes (34, 37, 177). Both steps are required for promoting degradation of aggregate-prone substrate proteins sequestered by autophagosomes.

Cytoskeleton. Efficient protein trafficking during autophagosome formation is presumably mediated by cytoskeletal networks. For example, functional actin cytoskeleton and the Arp (actin-related protein) 2/3 complex, which nucleates branching of actin filaments, are required for Atg9 anterograde transport to the PAS and the autophagy activity in yeast (130, 167). Microtubules are also involved in autophagy. In primary rat hepatocytes, the microtubule depolymerizing drug nocodazole inhibits autophagosome formation (98). In addition, microtubules, the tubulin deacetylase HDAC6 and the microtubule motor protein dynein are found to be required for the autophagic clearance of various aggregate-prone proteins in flies and mammalian cells (67, 153, 163). It seems that autophagosomes are formed at random locations in the cell, but transported directionally towards the nucleus after completion (69). Several lines of evidence suggest that autophagosomes associate with microtubule tracks, move to the microtubule-organizing center and fuse with endosomes or lysosomes, and the dynamic process is driven by the dynein motor (36, 69, 98).

Signaling pathways regulating autophagy

Nutrient Signaling

During nutrient deprivation autophagosome formation is dramatically induced. In both yeast and mammalian cells, two well-characterized signaling cascades that sense nutrient status, activate cell division and growth, and negatively regulate autophagy are the TOR and Ras-cAMP-PKA pathways.

TORC1 (TOR complex 1). TORC1 is sensitive to rapamycin. Inactivation of TORC1 by rapamycin stimulates autophagy in the presence of nutrients, suggesting that TOR downregulates autophagy (146). Extracellular amino acids enter mammalian cells through transporters such as SLC1A5 (solute carrier family 1 member 5) and SLC7A5 (141), and it is proposed that mTORC1 directly senses and is phosphorylated by nutrient signals (112); however, recent observations suggest that Rag proteins, the Ras-related small GTPases, interact with mTORC1 in response to amino acids, and mediate its translocation to a specific subcellular compartment that contains the mTORC1 activator Rheb (Ras homolog enriched in brain) (181). Other studies indicate that amino acids also activate mTOR via class III PI3K (hVps34) (13, 142) (Fig. 1.2A). The presence of amino acids stimulates hVps34, which leads to mTOR activation and autophagy inhibition. However, this creates a discrepancy with the role of class III PI3K in promoting nucleation and assembly of Atg proteins at early steps of autophagosome formation (71). A possible explanation is that PI3K exists in distinct subpopulations or protein complexes in the cell, which carry out different functions or function at different times.

Besides regulating the Atg1/ULK complex, in yeast TORC1 also suppresses autophagy via phosphorylation of Tap42, which activates the catalytic subunits of PP2A (the serine/threonine protein phosphatase 2A), a negative regulator of autophagy (233) (Fig. 1.2B). Although downstream targets of PP2A have not been identified, it is possible that Atg proteins may be directly involved, such as the Atg1 kinase complex (as described above) and other phosphorylated Atg proteins.

The Ras/PKA pathway. The RAS/cAMP-dependent protein kinase A (PKA) signaling pathway plays an important role in glucose sensing from yeast to mammals. Yeast PKA contains a heterotetramer composed of the regulatory subunit Bcy1 and three redundant catalytic subunits Tpk1, Tpk2 and Tpk3. In nutrient-rich conditions, small GTPases Ras1 and Ras2 are active and enhance cAMP generation by the adenylyl cyclase. Elevated cAMP binds to Bcy1 and releases its inhibitory effect on PKA. Constitutive activation of the Ras/PKA pathway suppresses autophagy induced by TOR inhibition in yeast (12, 185), suggesting that the Ras-PKA pathway downregulates autophagy in parallel with the TOR-Tap42 axis. Autophagy inhibition by Ras/PKA is likely mediated through regulation of Atg1, since Atg1 is identified as a phosphorylation substrate of PKA (11) (Fig. 1.2B). In the presence of nutrients, PKA phosphorylation causes Atg1 largely cytosolic and dissociated from the PAS; whereas during starvation, Atg1 is dephosphorylated and localized to the PAS. It should be noted that Atg1 may not be the sole PKA target, because a hyperactive Ras mutant Ras2 G19V, which constitutively activates PKA signaling, is still able to inhibit autophagy in cells expressing an Atg1 variant lacking the PKA phosphorylation sites.

In addition, the protein kinase Sch9, the closest yeast homolog to the mammalian protein kinase B (PKB)/Akt as well as to the TOR target S6 kinase (S6K), is involved in nutrient sensing (241). Simultaneous inactivation of PKA and Sch9 induces autophagy, which can be further increased by inactivation of TORC1 (237), suggesting that autophagy is negatively regulated by three parallel pathways in yeast, TORC1, Ras/PKA and Sch9 (Fig. 1.2B). Ras/PKA and Sch9 may regulate autophagy at the transcriptional level, as the transcriptional factors Msn2/4 and the Rim15 kinase are required for autophagic flux induced by inactivation of both PKA and Sch9, but not for that induced by inactivation of TOR (237).

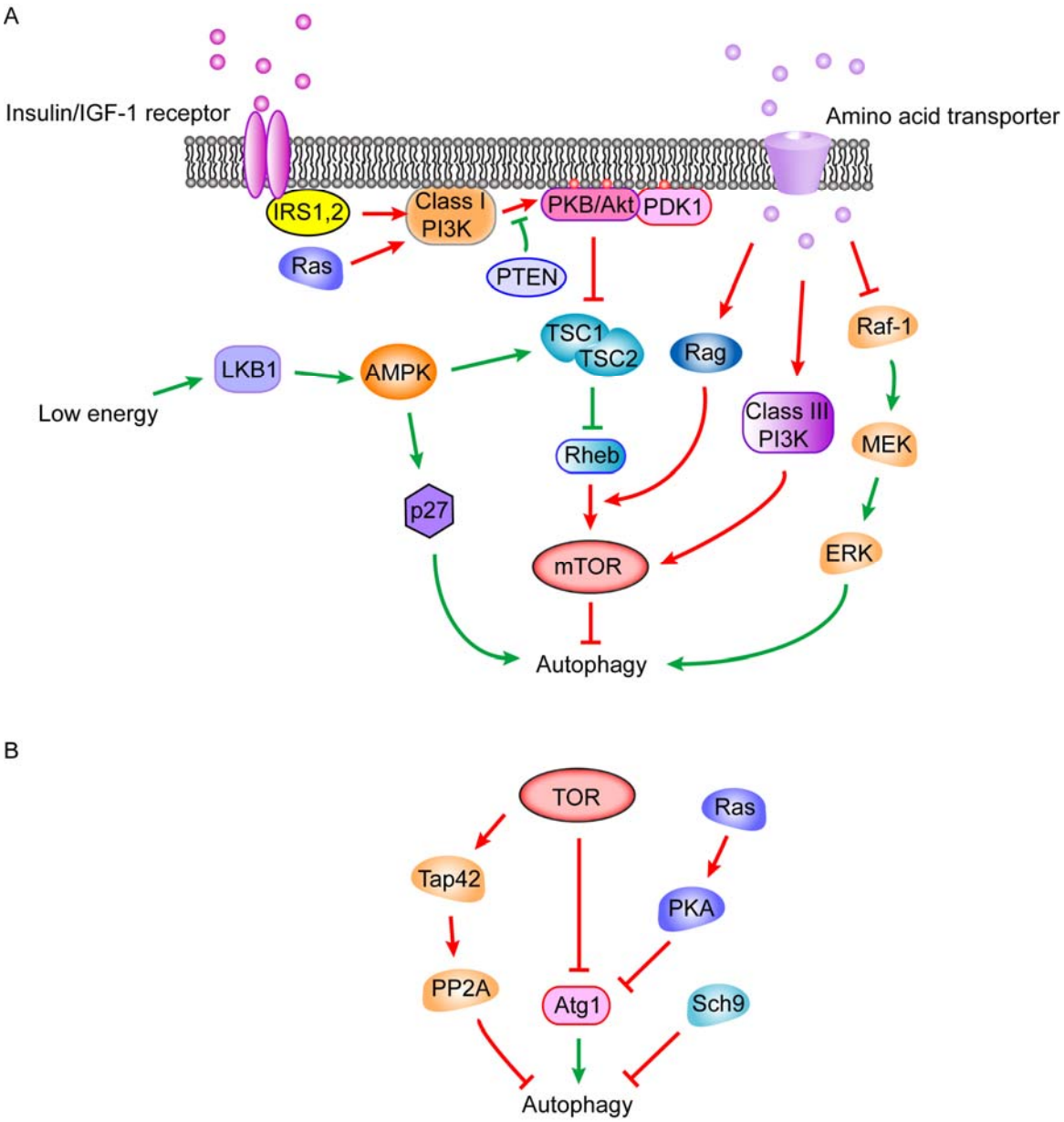

Figure 1.2. Autophagy is induced by deprivation of nutrients, hormones and energy. (A) Regulatory pathways of autophagy by amino acids, hormones and energy in mammals. (B) Signaling of autophagy in yeast. Green arrows/bars represent steps that activate autophagy, and red arrows/bars indicate steps inhibiting autophagy.

Insulin/Growth Factor Pathways

When growth factors are withdrawn from the extracellular milieu, in spite of sufficient nutrients, autophagy is induced and indispensable for maintaining cellular functions and energy production (114). In higher eukaryotes such as Drosophila and mammalian cells, the pathway that hormones regulate autophagy is different from that of nutrients but both converge on TOR (Fig. 1.2A). Insulin and insulin-like growth factors regulate mTOR through class I PI3K. Upon insulin binding, autophosphorylation of the insulin receptor on tyrosine residues recruits and phosphorylates IRS1 and IRS2 (insulin receptor substrate 1 and 2), which creates a docking scaffold that allows binding of adaptor proteins, including subunits of class I PI3K such as p85. Generation of PIP_3 (Fig. 1.2A, red circles in the membrane) by class I PI3K increases membrane recruitment of both protein kinase B (PKB)/Akt and its activator PDK1 (phosphoinositide-dependent protein kinase 1), leading to phosphorylation and activation of PKB/Akt by PDK1 (3, 196). The 3'-phosphoinositide phosphatase PTEN reverses the PIP_3 production, decreases the downstream PKB/Akt signaling and thus positively regulates autophagy (4). Activated PKB/Akt promotes phosphorylation of the protein encoded by TSC2 tumor suppressor gene that is mutated in the tuberous sclerosis complex (TSC) tumor syndrome. The phosphorylation blocks TSC2 to interact with TSC1 and form the TSC1/2 complex (118), which induces Rheb into the active GTP-bound form (62, 243) and allows it to directly bind and activate mTORC1 (111). When hormones are absent, mTOR is inactivated, which releases the inhibitory effect on autophagy.

Besides TOR, Ras signaling also plays a role in autophagy regulation by growth factors (Fig. 1.2A). Ras transduces signals from growth factor receptor tyrosine kinases

to intracellular effectors, such as Raf-1/MAP (mitogen-activated protein) kinases and class I PI3K. In NIH3T3 mouse embryonic fibroblast cells, activated Ras suppresses autophagy through class I PI3K, but not through Raf-1 (40). In contrast to PI3K, the Ras effector Raf-1 is found to be an amino acid sensor and positively regulate autophagy in HT-29 human colon cancer cells (157). In this situation, amino acids target and inhibit the activity of the Raf-1 kinase, which downregulates the downstream MEK1/2 and ERK1/2 (extracellular signal-regulated kinase 1/2) kinases and autophagy activity. Amino acid deprivation reverses this inhibition and induces ERK1/2 and autophagy. As a consequence, two downstream effector cascades of Ras, the Ras-PI3K and Ras-Raf-1-ERK1/2 pathways, are likely to counteract with each other in autophagy regulation through signaling from growth factors versus amino acids, or the genetic differences between normal and cancer cell lines determine how the Ras signaling controls autophagy.

Energy Sensing

During periods of intracellular metabolic stress, activation of autophagy is essential for cell viability, and the underlying pathways are understood in considerable detail. In mammalian cells, reduced cellular energy (ATP) level is sensed by AMPK (5'-AMP-activated protein kinase) (Fig. 1.2A). AMPK is activated by a decreased ATP/AMP ratio through the upstream LKB1 kinase (the Peutz-Jeghers syndrome protein). Active AMPK leads to phosphorylation and activation of the TSC1/2 complex, which inhibits mTOR activity through Rheb (63). Autophagy stimulated by mTOR downregulation results in elevated ATP production via recycling of nutrients. In addition, the LKB1-

AMPK pathway phosphorylates and activates $p27^{kip1}$, a cyclin-dependent kinase inhibitor leading to cell-cycle arrest, which is essential to prevent cells from apoptotic death and to induce autophagy for survival in response to bioenergetic stress during growth factor withdrawal and nutrient deprivation (108). Similarly, Snf1, the yeast homolog of mammalian AMPK, also positively modulates autophagy, possibly through independent mechanisms involving regulation of Atg1 (220).

Stress Response

ER stress. The endoplasmic reticulum (ER) is the key compartment in the cell to facilitate folding of newly synthesized proteins and vesicular secretion of membrane and proteins to various organelles and the cell surface, and it also serves as the major intracellular Ca^{2+} reservoir. A number of ER stress stimuli, for example, expression of aggregate prone proteins, glucose deprivation (reduced glycosylation), hypoxia and oxidative stress (decreased disulfide bond formation), and Ca^{2+} efflux from the ER, lead to accumulation of unfolded proteins in the ER, which exceeds its folding capacity. Increasing studies indicate that autophagy is potently induced by ER stress in organisms from yeast to mammals. However, the signaling mechanisms linking ER stress to autophagy vary, dependent on specific stress conditions and organisms (Fig. 1.3A).

In yeast, ER chemical stressors blocking formation of disulfide bonds or protein glycosylation, such as DTT and tunicamycin, effectively trigger autophagy, which requires the Atg1 kinase activity (236). ER stress-induced autophagy is required for cell survival in the presence of tunicamycin, likely through compensatory removal of expanded and disorganized ER, together with misfolded proteins in it, which result from

the unfolded protein response (UPR) (8). The UPR signaling pathway in yeast is mediated by Ire1 (inositol-requiring kinase 1), an ER transmembrane protein with a luminal stress-sensing domain and a cytosolic endoribonuclease domain. In response to accumulation of unfolded proteins, an ER-specific member of heat shock protein 70 family, Grp78/Bip, dissociates from its ER-sensing domain and activates the cytosolic endonuclease domain of Ire1, which triggers the splicing of the Ire1 substrate Hac1. The latter encodes a transcription factor (the yeast homolog of mammalian XBP1) that activates transcription of target genes involved in protein modification/folding, vesicle transport, phospholipids biosynthesis and ER-associated degradation (115). Although the Ire1-Hac1 pathway is required for autophagy induction by ER stress, it seems dispensable for the transcriptional upregulation of *ATG* genes (8). How Ire1 and Hac1 exert their function to stimulate autophagy in yeast remains to be understood.

In mammalian cells, knockdown of the upstream UPR regulator Grp78/Bip by siRNA inhibits autophagosome formation, but not LC3 conversion, induced by both ER stress and nutrient deprivation, suggesting that Grp78/Bip is an obligatory factor for autophagy and may function at the phagophore expansion rather than induction step (107). It should be noted that the conclusion is mainly based on knockdown of Grp78/Bip, an artificial condition that spontaneously activates UPR pathways and induces LC3 conversion, which may cause difficulties to differentiate the roles of Grp78/Bip and UPR signaling in autophagy induction.

Additional studies focusing on the downstream UPR targets have provided useful information on the mechanisms of ER stress-induced autophagy in mammals. Mammalian UPR signaling is more complex than yeast and involves three distinct

downstream pathways, IRE1 (similar to yeast Ire1), ATF6 (activating transcription factor 6) and PERK (RNA-dependent protein kinase-like ER kinase). They signal misfolded protein levels in the ER and activate transcription of different target genes. One downstream target of IRE1 is c-Jun N-terminal kinase (JNK), which is shown to be essential for lipid conjugation of LC3 induced by tunicamycin or by accumulation of cytosolic misfolded proteins due to proteasome inhibition in MEFs and cancer cells (30, 150), and recent data using murine cells suggest that in response to ER stress induced by expression of misfolded polyQ72 or mutant dysferlin proteins, phosphorylation of eIF2α (eukaryotic initiation factor 2 α) by the eIF2α kinase PERK is required for mediating LC3 conversion and autophagic degradation of the mutant proteins in the ER (38, 99). Thus, both the IRE1-JNK and the PERK-eIF2α pathways seem to play a pivotal role in UPR-induced autophagy.

In addition to the UPR signaling, ER stress also induces release of lumenal Ca^{2+} to the cytosol. Calcium-activated calmodulin-dependent kinase kinase-β (CaMKKβ) is stimulated by the increase in the intracellular Ca^{2+} level and further activates AMPK, the latter potently inducing autophagy (57). Elevated Ca^{2+} level also triggers phosphorylation of protein kinase Cθ (PKCθ), which induces LC3 conversion and autophagy in immortalized hepatocytes in response to ER stressors thapsigargin and tunicamycin (180).

Although the above studies show that ER stress-induced autophagy has a pro-survival role in mammalian cells, others implicate that ER stressors may cause autophagic cell death. Injection of tunicamycin into renal tubules in mice induces kidney tubular cell death via both apoptosis and autophagy, which are mediated by the catalytic activity of a tumor suppressor DAPk (calmodulin-regulated serine/threonine kinase

death-associated protein kinase). DAPk is activated by dephosphorylation of an inhibitory serine autophosphorylation on DAPk by a PP2A-like phosphatase (46), and activated DAPk induces autophagy likely through its ability to phosphorylate Beclin 1 and promote Beclin 1 dissociation from Bcl-2 (240). It is possible that autophagy plays dual roles in determining cell fate, depending on specific cell types and stimuli tested (29).

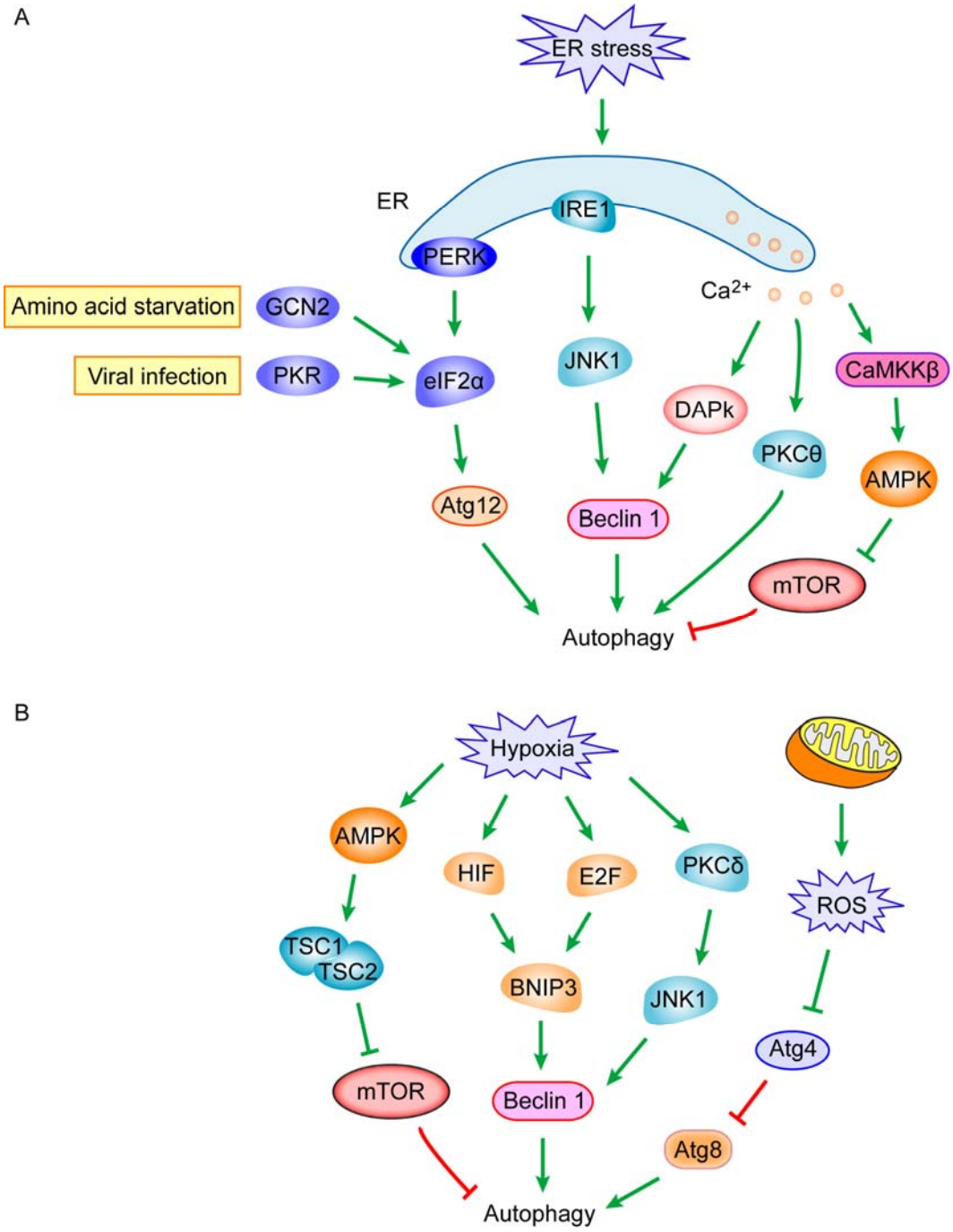

Figure 1.3. Autophagy regulation in response to stress. (A) ER stress stimulates autophagy through the PERK-eIF2α pathway, the IRE1-JNK1 pathway and Ca^{2+} release. Activation of eIF2α by PERK may upregulate transcription of certain autophagy genes, such as Atg12. Phosphorylation and activation of eIF2α by two other eIF2α kinases, CCN2 and PKR, upon amino acid starvation and viral infection, respectively, are also depicted. (B) Autophagy induction by mechanisms sensing hypoxia or oxidative stress. JNK1, DAPk and BNIP3 induce autophagy by disrupting Bcl-2-Beclin 1 interaction and activating Beclin 1. Green arrows/bars, steps activating autophagy; red bars, steps inhibiting autophagy.

Hypoxia. Low levels of oxygen at or below 1% (hypoxic stress) versus 2-9% (normoxia for most mammalian cell types), exist in physiologically developing embryos as well as a lot of pathological conditions, such as solid tumors, cardiovascular ischemia and brain injuries. Accumulating data show that hypoxia induces autophagy in mammalian cells, yet the area of study is at a beginning stage and the signaling pathways responsible for autophagy induction and its cellular consequences seem to be different, contingent on types of cells and autophagic pathways (Fig. 1.3B), for example, enhanced mitochondrial autophagy (mitophagy) during hypoxia is suggested an adaptive response, reducing ROS levels and protecting cell integrity, although in several glioma and breast cancer cell lines, prolonged hypoxia mediates autophagic cell death (5).

Hypoxia-inducible factor-1 (HIF-1) is the primary transcription factor acutely induced by the hypoxic condition and drives transcription of hundreds of genes that promote erythropoiesis and angiogenesis and decrease mitochondrial biogenesis and respiration, counterbalancing deleterious effects caused by O_2 deficiency. It is shown that in MEFs, mitochondria are removed by mitophagy in response to hypoxia, which is dependent on HIF-1 and the induction of its downstream target BNIP3 (Bcl-2 adenovirus E1a nineteen kDa interacting protein 3, a pro-death Bcl-2 family member) (242). In addition, during reticulocyte maturation in mice, BNIP3L (BNIP3-like protein, also known as NIX), another HIF-1-induced target, is also required for programmed mitochondrial clearance by autophagy (182, 186). BNIP3 competes with Beclin 1 for binding Bcl-2 and thus releases Beclin 1 for participating in mitophagy. It should be noted that, besides under the control of HIF, BNIP3 is also a target gene of the E2F transcription factors, which is inhibited by the RB tumor suppressor during RB-induced

cell cycle arrest (213). Therefore, hypoxia induces BNIP3 transcription via binding of HIF-1 and/or E2F to the BNIP3 promoter, and the RB-E2F-BNIP3 signaling is also involved in hypoxia-induced autophagy.

Indeed, upregulation of bulk autophagy by hypoxia in tumor cells seems independent of the HIF-1 pathway; instead, the AMPK-TSC2 (155) and PKCδ (protein kinase Cδ)-JNK1 (21) cascades are responsible for signaling autophagy induction. It is also found that hypoxia inhibits TOR and blocks eIF4F (eukaryotic initiation factor 4F) complex formation and mRNA translation (10, 172). Thus, autophagy induced by hypoxia can be at least partially TOR-dependent, and hypoxia-stimulated ER stress may also play a role in autophagy induction.

Oxidative stress. A common intracellular stress that potently leads to induction of autophagy is the formation of reactive oxygen species (ROS). Mitochondria are the major source generating ROS, which will in turn damage mitochondria. ROS-generating agents (such as hydrogen peroxide/H_2O_2 and 2-methoxyestradiol), or chemicals inhibiting the mitochondrial electron-transport-chain, induce ROS production and autophagic cell death in transformed and cancer cell lines (22, 23). Intriguingly, these drugs induce a much lower level of ROS in non-transformed primary mouse astrocytes compared to cancer cells, and fail to stimulate autophagy, suggesting that normal cells effectively maintain ROS at a tolerable level and protect themselves from mitochondrial damages, likely through antioxidant mechanisms such as the redox system, superoxide dismutase (SOD) and catalase, because applying ROS scavengers or overexpressing SOD2 reduces autophagy (22, 23). In addition, it is suggested that impaired mitochondria are selectively degraded through mitophagy in yeast and mammalian cells (135, 160, 174, 217), which

may constitute another mechanism to reduce ROS levels and maintain cell survival. Therefore, ROS selectively targets malignant but not normal cells for autophagy induction, providing important implications for anticancer therapy.

The link between ROS and autophagy induction may be the cysteine protease Atg4 (Fig. 1.3B), which cleaves Atg8/LC3 from the autophagosome membrane before autophagosome-lysosome fusion. ROS targets a conserved Cys 81 on Atg4, which is in the vicinity of its catalytic Cys 77 residue, and inhibits Atg4 protease activity and promotes lipidation of Atg8/LC3, an essential step for autophagy (184). It is not known yet how ROS levels are temporally and spatially controlled inside the cell, so that Atg4 can be locally activated to allow delipidation and recycling of Atg8/LC3; it is likely that mitochondria may actively participate in ROS production to regulate Atg4 activity. Future studies will clarify whether Atg4 is the sole molecule that underlies the redox regulation of autophagy.

Pathogen Infection

Autophagy has an important role in eliminating invading pathogens, and pathogen-induced autophagy appears to be TOR-independent (219). Although a lot of studies report autophagy induction in host cells by a number of bacteria and viruses and autophagic incorporation and degradation of the pathogens, the signaling pathways activating autophagy in innate and adaptive immunity have only been revealed recently (Fig. 1.4).

The innate immune system is an evolutionarily ancient and conserved defense mechanism and is found in almost all types of multicellular organisms, including insects,

plants and mammals. In Drosophila, which depend nearly entirely on innate immunity to fight against infection, the peptidoglycan-recognition protein (PGRP) family members play crucial roles in surveillance and microbe sensing. The PGRP receptors are present in immune cells, recognize bacterial-derived peptidoglycans, and activate the production of antimicrobial peptides. A PGRP family member, PGRP-LE, is the first identified cytoplasmic sensor in insects that recognizes presence of intracellular bacteria and triggers autophagy in host cells, which is required for suppressing the growth of *Listeria monocytogenes* in hemocytes and enhancing host viability (230). The pathway that transduces signals from the PGRP-LE receptor to the autophagy machinery, and whether it crosstalks to the classical signaling pathways downstream of PGRP receptors that activate genes encoding antimicrobial peptides, remain to be investigated.

Signaling of Toll-like receptors (TLRs) triggers autophagy during mammalian innate and adaptive immunity. TLRs are membrane receptors localized at the cell surface and endosomes, and TLR signaling activates transcription of genes responsible for T cell stimulation, inflammation and antiviral immune responses. Different TLRs are involved in autophagy induction upon binding their specific pathogen-derived ligands. For example, viral ssRNA (single-stranded RNA) induces autophagy via TLR7 (28), and yeast zymosan stimulates LC3 translocation to phagosomes by activating TLR2 (183); whereas lipopolysaccharide (LPS), which is derived from cell walls of Gram-negative bacteria, triggers autophagy through TLR4 (190, 228). TLRs recruit adaptor proteins to transduce signals to downstream effectors. MyD88 (myeloid differentiation factor 88) is the major adaptor protein used by almost all activated TLRs and mediates the autophagy induction downstream of TLR7 (28). In human and murine macrophages, the TLR4

adaptor protein TRIF (Toll-interleukin-1 receptor domain-containing adaptor-inducing interferon-β) is suggested to mediate LPS-induced autophagy and the same downstream signaling pathway is shared by both innate immunity and autophagy upregulation (228). In addition, a unique mechanism is proposed for induction of macrophage autophagy; in murine macrophages, MyD88, together with TRIF, interact with Beclin 1 more strongly in the presence of LPS or poly(I·C) (ligands for TLR4 and TLR3, respectively), which reduces the binding of Beclin 1 and Bcl-2 and thus triggers autophagy activation (190). Moreover, interferon (IFN)-γ and its effector Irgm1 (the IFN-inducible immunity-related GTPase family M member 1; also known as LRG-47) are also required to stimulate autophagy in macrophages and inhibit the survival of intracellular mycobacteria (48, 194).

In response to viral infection, the antiviral eIF2α kinase signaling pathway, including eIF2α and the IFN-inducible double-stranded RNA-dependent protein kinase R (PKR), is activated and upregulates autophagy (203, 204). Some viral proteins may antagonize autophagy induction by directly modulating autophagy proteins. An example is the HSV-1 (herpes simplex virus type 1)-encoded neurovirulence protein ICP34.5, which inhibits autophagy via interaction and sequestration of Beclin 1 (152). It is also reported that viral infection, such as infection of Hepatitis C virus, induces ER stress, and autophagy is triggered through the unfolded protein response, including the downstream IRE1, ATF6 and PERK signaling pathways (195).

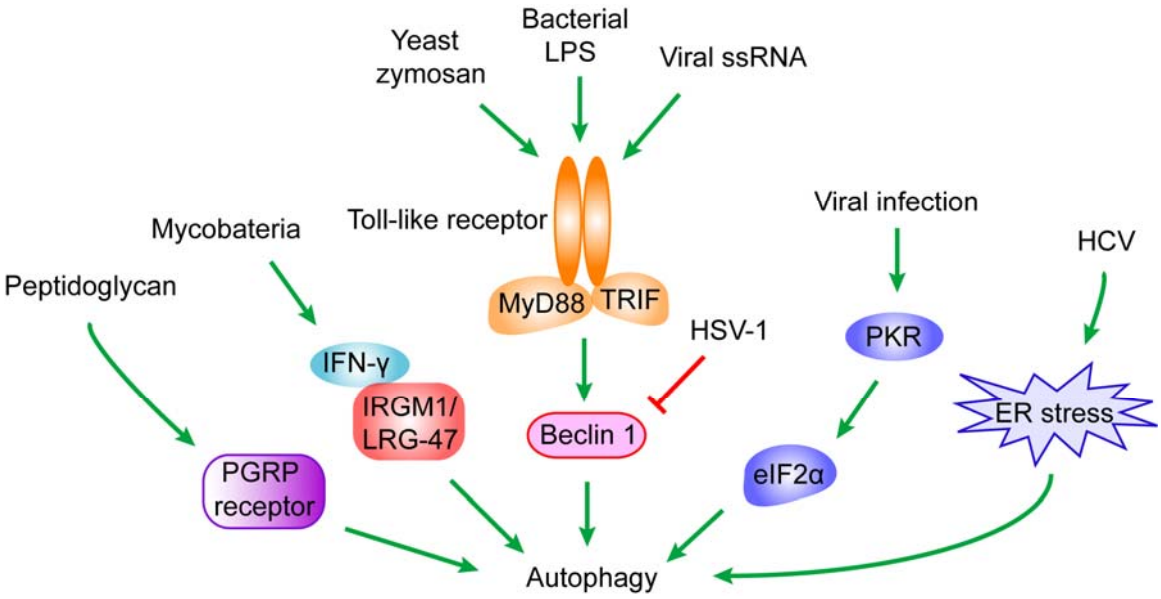

Figure 1.4. Different mechanisms that regulate autophagy by pathogen invasion. Toll-like receptor adaptor proteins, MyD88 and TRIF, dissociate Beclin 1 from its inhibitor Bcl-2 and induce autophagy, whereas HSV-1 protein ICP34.5 blocks autophagy by binding and sequestering Beclin 1. Green arrows, steps activating autophagy; the red bar, the step inhibiting autophagy. HSV-1, Herpes simplex virus type 1; HCV, Hepatitis C virus.

Transcriptional and epigenetic regulation of autophagy

Transcription

Autophagy genes are regulated at a transcriptional level in response to stress, for example, under starvation conditions, transcription of the autophagosome marker Atg8/LC3 is rapidly upregulated in yeast and mammalian cells. However, not much is known about the underlying transcription machinery. Foxo is the first transcription factor that is shown necessary and sufficient to induce autophagy in Drosophila larval fat body (73), and microarray analysis in yeast suggests that the transcription factor Ume6 is involved in the repression of *ATG8* expression during growth (224), although it remains to be seen whether it is direct or indirect effects on *ATG8* transcription. For mammalian models, discovery of a transcription-dependent mechanism via FoxO3 (forkhead box O 3) comes from studies on protein degradation during muscle atrophy (117, 245). FoxO3 induces the transcription of multiple autophagy genes, including *LC3B*, *Gabarapl1*, *atg12*, *atg4B*, *vps34*, *ulk2*, *beclin 1*, *Bnip3* and *Bnip3l*. FoxO3 directly binds to the promoters of *LC3B*, *Gabarapl1*, *atg12*, *Bnip3l* and *Bnip3* to activate gene transcription. Constitutive active FoxO3 is sufficient to induce autophagosome formation in adult mouse skeletal muscle, which promotes lysosomal proteolysis and leads to muscle wasting. Importantly, FoxO3 functions in parallel to the mTOR pathway; while both pathways are downstream of IGF-1/insulin-PI3K-PKB/Akt signaling. Thus, autophagy is regulated by two different mechanisms: non-transcriptional inhibition by mTOR and transcription-dependent upregulation through FoxO3. Nevertheless, transcriptional mechanisms that

physiologically regulate expression of autophagy genes in tissues other than myotubes have not been characterized.

Autophagy induction inversely correlates with active protein synthesis. In the presence of abundant nutrients, proteins are synthesized and autophagy suppressed, whereas in response to stress stimuli, cells trigger translational arrest and autophagy induction. Recent studies suggest that translational initiation factors, for example, eIF4GI, that specifically activate mRNA translation of genes controlling cell growth and proliferation, block the induction of autophagy downstream of TOR (162); whereas signaling pathways that induce translational arrest, such as the eEF-2 (eukaryotic elongation factor-2) kinase and the eIF2α kinase signaling pathway, positively regulate autophagy (203, 225). Phosphorylation of eIF2α at Ser-51 by the conserved eIF2α protein kinase family is essential for the global translational arrest and selective upregulation in the translation of the transcriptional activators (such as GCN4) that stimulate transcription of starvation-induced genes. Yeast has one eIF2α kinase, GCN2 (general control nonderepressible-2), which is negatively regulated by TOR (101); whereas mammals have four known eIF2α kinases, GCN2, PKR, PERK and HRI (heme-regulated inhibitor), activated by amino acid starvation, viral infection, ER stress and heme deprivation, respectively (Fig. 1.3A). In both yeast and MEFs, eIF2α phosphorylation by the eIF2α kinase GCN2 is required for starvation-induced autophagy, and in MEFs, PKR is required for autophagy induced by viral infection (203). The downstream effect of eIF2α phosphorylation in autophagy is likely to be transcriptional, as transcription of Atg12 is upregulated by phosphorylated eIF2α in polyQ72 loaded mammalian cells (99). In yeast, selective translation of Gcn4 (rather than the global translational arrest) by

eIF2α phosphorylation is essential for autophagy, consistent with a report indicating several autophagy genes, including *ATG1*, *ATG13* and *APE1*, as downstream transcription activation targets of Gcn4 (136). However, the study is largely based on microarray analysis, and independent assays are needed to test the functions of transcriptional activators in yeast autophagy.

Chromosome Modification

Accumulating data implicate an important role of epigenetic factors in regulating autophagy in various pathological conditions. Alteration of acetylation status of histones through histone deacetylases (HDAC) is a key mechanism that controls chromatin structural remodeling and gene transcription. Chemical or genetic inhibition of HDACs leads to autophagy induction (151). Various HDAC chemical inhibitors, including SAHA (suberoylanilide hydroxamic acid) and butyrate, promote hyperacetylation of histones and have been shown to preferentially target cancer cells for both apoptotic and caspase-independent autophagic cell death in cell lines and animal models (119, 189). Although there are debates on the anticancer role of autophagy induced by HDAC suppression (17), a number of mechanisms have been proposed for autophagy induction by HDAC inhibitors based on studies in different diseases. It is suggested that autophagy is stimulated by SAHA via a decreased level of mTOR expression and activity in the solid tumor endometrial stromal sarcoma cells, and via PKB/Akt inhibition and Beclin 1 induction in HeLa cells (15, 58), whereas in malignant rhabdoid tumor cells, the HDAC inhibitor FK228 induces autophagy by triggering translocation of AIF (apoptosis

inducing factor) into the nucleus, which mediates caspase-independent tumor cell death (221).

Specific transcriptional effect on *ATG* genes by HDAC suppression has also been reported. In lung tissues obtained from patients with the chronic obstructive pulmonary disease caused by cigarette smoking, inhibition of HDAC activity by cigarette smoke extract increases binding of Egr-1 (early growth response-1) and E2F family of transcription factors to the *LC3B* promoter region and activates *LC3B* expression. In addition, expression of *ATG4B* also depends on Egr-1 (24). Although one cannot rule out the possibility that enhanced autophagy by HDAC inhibition may be due to global cell cycle arrest (110) or nonspecific effects on the overall chromosomal structure, it opens up opportunities for regulating autophagy by chromosome modifiers as a therapeutic target for clinical intervention. Much awaits study to define the specific functions of different histone deacetylases on autophagy genes.

Post-translational regulation of the autophagy machinery

In addition to aforementioned ubiquitin-like modification of Atg12 and Atg8/LC3, and TOR/PKA-dependent phosphorylation of the Atg1 kinase complex, a number of other post-translational modifications on various Atg proteins have been recently studied and suggested to be crucial in regulating autophagy activity.

Phosphorylation

A major function of protein phosphorylation is to form a docking scaffold and recruit other proteins. An example is during pexophagy in the yeast *Pichia pastoris*, the receptor protein for peroxisomes, PpAtg30, is phosphorylated. Through phosphorylated residues PpAtg30 interacts with the autophagy machinery components, such as PpAtg11, and links peroxisomes for autophagic breakdown (35).

On the other hand, phosphorylation serves a role to sterically prevent protein-protein interaction. In mammalian cells, in response to ceramide or starvation, the Beclin 1 binding partner and inhibitor Bcl-2 is phosphorylated on three residues T69, S70 and S87 located in its cellular loop by JNK1 (156, 222). Hyperphosphorylated Bcl-2 dissociates from Beclin 1 and releases it for autophagy induction; whereas viral Bcl-2 (derived from Kaposi's sarcoma-associated herpesvirus), which lacks the phosphorylation loop, cannot dissociate from Beclin 1 and thus inhibits autophagy. In addition, phosphorylation of Beclin 1 on Thr 119 in its BH3 domain by DAPk also reduces Beclin 1-Bcl-2 interaction and activates autophagy (240). Thus, phosphorylation of autophagy-related proteins provides additional aspects for autophagy regulation.

Acetylation

Deacetylation modification of the autophagy machinery proteins is also required for autophagy (102, 103). A number of Atg proteins, including Atg5, Atg7, Atg8 and Atg12, are acetylated in nutrient-rich conditions and deacetylated during starvation, both in HeLa cells and in vivo. Acetylation of Atg proteins is dependent specifically on the p300 acetyltransferase, but not on two other acetyltransferase CBP and PCAF, and the deacetylation process dependent on the NAD-dependent deacetylase Sirt1 (a sirtuin family member). It is shown that components of the autophagy machinery physically interact with p300 or Sirt1, which is regulated by nutrient availability and contributes to changes in the acetylation status.

Sirt1 expression is induced by caloric restriction, which plays an important role in promoting longevity (231). Therefore, direct deacetylation of the autophagy machinery by Sirt1 provides an important mechanistic link between autophagy induction and life span extension. However, the molecular function of deacetylation of Atg proteins in autophagy is essentially unknown, although deacetylation may help remove spatial blockade for protein interaction or recruitment, or modify protein activity. In addition, the mechanisms by which Sirt1 and p300 sense upstream input signals have not been demonstrated. It is possible that the insulin/growth factor pathway is involved in the control of the reversible acetylation process.

Concluding remarks

Substantial progress has been made in the past few years on the molecular mechanism and regulatory network of autophagy from yeast to mammals. As a major cellular catabolic system targeting a variety of substrates, the autophagic process needs to be tightly controlled. The coordination of Atg proteins with other subcellular components, including cytoskeleton, the secretory pathway, oncogenes and tumor suppressors, and immunoproteins, is crucial for autophagy induction. Both canonical (such as the insulin and growth factor pathway) and novel signaling cascades have been implicated in regulating autophagy, in response to different intra- or extracellular stimuli. Current knowledge and further investigation on genetic regulation of autophagy will provide a broad spectrum of potential pharmacological targets for modulating autophagy in various disease conditions.

Summary points

1. Autophagy mediates the lysosomal degradation of cytosolic proteins, damaged or excess organelles, protein aggregates and invaded microbes.
2. Autophagy can non-selectively degrade bulk cytosol, or selectively target specific cargos through receptor proteins.
3. Autophagy-related (*ATG*) genes cooperatively function at multiple steps to facilitate the formation of a double-membrane autophagosome.
4. Various stress conditions stimulate induction of autophagy, and the signal transduction mechanisms of autophagy are being identified.
5. Not much is known about transcriptional regulation of autophagy genes, yet several transcription factors have been suggested to activate or suppress expression of certain *ATG* genes in yeast, Drosophila and mammalian tissues.
6. Autophagy proteins undergo phosphorylation and acetylation modifications to accomplish autophagy activity.

Future issues

1. Crosstalks between signaling pathways in controlling autophagy, and detailed studies on a convergent molecule of several upstream pathways, such as the link between TOR downregulation and autophagy induction, should be further explored.
2. Characterization of Atg1 kinase substrates and new components in the Atg1 complex in both yeast and higher eukaryotes will provide useful information on the exact functions this important kinase carries out during autophagy.
3. How substrate specificity is achieved by selective autophagic degradation in a lot of circumstances, for example, cell cycle progression, cell karyogamy or division, development, differentiation and diseases, deserves extensive investigation. It should be noted that homologs of many *ATG* genes required for selective autophagy in yeast have not been identified in higher eukaryotes, such as Atg11; thus it is likely that they may share functional and structural similarities but not sequence homology.
4. Future studies on the mechanistic aspects of autophagosome formation can be performed either in vivo or in vitro, for instance, how small GTPases and SNARE proteins may collaborate with the autophagy machinery during phagophore assembly if any of them is involved, and what regulate dissociation of various Atg proteins from a completed autophagosome before fusion.
5. Transcriptional and translational regulation of autophagy genes, such as mRNA expression and stability, and whether there is tissue specificity, need to be better understood in both physiological and pathological stress conditions.

6. Discovery of new posttranslational modifications on Atg proteins and their regulating mechanisms will add to our current understanding of genetic regulation of autophagy.

CHAPTER 2

Recruitment of Atg9 to the preautophagosomal structure by Atg11 is essential for selective autophagy in budding yeast

Abstract

Autophagy is a conserved degradative pathway that is induced in response to various stress and developmental conditions in eukaryotic cells. It allows the elimination of cytosolic proteins and organelles in the lysosome/vacuole. In the yeast *Saccharomyces cerevisiae*, the integral membrane protein Atg9 cycles between mitochondria and the pre-autophagosomal structure (PAS), the nucleating site for formation of the sequestering vesicle, suggesting a role in supplying membrane for vesicle formation and/or expansion during autophagy. To better understand the mechanisms involved in Atg9 cycling, we performed a yeast two-hybrid-based screen and identified a peripheral membrane protein, Atg11, which interacts with Atg9. We show that Atg11 governs Atg9 cycling through the PAS during specific autophagy. We also demonstrate that the integrity of the actin cytoskeleton is essential for correct targeting of Atg11 to the PAS. We propose that a pool of Atg11 mediates anterograde transport of Atg9 to the PAS dependent on the actin cytoskeleton during yeast vegetative growth.

Introduction

As one of the major degradative mechanisms conserved among eukaryotic cells, autophagy mediates the turnover and recycling of long-lived cytosolic proteins and excess or damaged organelles (166). The cargo destined for autophagic degradation is sequestered in a double-membrane vesicle called an autophagosome, which fuses with the lysosome in mammalian cells or the vacuole in yeast. Eventually the cargo is degraded by lysosomal/vacuolar resident hydrolases. Autophagy occurs in response to physiological stress or developmental signals (106). Recently, autophagy has been implicated in a variety of human diseases, including cancer, neurodegeneration, and pathogen infection (192). The identification of over 30 *ATG* (*a*u*t*opha*g*y-related) genes in the budding yeast *Saccharomyces cerevisiae* has highlighted this single-cell organism as a perfect model to study the molecular mechanism of autophagy, although orthologs of some yeast *ATG* genes have been found in higher eukaryotes.

In yeast, autophagy can be induced under starvation conditions to reuse nutrients for essential cellular activities and proper cellular remodeling; this starvation-induced bulk autophagy is considered nonspecific. Studies in yeast have also revealed that *S. cerevisiae* has selective autophagic pathways that target specific cargos. These pathways mechanistically and genetically resemble bulk autophagy. One such route is the cytoplasm to vacuole targeting (Cvt) pathway (133). In this pathway, two vacuolar hydrolases, the precursor form of aminopeptidase I (prApe1) and α-mannosidase (Ams1), are transported to the vacuole in a double-membrane vesicle called a Cvt vesicle, with the former subsequently being processed into mature Ape1. Compared with starvation-

induced autophagy, the Cvt pathway occurs constitutively in growing conditions. Although some Atg proteins appear to be pathway-specific, most are involved in both the specific and nonspecific pathways; however, it is not fully understood how these proteins coordinate and function at the molecular level in either bulk or selective autophagy.

Most yeast Atg components localize at a perivacuolar punctate structure called the preautophagosomal structure or phagophore assembly site (PAS), which is proposed to be the site of autophagosome and Cvt vesicle formation (86, 147). In most endomembrane trafficking systems, such as the early secretory pathway, vesicles form by budding from the surface of a pre-existing organelle. However, in autophagy-related processes, the double-membrane sequestering vesicles appear to form de novo; that is, they expand by membrane addition during the formation process rather than being generated from a single piece of contiguous membrane (166). One of the major current challenges is to unveil where the membrane materials for autophagosomes or Cvt vesicles come from and how the lipids are transported to the assembly site. Among all Atg proteins, Atg9 is the best candidate that can help us understand this pivotal issue. Atg9 is the only characterized integral membrane protein required for both autophagosome and Cvt vesicle formation (144). However, this protein is absent from the completed vesicles, suggesting it is retrieved prior to the vesicle sealing/completion step. Atg9 localizes to multiple punctate sites, with one of them corresponding to the PAS and others to mitochondria, in addition to unidentified structures (168). Recent studies reveal that Atg9 cycles between mitochondria and the PAS vesicle assembly site (168, 169). These characteristics make Atg9 a potential membrane-carrier for vesicle formation.

We decided to investigate the molecular regulatory mechanisms underlying Atg9 cycling, and in particular what factors regulate the anterograde transport of Atg9 to the site of vesicle formation. In this study, we discovered that a peripheral membrane protein, Atg11 (87), is an interaction partner of Atg9. The interaction requires the second coiled-coil domain of Atg11 and the Atg9 N-terminal cytosolic domain. A missense mutation (H192L) in the Atg9 N-terminal domain that disrupts its interaction with Atg11, results in impaired cycling of Atg9 and a defect in selective autophagy. In addition, we found that in actin mutant cells Atg11 colocalized with Atg9 and was retained on mitochondria, indicating that Atg11 is not able to direct Atg9 to the PAS in the absence of an intact cytoskeletal network. These data support a model that a pool of Atg11 links Atg9 to the PAS along the actin cable under vegetative growth conditions.

Results

Atg11 is an interaction partner of Atg9

Atg9 is the only known transmembrane protein required for both bulk autophagy and selective autophagic processes, e.g., the Cvt pathway (144). Unlike most other Atg proteins, which are restricted to the perivacuolar PAS, Atg9 localizes to several punctate structures; one of them is at the PAS, whereas the others are primarily confined to mitochondria (168). Atg9 cycles between the two compartments, suggesting that it plays a role in providing lipids to the forming autophagosomes or Cvt vesicles (169); however, other than actin (167), the factors that regulate the anterograde transport of Atg9 to the PAS have not been identified. Therefore, we performed a yeast two hybrid-based screen of Atg proteins to identify potential Atg9-interacting proteins. Yeast two-hybrid cells harboring Atg9 and a peripheral membrane protein, Atg11, showed robust growth on plates lacking histidine, indicating that Atg11 could interact with Atg9 (Fig. 2.1A). The same result was obtained on plates lacking adenine (data not shown).

Atg11 functions in selective types of autophagy, i.e., the Cvt pathway and pexophagy, but is not essential for bulk autophagy (87). Atg11 plays a role in organizing the PAS and linking cargo to the vesicle-forming machinery at the PAS (191, 234). This protein is a component of at least two complexes in yeast. One is the Atg1-Atg11 complex, which is involved in induction of bulk and selective autophagy (79). The other is the Atg19-Atg11 complex, which recognizes and delivers prApe1 and Ams1 to the PAS (191, 234). We decided to determine whether these complexes are involved in Atg11 and Atg9 interaction. To address this issue, we utilized a biochemical approach to

examine whether Atg11 was able to form a complex with Atg9. We tagged Atg11 with GFP, and Atg9 with protein A (PA), at the chromosomal locus. Wild-type, *atg1*Δ, and *atg19*Δ cells expressing the integrated Atg9-PA and Atg11-GFP fusions were lysed, and the PA-tagged protein was isolated with IgG-sepharose beads. Atg11 was coprecipitated with Atg9-PA in all three strains (Fig. 2.1B), which verifies that these two proteins are present in a complex, although we do not know if they interact directly. Thus, the absence of either Atg1 or Atg19 did not affect the formation of a complex between Atg9 and Atg11. This finding suggests that there might be multiple populations of Atg11 within the cell, which interact with different sets of Atg proteins.

Our recent data show that two other Atg proteins, Atg23 and Atg27, interact with Atg9 and are required for Atg9 cycling. The interaction between Atg9 and either Atg23 or Atg27 is not mediated through Atg11 (105, 216). Thus, we extended the analysis by determining whether the Atg9-Atg11 interaction was dependent on these other Atg9-interacting proteins. We found that Atg11 was co-precipitated with Atg9 in *atg23*Δ and *atg23*Δ *atg27*Δ cells despite a lower overall efficiency of recovery (Fig. 2.1C), suggesting that Atg9 and Atg11 were able to form a complex in the absence of Atg23 and Atg27, although these two proteins may facilitate the interaction. The interaction between Atg9 and Atg11 in the *atg23*Δ or *atg27*Δ strains was confirmed by yeast two-hybrid analyses; the *atg23*Δ or *atg27*Δ two-hybrid cells expressing Atg9 and Atg11 were able to grow on -his selective plates, which is comparable to the wild-type cells (data not shown).

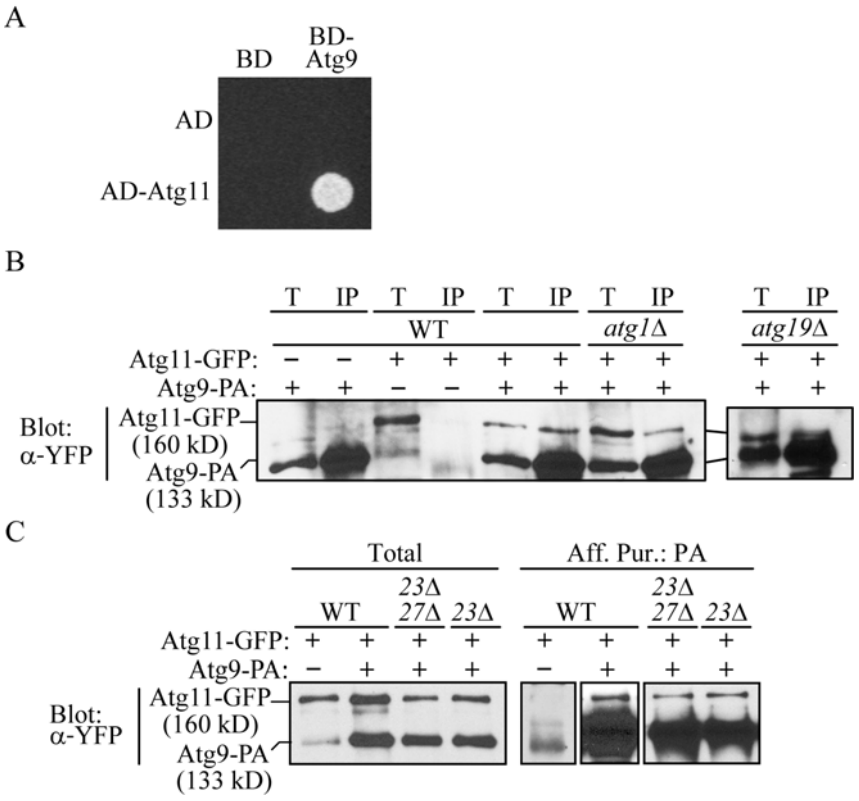

Figure 2.1. Atg9 interacts with Atg11. (A) A yeast two-hybrid assay reveals that full-length Atg9 interacts with full-length Atg11. The two-hybrid strain PJ69-4A was co-transformed with plasmids containing the activation domain (AD)-fused Atg11 and the binding domain (BD)-fused Atg9, or with empty vectors (AD and BD). Interactions were monitored by the ability of cells to grow on plates without histidine for 3 d. (B) Atg11 is co-precipitated with Atg9 independent of Atg1 and Atg19. Wild-type (TYY161), *atg1*Δ (TYY162), and *atg19*Δ (CCH005) strains expressing integrated Atg11-GFP and Atg9-protein A (PA) fusions were used for affinity isolation. Wild-type strains expressing integrated Atg9-PA alone (FRY171), or integrated Atg11-GFP (PSY101) and *CUP1* promoter-driven protein A (pCuPA(414)), were used as controls. Eluted polypeptides were separated by SDS-PAGE and detected with anti-YFP antibody. The same amounts of the total lysate (Total) and immuno-affinity purified isolate (IP) were loaded per gel lane. (C) Atg11 is co-precipitated with Atg9 in the absence of Atg23 and Atg27. Wild-type (TYY161), *atg23*Δ (CCH004), and *atg23*Δ *atg27*Δ (CCH006) strains expressing integrated Atg11-GFP and Atg9-PA fusions were used for affinity isolation. Total lysates (Total) and eluted polypeptides (Aff. Pur.) were separated by SDS-PAGE and visualized by immunoblotting with antibody to YFP. An Atg11-GFP strain (PSY101) expressing *CUP1*-driven protein A (pCuPA(414)) alone was used as control.

Table 2.1. Yeast strains used in this study.

Strain	Genotype	Reference
BY4742	*MATα ura3*Δ *leu2*Δ *his3*Δ *lys2*Δ	Invitrogen
CCH001	SEY6210 *atg9*Δ*::HIS5 atg1*Δ*::LEU2*	This study
CCH002	YTS158 *atg9*Δ*::HIS5*	This study
CCH004	TYY161 *atg23*Δ*::URA3*	This study
CCH005	TYY161 *atg19*Δ*::URA3*	This study
CCH006	TYY161 *atg23*Δ*::URA3 atg27*Δ*::LEU2*	This study
CCH007	PSY101 *atg9*Δ*::LEU2*	This study
DDY1493	*MATα ura3-52 leu2-3,112 his3-*Δ*200 tub2-201 act1-159::HIS3*	(31)
FRY136	SEY6210 *ATG9-YFP::HIS3*	(26)
FRY138	SEY6210 *ATG9-YFP::HIS3 atg1*Δ*::URA3*	(169)
FRY171	SEY6210 *ATG9-PA::TRP1*	This study
FRY172	SEY6210 *ATG9-PA::TRP1 pep4*Δ*::LEU2*	(169)
FRY245	SEY6210 *ATG9-RFP::HIS3*	(168)
IRA004	DDY1493 *ATG9-RFP::KAN*	(168)
JKY007	SEY6210 *atg9*Δ*::HIS3*	(144)
JLY87	PJ69-4A *atg23*Δ*::KAN*	(105)
JLY88	PJ69-4A *atg27*Δ*::KAN*	(105)
KTY53	SEY6210 *ATG9-YFP::HIS3 atg11*Δ*::URA3*	(169)
PJ69-4A	*MATα leu2-3,112 trp1-*Δ*901 ura3-52 his3-*Δ*200 gal4*Δ *gal80*Δ *LYS2::GAL1-HIS3 GAL2-ADE2*	

	met2::GAL7-lacZ	(70)
PSY101	SEY6210 *ATG11-GFP::HIS3*	This study
SEY6210	*MATα ura3-52 leu2-3,112 his3-Δ200 trp1-Δ901*	
	lys2-801 suc2-Δ9 mel GAL	(173)
TVY1	SEY6210 *pep4Δ::LEU2*	(45)
TYY127	YTS158 *atg1Δ::HIS5*	This study
TYY161	SEY6210 *ATG11-GFP::HIS3 ATG9-PA::TRP1*	This study
TYY162	TYY161 *atg1Δ::URA3*	This study
YTS150	SEY6210 *ATG9-YFP::HIS5 atg1Δ::URA3*	
	atg11Δ::LEU2	(193)
YTS158	BY4742 *pho8::pho8Δ60 pho13Δ::KAN*	This study

Atg11 is predicted to contain four coiled-coil (CC) domains (234) (Fig. 2.2A). Each CC domain mediates interactions of Atg11 with different Atg proteins. To test whether these CC domains are responsible for the interaction between Atg11 and Atg9, we used CC domain deletion mutants in a series of yeast two-hybrid assays. As shown in Fig. 2.2B, the two-hybrid mutant AD-Atg11 C-terminal truncation (11N; Δ627-1178, lacking CC3-4) allowed the cells to grow in the presence of BD-Atg9, as well as the full-length AD-Atg11. In contrast, cells expressing an AD-Atg11 N-terminal truncation (11C; Δ1-817, lacking CC1-3) could not grow on selective -his plates (Fig. 2.2B). Thus, the Atg11 N terminus is sufficient for the Atg9-Atg11 interaction. In addition, Atg11ΔCC2 (Δ536-576) abolished the interaction with Atg9, whereas cells containing mutants Atg11ΔCC1 (Δ272-321), Atg11ΔCC3 (Δ627-858), or Atg11ΔCC4 (Δ859-1178) grew well on selective plates (Fig. 2.2C). These data indicated that Atg11 coiled-coil domain 2 is required for the Atg9-Atg11 interaction.

From a hydropathy plot analysis, Atg9 contains hydrophilic NH_2- and COOH-termini flanking 6-8 transmembrane domains (144). To define the topology of Atg9, we investigated the protease sensitivity of the Atg9 N and C termini. Spheroplasts derived from *pep4*Δ cells expressing either the N-terminal tagged PA-Atg9 fusion or the C-terminal tagged Atg9-PA fusion were osmotically lysed and centrifuged at 13,000 x *g*. In agreement with previous studies, approximately two-thirds of the total Atg9 was present in the S13 supernatant fraction that contained the PAS, and one-third was present in the P13 pellet fraction (Fig. 2.2D) (168). When the P13 fraction was treated with exogenous proteinase K, both the N- and C-terminal PA tags were cleaved in the absence or presence of detergent, and no bands of smaller molecular mass were detected (Fig. 2.2D),

indicating that both the N and C termini of Atg9 were accessible to protease on the cytosolic side of the membrane. To verify that intracellular membranous structures were intact after osmotic lysis, we simultaneously monitored the protease sensitivity of an endogenous vacuole membrane protein, Pho8. The precursor form of Pho8 that accumulated in the *pep4*Δ background contains a small cytosolic tail and a lumenally oriented propeptide (Fig. 2.2D). In the absence of detergent, only the Pho8 cytosolic tail, but not the lumenal propeptide, was accessible to proteinase K. Upon addition of both detergent and proteinase K, the Pho8 lumenal propeptide was removed due to disruption of all membranous compartments, shown as a further shift of the molecular mass (Fig. 2.2D). Thus, these data verified the integrity of the relatively fragile vacuole and presumably other intracellular membranous compartments following osmotic lysis, suggesting that both the N and C termini of Atg9 are exposed to the cytosol (Fig. 2.2D). Accordingly, the topology of Atg9 appears to be conserved between yeast and mammalian cells (239).

So far no known functional domains have been identified in the Atg9 N- or C-terminal regions. To further analyze the Atg9-Atg11 interaction, we generated truncated Atg9 mutants containing the N terminus, C terminus, or transmembrane region, respectively. As shown in Fig. 2.2E, in the presence of Atg11, the Atg9 N-terminal domain supported growth of two-hybrid cells as well as the full-length Atg9, whereas neither the C-terminal nor the transmembrane domains of Atg9 were able to do so (Fig. 2.2E). This result showed that Atg11 interacts with the N-terminal region of Atg9. We further constructed a series of Atg9 N-terminal truncation mutants and analyzed them for interaction with Atg11 by yeast two-hybrid. Atg9 N-terminal amino acids 159-255

appeared to be the minimal region that mediates the interaction with Atg11 (Fig. 2.2F). Taken together, we concluded that Atg11 and Atg9 interact through the Atg11 coiled-coil domain 2 and the Atg9 N terminus.

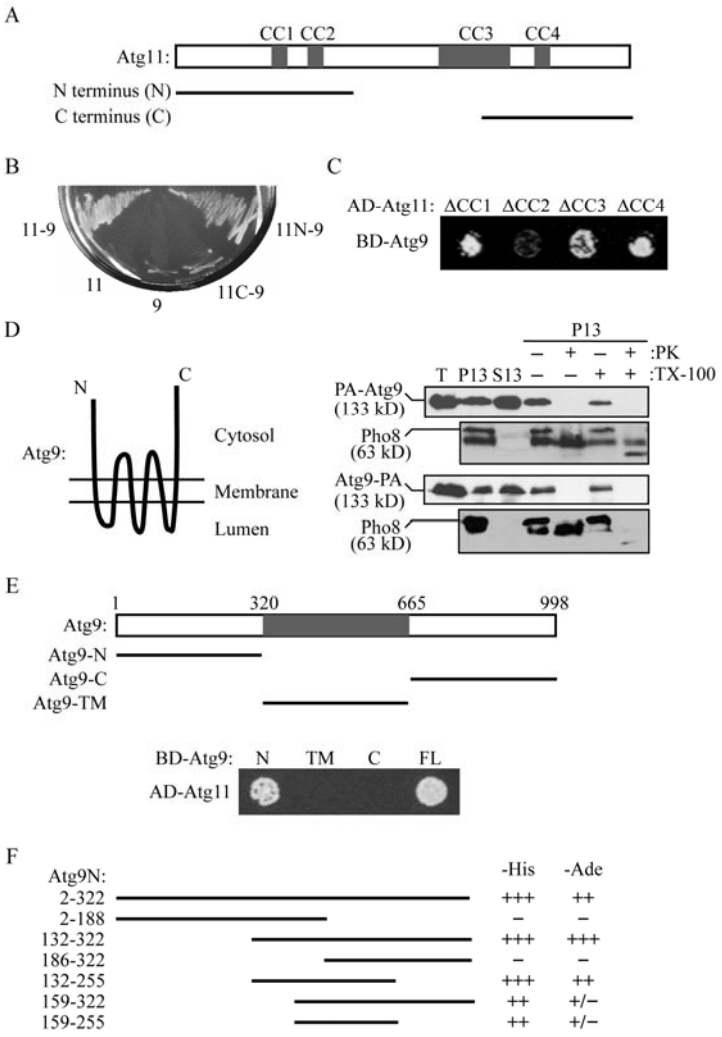

Figure 2.2. The Atg9-Atg11 interaction is mediated by the Atg11 CC2 domain and the Atg9 N-terminal region. (A) Schematic representation of Atg11 highlighting the position of the four coiled-coil domains and indicating the extent of the N- and C-terminal domains used in the two-hybrid analysis. (B) The Atg11 N terminus is sufficient to interact with Atg9 as demonstrated by the yeast two-hybrid assay. Cells expressing an Atg11 N-terminal fragment and Atg9 (11N-9), full-length Atg11 and Atg9 (11-9), the Atg11 C terminus and Atg9 (11C-9), or Atg11 (11) or Atg9 (9) with the corresponding empty vector were grown for 3 days on plates lacking histidine. (C) Atg11 coiled-coil domain 2 is essential for Atg11-Atg9 interaction. Cells expressing Atg9 and Atg11 lacking the indicated coiled-coil (CC) domains were grown for 3 days on -histidine plates. (D) Both the N- and C-termini of Atg9 are protease-sensitive. A schematic representation of Atg9 topology is shown on the left. *pep4*Δ cells expressing either integrated C-terminally-tagged Atg9-protein A (FRY172), or *CUP1*-driven N-terminally-tagged protein A-Atg9 (TVY1; pCuPAAtg9(416)) were converted to spheroplasts, osmotically lysed and the pellet fraction subjected to proteinase K (PK) treatment in the presence or absence of Triton X-100 (TX-100). Fractions were analyzed by immunoblot with antibodies to PA and Pho8. (E) The Atg9 N terminus interacts with Atg11. A schematic diagram of Atg9 and domains used for two-hybrid analysis are depicted. Cells expressing Atg11 and the Atg9 N-terminal fragment (N), transmembrane domain (TM), C terminus (C), or full-length Atg9 (FL) were grown for 3 days on -histidine plates. (F) Atg9 N-terminal amino acids 159-255 are the minimal sufficient region needed to interact with Atg11. A truncation series of the Atg9 N-terminal region in the binding domain (BD) two-hybrid plasmid is depicted. The strength of the corresponding proteins to interact with AD-Atg11 is indicated on the right, by robustness of cell growth on plates without histidine (-His) or adenine (-Ade) for 5 d.

Atg11 recruits Atg9 to the PAS

In wild-type cells, Atg11 localizes at the PAS (87) and Atg9 cycles between the PAS and mitochondria (168, 169). To examine the role of the interaction between Atg9 and Atg11, we analyzed the cycling of Atg9 in the presence of overexpressed Atg11, or in the absence of this protein. The chromosomally-tagged Atg9-YFP chimera displayed a multiple-punctate distribution in wild-type cells, with one of the puncta colocalizing with the PAS marker BFP-Ape1 (Fig. 2.3A). In contrast, in the *atg1*Δ background, Atg9 was restricted to the PAS, in agreement with previous observations that indicated a role for Atg1 in retrograde transport of Atg9 from the PAS to mitochondria. In 91% (109/120) of the cells overexpressing Atg11, Atg9-YFP localized solely to the perivacuolar PAS (represented by CFP-Atg11), similar to the situation observed in *atg1*Δ cells (Fig. 2.3A) (86), and did not localize to mitochondria (data not shown). Thus, excess Atg11 was able to restrict Atg9 to the PAS. Overexpressed Atg11 displays a dominant negative phenotype, interfering with vacuolar import of prApe1 through the Cvt pathway (unpublished results). The dominant negative phenotype presumably reflects the defect in Atg9 cycling.

To further examine the role of Atg11 in recruiting Atg9 to the PAS, we used the TAKA (Transport of Atg9 after Knocking out *ATG1*) assay (26). This assay examines the epistasis of a second mutation relative to *atg1*Δ with regard to Atg9 localization at the PAS. We visualized chromosomally tagged Atg9-YFP in *atg11*Δ single and *atg1*Δ *atg11*Δ double deletion cells, and simultaneously labeled the vacuolar membrane with FM 4-64. As shown previously, in *atg1*Δ cells, Atg9-YFP localized to a single perivacuolar punctum, which corresponds to the PAS (Fig. 2.3B). In contrast, in nearly

90% of the *atg11*Δ or *atg1*Δ *atg11*Δ mutants, Atg9-YFP fluorescence showed multiple puncta and did not localize at a single perivacuolar structure, suggesting its anterograde transport was blocked due to the *ATG11* deletion (Fig. 2.3B). These results suggest that Atg11 is involved in the anterograde transport of Atg9.

Our mapping of the Atg9 and Atg11 interaction domains indicated that Atg11ΔCC2 but not Atg11 lacking its other coiled-coil domains was defective in forming a complex with Atg9 (Fig. 2.2). Accordingly, we examined the effect of Atg11 coiled-coil deletions on Atg9 subcellular distribution. As shown in Fig. 2.3C, in cells expressing Atg11ΔCC1 in the *atg1*Δ background, Atg9 localized to the PAS, similar to the result seen in *atg1*Δ cells expressing wild-type Atg11. In contrast, in cells expressing Atg11ΔCC2, which lacks the Atg9-interacting domain, Atg9 displayed a multiple punctate distribution (Fig. 2.3C), resembling that observed in *atg1*Δ *atg11*Δ cells even though the mutant protein was expressed at a level similar to the wild-type protein (234). Thus, we concluded that interaction of Atg9 with Atg11 coiled-coil domain 2 is required to direct Atg9 to the PAS.

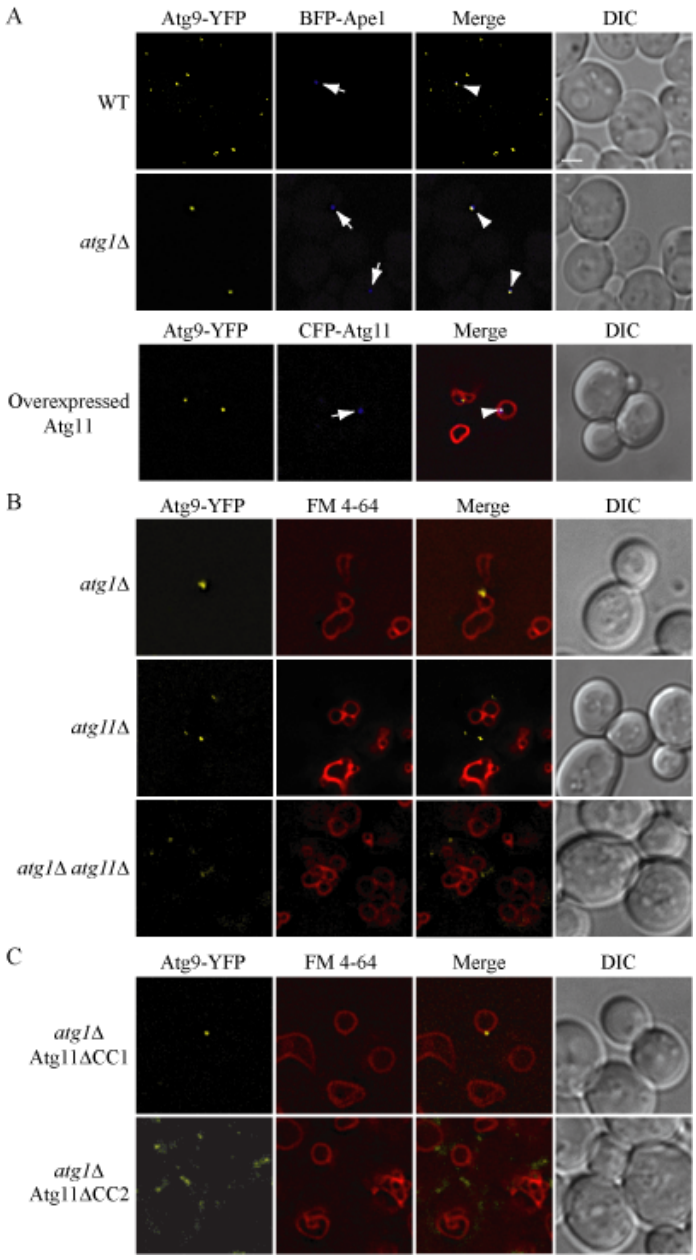

Figure 2.3. Atg9 cycles through the PAS in an Atg11-dependent manner. (A) Atg11 overexpression restricts Atg9 to the PAS. Wild-type or *atg1*Δ strains expressing an integrated Atg9-YFP fusion (FRY136 and FRY138, respectively) were transformed with a plasmid containing BFP-Ape1 (pBFPApe1(414)) as the PAS marker. In addition, an *atg11*Δ strain (KTY53) expressing an integrated Atg9-YFP fusion was transformed with a centromeric plasmid containing *CUP1* promoter-driven CFP-Atg11 (pCuHACFPCVT9(414)). Cells were grown to mid-log phase and visualized by fluorescence microscopy. Arrows mark the PAS localization of BFP-Ape1 and arrowheads mark the sites of co-localization. (B) Atg9 fails to transport to the PAS in mutants deleted for Atg11. *atg1*Δ (FRY138), *atg11*Δ (KTY53), or *atg1*Δ *atg11*Δ (YTS150) strains expressing chromosomally-tagged Atg9-YFP were imaged by fluorescence microscopy. (C) The second Atg11 coiled-coil domain is needed for correct Atg9 cycling. The *atg1*Δ *atg11*Δ strain (YTS150) was transformed with a plasmid encoding the Atg11ΔCC1 or Atg11ΔCC2 mutants and the YFP fluorescence visualized by fluorescence microscopy. In all panels, cells were stained with FM 4-64 to label the vacuole before being imaged by fluorescence microscopy. DIC, differential interference contrast. Scale bar, 2 μm.

The Atg9^{H192L} mutant is defective for the Cvt pathway

To further clarify the physiological functions of the Atg9-Atg11 interaction, we decided to test whether autophagic processes were affected by its disruption. It has been reported that Atg11 coiled-coil domain 2, the Atg9-interacting domain, interacts with multiple Atg proteins, including at least one, Atg1, that is involved in Atg9 retrograde transport (234). Thus, Atg11ΔCC2 may cause pleiotropic effects when used in functional studies. To bypass this problem, we decided to use native Atg11 and instead to isolate mutations within the Atg9 N-terminal region that disrupt the interaction with Atg11. We performed a PCR-based random mutagenesis on the N-terminal region of Atg9, followed by a yeast two-hybrid screen for loss-of-interaction mutants. A missense mutation was identified, with a single histidine-to-leucine substitution at position 192 (H192L), which is located in the minimal region (amino acids 159-255) needed for the Atg9-Atg11 interaction (Fig. 2.2E). Two-hybrid cells harboring this mutation completely lost the capacity for growth on selective -ade plates in the presence of Atg11 (Fig. 2.4A), whereas the expression level of the mutant protein was comparable to that of the wild-type (data not shown), indicating that the interaction between Atg9 and Atg11 was abolished by the H192L mutation. The loss of Atg9-Atg11 interaction was confirmed by a co-immunoprecipitation assay. As shown in Fig. 2.4B, endogenous Atg11 was recovered only with wild-type Atg9, but not with the Atg9^{H192L} mutant. In contrast, yeast two-hybrid data indicated that the interaction between Atg9 and either Atg2 or Atg18, two proteins involved in retrograde transport of Atg9, was unaffected (data not shown).

Because both *ATG9* and *ATG11* are essential genes for the Cvt pathway, a type of selective autophagy, we monitored the processing of prApe1 as a marker protein for this

transport route. As shown in Fig. 2.4C, cells expressing Atg9^{H192L} did not generate the mature form of Ape1, compared with cells expressing wild-type Atg9, indicating that the Cvt pathway was impaired by the Atg9 H192L mutation.

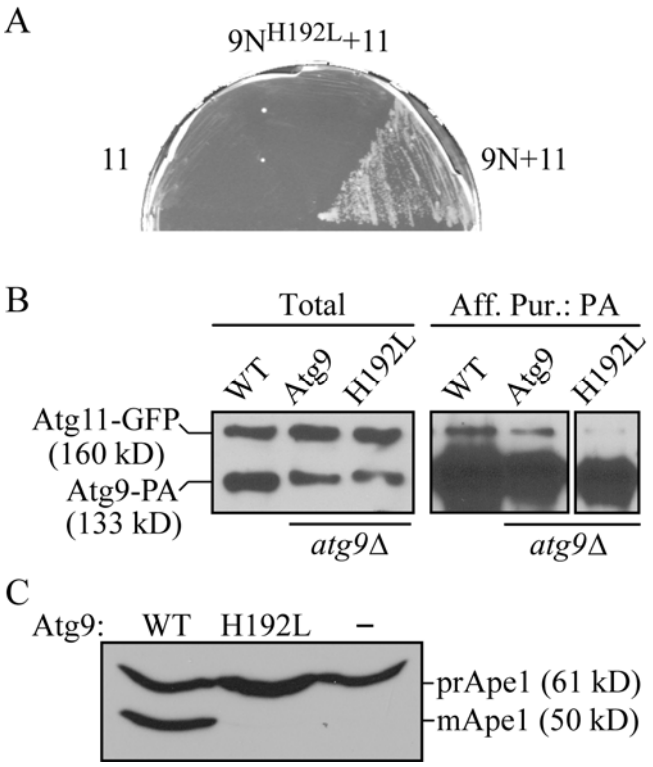

Figure 2.4. The Atg9^{H192L} mutant is defective for the Cvt pathway. (A) The Atg9 H192L mutation disrupts the interaction between Atg9 and Atg11 by yeast two-hybrid assay. Cells expressing Atg11 (AD-Atg11) and either the empty plasmid (11), the Atg9 N terminus harboring the H192L mutation (BD-Atg9N^{H192L}; 9N^{H192L}+11), or the wild-type Atg9 N-terminal fragment (9N+11) were grown for 5 days on -adenine plates. (B) Atg11 is co-precipitated with wild-type Atg9 but not with Atg9^{H192L}. An *atg9*Δ strain expressing an integrated Atg11-GFP fusion (CCH007) was transformed with a plasmid expressing either wild-type Atg9-PA (pAtg9PA(314); Atg9) or Atg9^{H192L}-PA (pAtg9^{H192L}PA(314); H192L) driven by the Atg9 native promoter. The affinity isolation was performed as described in Materials and methods. Eluted polypeptides were separated by SDS-PAGE and detected with anti-YFP antibody. A wild-type strain expressing integrated Atg11-GFP and Atg9-PA fusions (TYY161) was used as a control (WT). (C) Precursor Ape1 maturation is blocked in cells expressing Atg9^{H192L}. The *atg9*Δ strain (JKY007) was transformed with a plasmid expressing wild-type Atg9 (pAPG9GFP416; WT), Atg9^{H192L} (pAtg9^{H192L}GFP416; H192L), or an empty vector (pRS416; -). Cells were grown to mid-log phase, and protein extracts analyzed by western blot using antiserum to Ape1. The positions of precursor and mature Ape1 are indicated.

Anterograde movement of Atg9^{H192L} is blocked in growing conditions

We were interested in determining whether the impairment of the Cvt pathway seen with Atg9^{H192L} (Fig. 2.4B) was caused by defects in Atg9 cycling, in particular anterograde movement to the PAS. Accordingly, we used the TAKA assay to visualize the cycling of Atg9^{H192L}-GFP in growing conditions, and concurrently stained mitochondria with the dye MitoFluor Red. In the *atg1*Δ background, wild-type Atg9-GFP was restricted to the PAS as marked with BFP-Ape1 in 94% (116/123) of the cells examined (Fig. 2.5). In contrast, Atg9^{H192L}-GFP distributed to multiple punctate structures in 84% (131/156) of the *atg1*Δ cells, which colocalized in part with the mitochondrial labeling but not with the PAS. Thus, the Atg9^{H192L} mutation acted epistatically to *atg1*Δ, suggesting that the anterograde movement of Atg9^{H192L} from mitochondria to the PAS was defective.

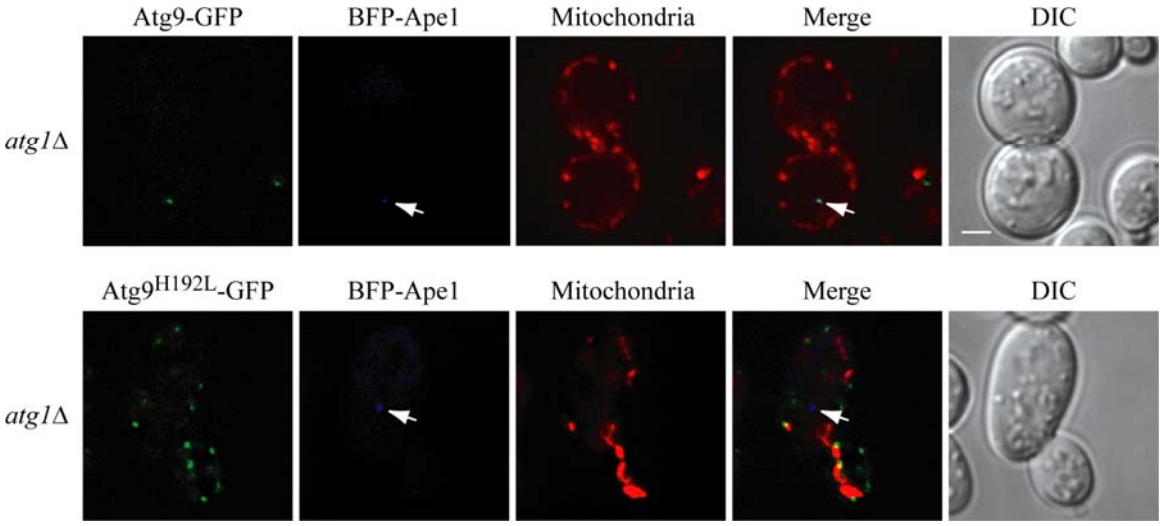

Figure 2.5. Anterograde transport of Atg9 to the PAS is impaired in the Atg9^{H192L} mutant under growing conditions. The *atg1*Δ *atg9*Δ strain (CCH001) was co-transformed with a BFP-Ape1 plasmid (pBFPApe1(414)) and a plasmid expressing wild-type Atg9-GFP (pAPG9GFP(416)), or Atg9^{H192L}-GFP (pAtg9^{H192L}GFP(416)). Cells were cultured to mid-log phase and stained with MitoFluor Red 589 as described in Materials and methods prior to imaging by fluorescence microscopy. DIC, differential interference contrast. Scale bar, 2 μm.

Bulk autophagy is not affected by disruption of the Atg9-Atg11 interaction

Atg9 is essential for both bulk autophagy and the Cvt pathway, whereas Atg11 is required solely in the Cvt pathway (87, 144). To clarify whether Atg9 anterograde transport via Atg11 is involved in bulk autophagy, we utilized the Atg9^{H192L} mutant to analyze the progression of bulk autophagy by several established assays.

Atg8 conjugated to phosphatidylethanolamine (PE) remains associated with the completed autophagosome and is a marker for autophagic delivery to the vacuole (60, 91, 92). Following delivery, of the GFP-tagged Atg8 chimera, the GFP moiety is cleaved and remains relatively stable in the vacuole, whereas Atg8 is rapidly degraded. Thus, the accumulation of free GFP reflects the progression of bulk autophagy, which can be readily detected by western blot (26, 193). In *atg9*Δ cells, essentially no free GFP was detected, indicating that bulk autophagy was blocked by *ATG9* deletion (Fig. 2.6A). In cells expressing wild-type Atg9 or Atg9^{H192L}, free GFP was detectable starting at 2 h after cells were shifted to starvation conditions (SD-N) to induce bulk autophagy, although the GFP-Atg8 processing showed a delay in Atg9^{H192L} cells compared to wild-type cells. This result demonstrated that bulk autophagy retained similar activity even when Atg9 failed to interact with the Cvt-specific component Atg11.

To confirm the above result, we quantitatively measured the bulk autophagy activity using another marker protein, Pho8Δ60, which encodes an altered form of alkaline phosphatase that is only delivered to the vacuole via autophagy (145). The Pho8Δ60 enzymatic activity was measured in wild-type and *atg1*Δ cells, and in *atg9*Δ cells transformed with a plasmid expressing wild-type Atg9 or Atg9^{H192L}, or an empty vector, in growing (SMD) and starvation (SD-N) conditions (Fig. 2.6B). The *atg1*Δ cells,

or the *atg9*Δ cells transformed with an empty vector, showed only the basal level of Pho8Δ60 activity after autophagy induction (SD-N), indicating bulk autophagy was defective after deleting either gene. In contrast, there was an increase of Pho8Δ60 activity in *atg9*Δ cells expressing either wild-type Atg9 or $Atg9^{H192L}$, indicating that $Atg9^{H192L}$ rescued the autophagy defect in *atg9*Δ cells, comparable to the wild-type Atg9 protein. Taken together, these data suggested that bulk autophagy does not depend on the interaction between Atg9 and an Atg protein that is needed for anterograde movement during specific autophagy, Atg11.

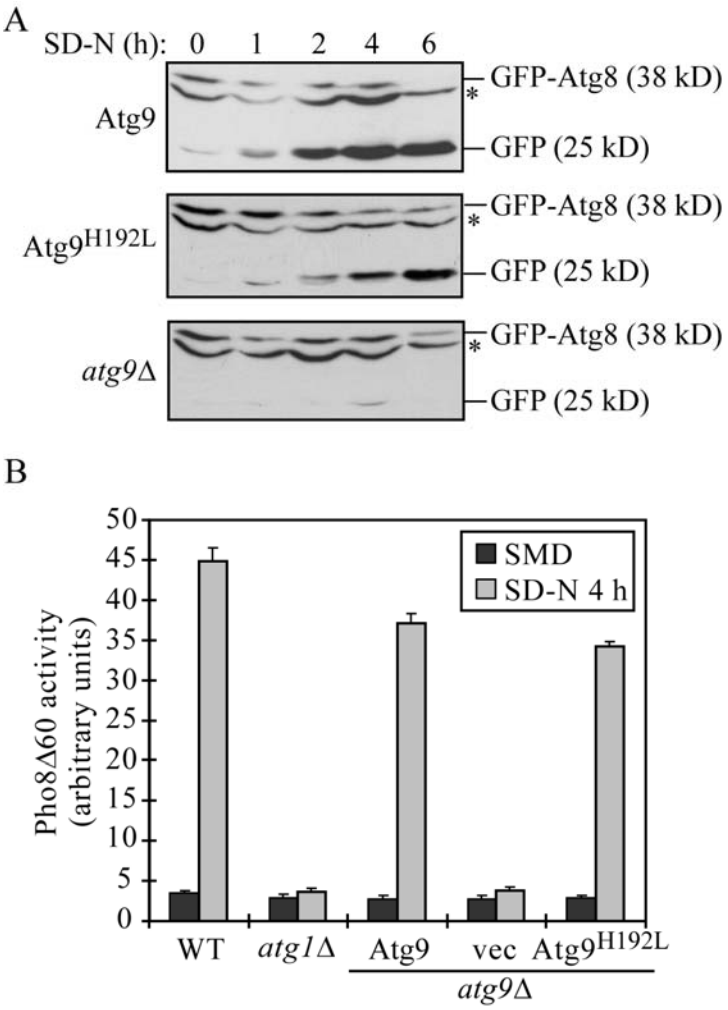

Figure 2.6. Bulk autophagy is normal with the Atg9^{H192L} mutant. (A) GFP-Atg8 processing is not affected by Atg9^{H192L}. The *atg9*Δ strain (JKY007) was co-transformed with a GFP-Atg8 plasmid (pGFPAUT7(414)) and a plasmid expressing wild-type Atg9 (pAPG9GFP(416); Atg9), Atg9^{H192L} (pAtg9^{H192L}GFP416; Atg9^{H192L}), or an empty vector (pRS416; *atg9*Δ). Cells were grown in SMD to mid-log phase and shifted to starvation conditions (SD-N). At the indicated time points, aliquots were taken and protein extracts analyzed by western blot using anti-GFP antibody. The positions of GFP-Atg8 and free GFP are indicated. The asterisk marks a nonspecific band. (B) Pho8Δ60 activity is normal in Atg9^{H192L}-expressing cells. The wild-type (YTS158) and *atg1*Δ (TYY127) strains, and the *atg9*Δ strain (CCH002) transformed with a plasmid expressing wild-type Atg9 (pAPG9(416)), Atg9^{H192L} (pAtg9^{H192L}416), or an empty vector (pRS416) were grown in SMD to mid-log phase and shifted to SD-N for 4 h. The Pho8Δ60 activity was measured as described in Materials and methods. Error bars indicate the S.E.M. of three independent experiments.

Atg9^{H192L} cycling is normal during bulk autophagy

Because bulk autophagy activity was not affected by the Atg9 H192L mutation, it was tempting to speculate that Atg9^{H192L} cycled normally under starvation conditions even though it was not capable of forming a complex with Atg11. To test this hypothesis, we visualized the movement of Atg9^{H192L} by the TAKA assay after autophagy induction. Cells were treated with the drug rapamycin, which mimics starvation conditions and induces bulk autophagy. As shown in Fig. 2.7, in the *atg1*Δ background without rapamycin treatment (-rap), wild-type Atg9-GFP was restricted to the PAS, whereas Atg9^{H192L}-GFP could not move to the PAS and displayed a multiple-punctate localization. After treatment with rapamycin (+rap), in 85% (41/48) of the cells Atg9^{H192L}-GFP colocalized with the PAS marker BFP-Ape1 similar to wild-type Atg9, indicating that Atg9 recruitment to the PAS was normal. Therefore, this result demonstrated that during bulk autophagy, the Atg9^{H192L} mutation did not interfere with the cycling of Atg9.

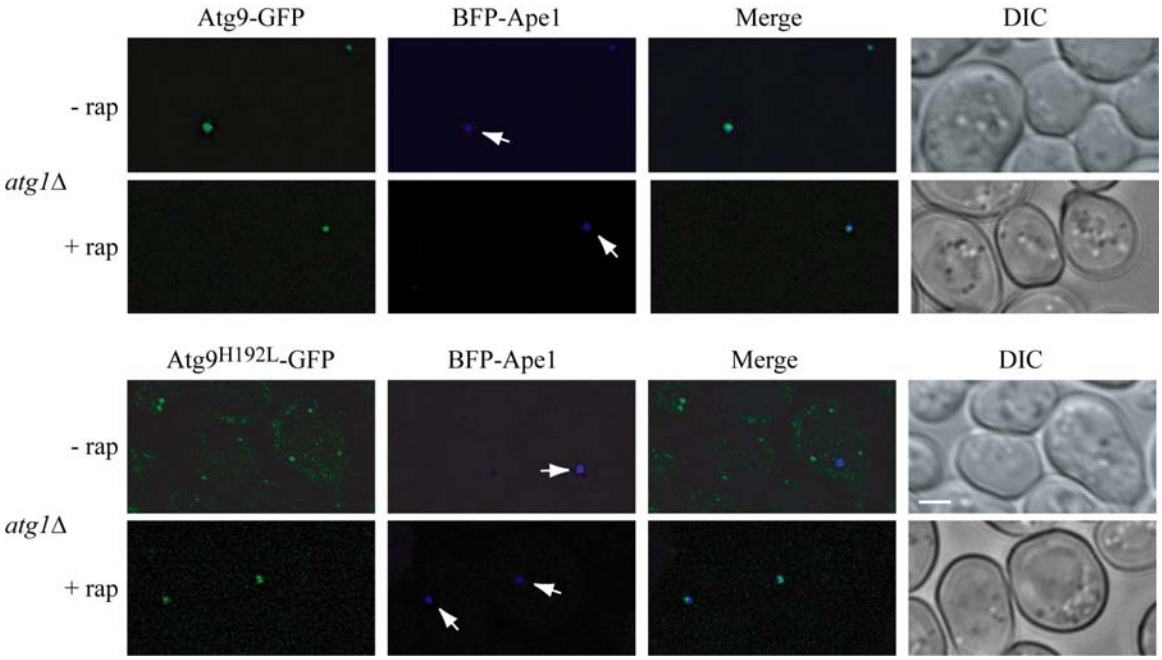

Figure 2.7. Anterograde transport of Atg9^{H192L} is normal upon bulk autophagy induction. The *atg1*Δ *atg9*Δ strain (CCH001) was co-transformed with a BFP-Ape1 plasmid (pBFPApe1(414)) and a plasmid expressing wild-type Atg9-GFP (pAPG9GFP(416)) or Atg9^{H192L}-GFP (pAtg9^{H192L}GFP(416)). Bulk autophagy was induced by rapamycin treatment (+rap) as described in Materials and methods prior to imaging by fluorescence microscopy. Arrows mark the PAS localization of BFP-Ape1. DIC, differential interference contrast. Scale bar, 2 μm.

Atg11 localization to the PAS is dependent on the actin cytoskeleton

Recently, we have shown that Atg9 anterograde traffic to the PAS is blocked when the actin cytoskeleton is disrupted by either treatment with the drug latrunculin A or point mutations in *ACT1*, the gene encoding actin (167). In particular, the impairment of actin function leads to a defect in the Cvt pathway, whereas bulk autophagy is normal; a similar phenotype was also observed with the Atg9^{H192L} mutant. Because Atg9 anterograde transport was also dependent on its interaction with Atg11 (Fig. 2.3), we wondered whether there was a functional connection between actin and Atg11 in Atg9 cycling and autophagic processes. Previous data show that Atg11 is needed to recruit prApe1 to the PAS (234). The *atg9* null mutant does not affect the recruitment of prApe1

to the PAS or localization of Atg11 (T. Yorimitsu and D.J. Klionsky, unpublished data), suggesting that Atg11 localization at the PAS is not dependent on the Atg9-Atg11 interaction. Thus, we propose that Atg11 mediates the actin-dependent Atg9 cycling in the Cvt pathway. To test this hypothesis, we utilized an actin mutant, *act1-159*, which has defects in actin cable depolymerization, Atg9 cycling and the Cvt pathway (167). As shown in Fig. 2.8A, in wild-type cells, GFP-Atg11 localized to the PAS as a single punctum; chromosomally-tagged Atg9-RFP displayed a multiple-punctate localization pattern. In the *act1-159* mutant, however, GFP-Atg11 redistributed to cytoplasmic patches, which partially colocalized with Atg9-RFP. To reveal the identity of these multiple compartments, we stained cells with the mitochondrial dye MitoFluor Red and the vacuolar membrane dye FM 4-64. As shown in Fig. 2.8B, in 81% (81/100) of the cells, the GFP-Atg11 patches were absent from the perivacuolar PAS position; instead, they colocalized with the mitochondrial labeling, indicating that Atg11 localized at mitochondria when the actin network was defective. Therefore, the proper localization of Atg11 to the PAS is dependent on the actin cytoskeleton and may underlie the actin-dependent Atg9 cycling during the Cvt pathway and other types of specific autophagy.

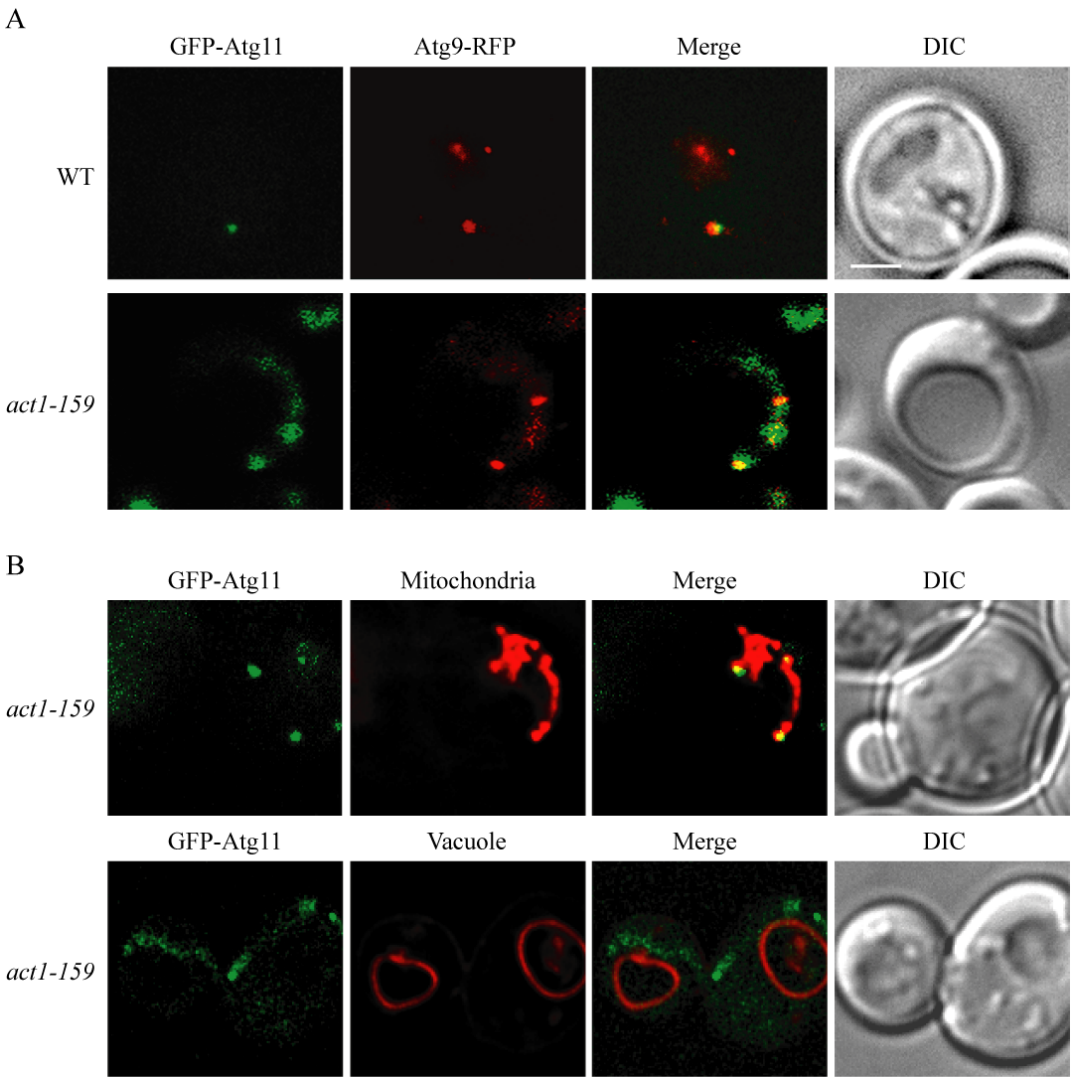

Figure 2.8. Atg11 localization at the PAS is dependent on the actin cytoskeleton. (A) Atg11 alters its distribution in the *act1-159* mutant and colocalizes with Atg9. Wild-type (FRY245) and *act1-159* (IRA004) strains expressing an integrated Atg9-RFP fusion were transformed with a plasmid containing GFP-Atg11 (pTS495). Cells were grown to mid-log phase at 30°C and imaged by fluorescence microscopy. (B) Atg11 is localized to mitochondria in the *act1-159* mutant. The *act1-159* (IRA004) strain was transformed with the GFP-Atg11 plasmid. Cells were treated with MitoFluor Red 589 or FM 4-64 as described in Materials and methods and imaged by fluorescence microscopy. DIC, differential interference contrast. Scale bar, 1 µm.

Discussion

Atg9 is the only characterized transmembrane protein that is involved in the formation of the sequestering vesicles that form during the Cvt pathway, pexophagy and autophagy. Accordingly, it is the best candidate to mark the source of the vesicle membrane. Recently, we have shown that Atg9 localizes to mitochondria in addition to the PAS, implicating this organelle in supplying membrane during autophagy-related processes (168). Only Atg19, which is a receptor for biosynthetic cargos, and Atg8 remain associated with the completed vesicles; most of the soluble Atg proteins involved in vesicle formation presumably dissociate from the membrane prior to or upon vesicle completion. In contrast, a specific retrieval mechanism operates in the cycling of Atg9 and the associated protein Atg23 (169). The retrograde movement of Atg9 from the PAS to mitochondria requires Atg1-Atg13, Atg2, Atg18 and the PtdIns 3-kinase complex. Transit of Atg9 to the PAS involves Atg23, Atg27 and actin (105, 167, 232); however, the mechanism by which actin mediates Atg9 movement is not known.

To identify other Atg components involved in anterograde movement of Atg9, we carried out a yeast two-hybrid screen for proteins that interact with Atg9 and identified Atg11 (Fig. 2.1). This result is intriguing because Atg11 has previously been shown to interact with Atg19 and Atg1, components involved in distinct steps of a specific autophagic process. In conjunction with the present result, we propose that Atg11 acts as a scaffold to coordinate the delivery of multiple components—including the cargo-receptor complex, components involved in vesicle formation, and proteins involved in supplying membrane—to the site of vesicle formation, the PAS (Fig. 2.9). The Atg11

second coiled-coil domain interacts with the N terminus of Atg9 (Fig. 2.2), and the interaction occurs in the absence of Atg1 or Atg19 (Fig. 2.1), suggesting that there are distinct and multiple populations of Atg11 within the cell. Atg11 self-interaction (234) may then allow these various populations of Atg proteins to be delivered to the PAS in a coordinated manner. Consistent with this model, overexpression of Atg11 restricted Atg9 to the PAS, presumably due to enhanced delivery (Fig. 2.3). In contrast, a mutation of H192L that disrupts interaction between Atg9 and the specific autophagy component Atg11 resulted in a defect in transporting Atg9 to the PAS (Fig. 2.5). Furthermore, the absence of Atg9 at the PAS due to this point mutation led to a block in the Cvt pathway (Fig. 2.4).

It is known that Atg11 is needed for specific types of autophagy, such as the Cvt pathway, but is not essential for nonspecific autophagy (87). We found that the Atg9 point mutant that disrupts the interaction with Atg11 imposed little effect on the bulk autophagy that is induced during starvation (Fig. 2.6). The essentially normal autophagy function was correlated with the normal localization/transport of the binding-defective Atg9 mutant in the presence of the autophagy inducer rapamycin (Fig. 2.7). This finding suggests that anterograde transport of Atg9 during bulk autophagy may be mediated by a different mechanism that is, at least relatively, independent of Atg11. Thus, other proteins that may interact with Atg9 deserve further investigation to reveal the Atg9 cycling machinery that operates during bulk autophagy; however, we cannot rule out the possibility that a low level of interaction between $Atg9^{H192L}$ and Atg11 allows anterograde transport of $Atg9^{H192L}$ following autophagy induction.

Finally, we found that actin is required for the localization of Atg11 to the PAS (Fig. 2.8). This observation, coupled with the role of Atg11 in Atg9 anterograde movement, but not vice versa, suggests that Atg11 mediates the connection between actin and Atg9 delivery from the mitochondria to the PAS (167-169). Actin is not needed for bulk autophagy in yeast (167), in agreement with our findings in the present paper that the $Atg9^{H192L}$ mutant is not defective for nonspecific autophagy. It is not known how Atg9 might move along actin cables. The third Atg11 coiled-coil domain displays some similarity with that of Myo2; however, Atg11 lacks the N-terminal motor domain that functions in Myo2 movement (131). Thus, it is not clear how Atg11 might actually mediate the anterograde movement of Atg9. Continued analysis of Atg9 cycling and its interactions with Atg11, and other Atg proteins, may provide insight into the underlying mechanisms of membrane delivery during Cvt vesicle and autophagosome formation.

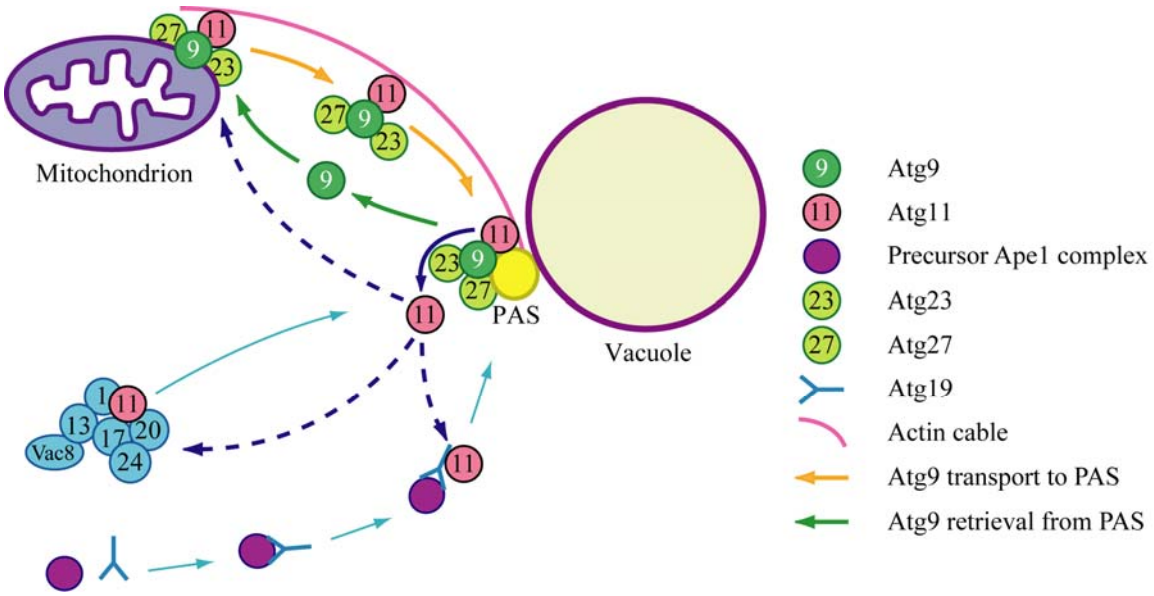

Figure 2.9. Model of Atg9 transport mediated by Atg11. The transmembrane protein Atg9 cycles between the PAS and mitochondria. The potential role of Atg9 cycling is to provide lipids for vesicle formation in bulk and selective autophagy. In the latter, a pool of the peripheral membrane protein Atg11, along with Atg23 and Atg27, regulates the anterograde movement of Atg9 from mitochondria to the PAS, dependent on actin function. The other two known Atg11 populations in yeast are indicated: the Atg1-Atg11 complex (consisting of Atg1, Atg11, Atg13, Atg17, Atg20, Atg24, and Vac8) and the Atg11-Atg19 complex (consisting of prApe1, the prApe1 receptor Atg19, and Atg11). The retrieval of Atg9 requires the Atg1-Atg13 complex, Atg2, Atg18, and the PtdIns3-kinase complex (not shown).

Materials and methods

Yeast strains and media

The *S. cerevisiae* strains used in this study are listed in Table 2.1. For gene disruption, the entire coding region was replaced by the *Saccharomyces cerevisiae TRP1*, the *Kluyveromyces lactis LEU2* or *URA3*, the *S. kluyveri HIS3*, or the *Escherichia coli* kan^r gene using PCR primers containing ~50 bases of identity to the regions flanking the open reading frame. For PCR-based integrations of the PA and GFP tags at the 3' end of the *ATG9* and *ATG11* genes, pHAB102 and pFA6a-GFP-HIS3 were used as templates to generate strains expressing fusion proteins under the control of their native promoters (2, 113).

Yeast cells were grown in rich medium (YPD; 1% yeast extract, 2% peptone, 2% glucose) or synthetic minimal medium (SMD; 0.67% yeast nitrogen base, 2% glucose, amino acids, and vitamins as needed). Starvation experiments were conducted in synthetic medium lacking nitrogen (SD-N; 0.17% yeast nitrogen base without amino acids, 2% glucose).

Plasmids

Plasmids expressing Atg11 truncations (234), GFP-Atg8 (pGFP-AUT7(414) (2)), Atg9 (pAPG9(416); essentially constructed the same as pAPG9(414) (144)), Atg9-GFP (pAPG9GFP(416) (144)), and CFP-Atg11 (pCuHACFPCVT9(414) (86)) have been described previously. BFP-Ape1 (pBFPApe1(414)) was constructed by introducing BFP (QBiogene) on a BamHI PCR-generated fragment into a unique BglII site situated after

the start codon of *APE1* (191). GFP-Atg11 (pTS495) was constructed in a similar manner starting with *ATG11* cloned into the pRS416 vector. PA-Atg9 (pCuPAAtg9(416)) was generated by cloning *ATG9* into the pRS416-CuProtA vector (86). Full length Atg9 (pBD-Atg9), and the Atg9 N-terminal (pBD-Atg9N), C-terminal (pBD-Atg9C), and transmembrane (pBD-Atg9TM) regions were amplified by PCR from pAPG9(416) and introduced into the two-hybrid vector pGBDU-C1 using BamHI and SalI sites. A total of 19 other *ATG* genes were amplified and cloned into the two-hybrid vector pGAD-C1 using BamHI and SalI sites. The serial deletion mutants of the Atg9 N terminus were generated by PCR amplification from pBD-Atg9N and ligated into the EcoRI and BamHI sites of pGBDU-C1. The plasmid expressing the $Atg9^{H192L}$ mutant ($pAtg9^{H192L}$(416)) was constructed by releasing the *ATG9* fragment containing H192L from $pAtg9^{H192L}$GFP(416) (see below) and cloned into pAPG9(416) using SacI and AgeI. pAtg9PA(314) and $pAtg9^{H192L}$PA(314) were constructed by PCR-amplifying *ATG9* and $ATG9^{H192L}$ together with its native promoter from pAPG9GFP(416) and $pAtg9^{H192L}$GFP(416), and incorporating them into pNopPA(314) using XhoI and XmaI sites. pNopPA(314) is a gift from Dr. Fulvio Reggiori (University of Utrecht).

Protein A affinity isolation

Cells were grown to OD_{600} = 0.8 in SMD, and 100 ml were harvested and resuspended in lysis buffer (PBS, 200 mM sorbitol, 1 mM $MgCl_2$, 0.1% Tween 20, 1 mM PMSF and protease inhibitor cocktail). The detergent extracts were incubated with IgG-sepharose beads overnight at 4°C. The beads were washed with lysis buffer 8 times and

eluted in SDS-PAGE sample buffer by incubating at 55°C for 15min. The eluates were resolved by SDS-PAGE and immunoblotted with anti-YFP antibody.

Random mutagenesis screen and generation of the Atg9 mutant

The gap-repair PCR mutagenesis method (149) was employed to generate the Atg11-binding-defective Atg9 mutant. An AvrII site at 942 bp was introduced into the pAPG9GFP(416) plasmid by site-directed mutagenesis. The Atg9 N-terminal region containing the AvrII site was amplified and introduced into pGBDU-C1 with EcoRI and BamHI to generate pBD-Atg9N(AvrII). A gapped pGBDU-C1 plasmid was generated by digesting with EcoRI and BamHI. The PCR reaction was carried out using Taq polymerase (New England Biolabs, Beverly, MA) with pBD-Atg9N(AvrII) as the template. The dATP concentration was lowered to three-fifths that of the other three dNTPs. The resulting mutagenized PCR product shares overlapping sequences of ~100 bp at both 5' and 3' ends with the gapped pGBDU-C1 plasmid. The PCR product and the gapped plasmid were co-transformed into the two-hybrid strain PJ69-4A. The transformants were replicated on both -his and -ade plates. The transformants that were not able to grow on either plate were selected and analyzed by western blot for protein stability using anti-Atg9 antiserum (144). Stable mutants were sequenced and pBD-Atg9N^{H192L} identified. The Atg9 N-terminal fragment containing the H192L mutation was then released from pBD-Atg9N^{H192L} by digestion at the introduced AvrII site and a natural NruI site. This fragment was cloned into pAPG9GFP(416) digested with the same restriction enzymes to generate pAtg9^{H192L}GFP(416).

Fluorescence microscopy

Cells expressing fusion proteins with fluorescence tags were grown in SMD media to OD_{600} = 0.8. For vacuolar membrane labeling, cells were pelleted, resuspended in fresh media at OD_{600} = 1.0, incubated with 2 μM FM 4-64 at 30°C for 15 min, and then pelleted and cultured in the same media without FM 4-64 at 30°C for 30 min. For mitochondrial fluorescent labeling, MitoFluor Red 589 (Molecular Probes, Eugene, OR) was added to the growing culture at a final concentration of 1 μM, and the culture incubated at 30°C for 30 min. Cells were then washed with the same culture medium before imaging to remove the excess dye. For rapamycin treatment, cells were cultured with 0.2 μg/ml rapamycin at 30°C for 1.5 h. When necessary, a mild fixation procedure was applied to visualize Atg9 without destroying various fluorescent proteins: Cells were harvested, resuspended in a half-volume of fixation buffer (50 mM KH_2PO_4, pH 8.0, 1.5% formaldehyde, 1 μM $MgCl_2$), and incubated at room temperature for 30 min with gentle shaking. Cells were then washed once with an equal amount of wash buffer (50 mM potassium phosphate, pH 8.0, 1 μM $MgCl_2$), and resuspended in 50 μl wash buffer. Fluorescence signals were visualized on an Olympus IX71 fluorescence microscope (Olympus, Mellville, NY). The images were captured by a Photometrics CoolSNAP HQ camera (Roper Scientific, Inc., Tucson, AZ) and deconvolved using DeltaVision software (Applied Precision, Issaquah, WA).

Additional assays

The GFP-Atg8 processing assay, the Pho8Δ60 activity assay and the protease protection assay were carried out as previously described (2, 26, 145, 193).

CHAPTER 3

Self-interaction is critical for Atg9 transport and function at the phagophore assembly site during autophagy

Abstract

Autophagy is the degradation of a cell's own components within lysosomes (or the analogous yeast vacuole), and its malfunction contributes to a variety of human diseases. Atg9 is the sole integral membrane protein required in formation of the initial sequestering compartment, the phagophore, and is proposed to play a key role in membrane transport; the phagophore presumably expands by vesicular addition to form a complete autophagosome. It is not clear through what mechanism Atg9 functions at the phagophore assembly site (PAS). Here we report that Atg9 molecules self-associate independently of other known autophagy proteins in both nutrient-rich and starvation conditions. Mutational analyses reveal that self-interaction is critical for anterograde transport of Atg9 to the PAS. The ability of Atg9 to self-interact is required for both selective and non-selective autophagy at the step of phagophore expansion at the PAS. Our results support a model in which Atg9 multimerization facilitates membrane flow to the PAS for phagophore formation.

Introduction

Autophagic degradation of unneeded or damaged cellular components is essential for various cellular functions including proper homeostasis. Along these lines, the malfunction of autophagy is implicated in a variety of diseases, including cancer, neurodegeneration, cardiac disorders and pathogen infection (192). During autophagy, cytosolic proteins and organelles are engulfed into a double-membrane vesicle, the autophagosome, which then fuses with a lysosome (or the vacuole in fungi and plants) where its cargos are degraded. The autophagy-related (Atg) protein Atg9 plays a central role in the nucleation step during autophagosome formation in eukaryotes ranging from yeast to mammals (144, 239). Being the only identified integral membrane protein that is absolutely required in autophagosome formation, Atg9 is proposed to be the "carrier" of lipids to the phagophore assembly site (PAS, also known as the preautophagosomal structure) (86). Atg9 is absent from the completed autophagosomes, suggesting that the protein is retrieved upon vesicle completion. Previous work done in the yeast *Saccharomyces cerevisiae* has shown that Atg9 interacts with multiple autophagy-related proteins via its two cytosol-facing termini (54, 105, 168, 232). However, the physiological role of such a multi-subunit complex in autophagy and the function of Atg9 in this complex are still unclear.

Selective autophagy, such as pexophagy (degradation of excess peroxisomes), mitophagy (clearance of damaged mitochondria) and the cytoplasm to vacuole targeting (Cvt) pathway, targets specific cargos (226). The Cvt pathway occurs during vegetative growth in yeast, in which two vacuolar hydrolases, α-mannosidase and the precursor

form of aminopeptidase I (Ape1 [prApe1]), are transported to the vacuole where prApe1 is processed into mature Ape1. Non-selective, bulk autophagy occurs at a basal level and is induced by developmental signals and/or stress conditions (106). For instance, during starvation, nutrients are provided to ensure cell survival through elevated autophagic degradation of bulk cytoplasm and subsequent release of the breakdown products from the lysosome. Previous studies in yeast show a cycling route of Atg9 transport between the PAS and some peripheral compartments including mitochondria, during vegetative growth: the anterograde transport of Atg9 to the PAS facilitated by Atg9 binding partners may deliver lipids to the PAS, and the retrieval of Atg9 from the PAS may recycle the protein back to the membrane origin for the next round of delivery (54, 169). Nevertheless, to date little is known about the mechanism targeting Atg9 to the PAS during starvation-induced bulk autophagy.

Unlike other intracellular trafficking vesicles that usually bud from the surface of a preexisting organelle, an autophagosome is thought to assemble by fusion of new membrane fragments with the phagophore, the initial sequestering compartment, at the PAS. However, the membranous structure at the PAS, or the expanding phagophore, has not been clearly elucidated; how small membranes are incorporated into this structure remains unknown. In this paper, we present data that Atg9 interacts with itself in both nutrient-rich and starvation conditions independent of other Atg proteins. The self-interaction, which is mediated by the C terminus of the protein, promotes the trafficking of Atg9 from its origins to the PAS and is required for both selective and non-selective starvation-induced autophagy. Through examining the expansion of Atg9-containing phagophores by fluorescence and immunoelectron microscopy, we found that the ability

of Atg9 to multimerize is an essential function during formation of a normal phagophore at the PAS. Our data provide new conceptual insights to the molecular mechanism governing Atg9 anterograde transport and assembly of the PAS during bulk autophagy, and hence refine the cycling model of Atg9 transport.

Results

Atg9 self-interacts independent of other autophagy proteins or nutrient status

Previously we showed that Atg9 is located at the PAS and multiple peripheral punctate sites (169). To determine whether Atg9 directly self-interacts, we took advantage of a new reagent, a yeast strain lacking twenty-four known *ATG* genes that function in *S. cerevisiae*, referred to as the multiple knockout (MKO) strain (16). Analyses by fluorescence microscopy revealed that Atg9-GFP fusion proteins were indeed organized in clusters (detected as large puncta) in this strain, as well as in the wild-type strain (Fig. 3.1A), while expressing GFP alone did not lead to observable cluster formation (Fig. 3.S1). These findings led us to propose that Atg9 may form clusters through direct self-association involving none of the other known Atg proteins. To test this hypothesis, we coexpressed Atg9 proteins fused with two different tags, GFP and DsRed, in MKO and wild-type strains. As shown in Fig. 3.1B, the Atg9-GFP and Atg9-DsRed fusion proteins were colocalized in the cell as assessed by fluorescence microscopy.

Table 3.1. Yeast strains used in this study.

Strain	Genotype	Reference
BY4742	*MATα ura3*Δ *leu2*Δ *his3*Δ *lys2*Δ	Invitrogen
CCH001	SEY6210 *atg9*Δ*::HIS5 atg1*Δ*::LEU2*	(54)
CCH002	YTS158 *atg9*Δ*::HIS5*	(54)
CCH010	YCY123 *ATG9-3GFP::URA3 ATG9-3DsRed::LEU2*	This study
CCH011	SEY6210 *ATG9-3GFP::URA3 ATG9-3DsRed::LEU2*	This study
CCH019	SEY6210 *ATG9-TAP::TRP1*	This study
CCH020	JLY68 *atg9*Δ*::LEU2*	This study
CCH025	SEY6210 *RFP-APE1::LEU2 atg9*Δ*::HIS3*	This study
CCH026	SEY6210 *ATG14-GFP::TRP1 RFP-APE1::LEU2 atg9*Δ*::HIS3*	This study
CCH027	SEY6210 *atg9*Δ*::TAP(URA3)*	This study
JKY007	SEY6210 *atg9*Δ*::HIS3*	(144)
JLY68	SEY6210 *ATG23-PA::HIS5 ATG27-HA::TRP1*	(105)
PJ69-4A	*MATα leu2-3,112 trp1-*Δ*901 ura3-52 his3-*Δ*200 gal4*Δ *gal80*Δ *LYS2::GAL1-HIS3 GAL2-ADE2 met2::GAL7-lacZ*	(70)
SEY6210	*MATα ura3-52 leu2-3,112 his3-*Δ*200 trp1-*Δ*901 lys2-801 suc2-*Δ*9 mel GAL*	(173)
UNY102	SEY6210 *TAP-ATG1*	(236)
YCY123	SEY6210 *atg1*Δ*, 2*Δ*, 3*Δ*, 4*Δ*, 5*Δ*, 6*Δ*, 7*Δ*, 8*Δ*, 9*Δ*, 10*Δ*, 11*Δ*, 12*Δ*, 13*Δ*, 14*Δ*, 16*Δ*, 17*Δ*, 18*Δ*, 19*Δ*, 20*Δ*, 21*Δ*, 23*Δ*, 24*Δ*, 27*Δ*, 29*Δ	(16)

YCY135	YCY123 *ATG9-3GFP::URA3*	This study
YTS158	BY4742 *pho8::pho8Δ60 pho13Δ::KAN*	(54)

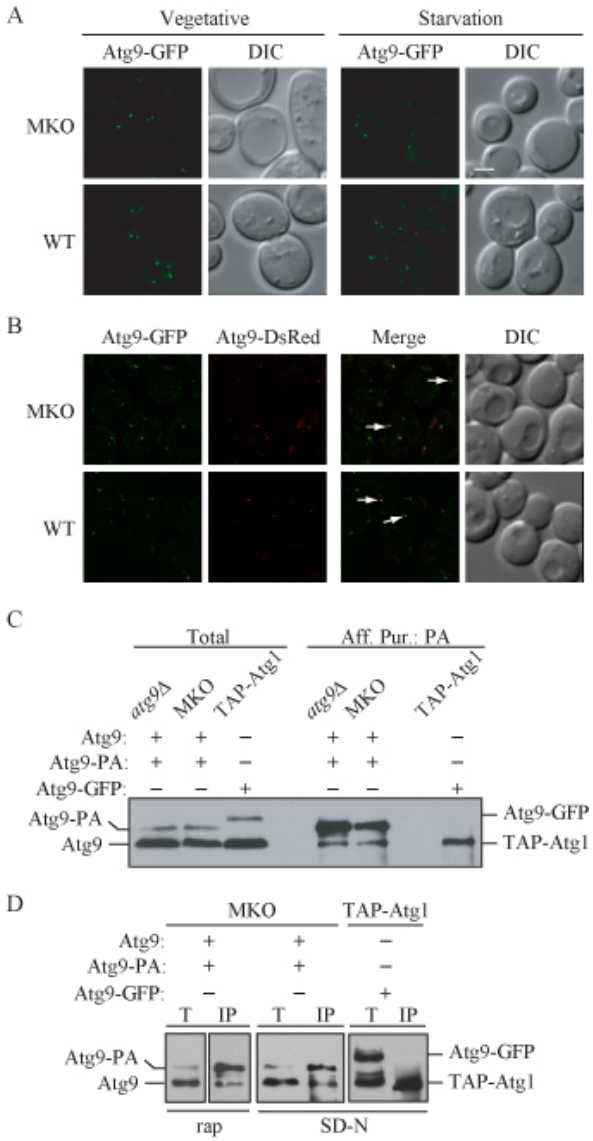

Figure 3.1. Atg9 self-associates independent of other Atg components or nutrient status. (A) Atg9 forms clusters independent of other Atg proteins under both nutrient rich and nitrogen starvation conditions. Wild-type (SEY6210; WT) or multiple knockout (YCY123; MKO) strains were transformed with a plasmid expressing Atg9-GFP driven by the Atg9 native promoter. Cells cultured in nutrient-rich medium (Vegetative) or nitrogen-starved for 3 h (Starvation) were visualized by fluorescence microscopy. (B) Atg9 molecules colocalize. WT (CCH011) or MKO (CCH010) strains expressing integrated Atg9-3GFP and Atg9-3DsRed fusions were grown to mid-log phase, subject to mild formaldehyde fixation and imaged by fluorescence microscopy. The arrows mark examples of the sites where the two chimeras colocalize. (C) Atg9 is coprecipitated by Atg9-protein A (PA) independent of other Atg proteins. *atg9*Δ (JKY007) or MKO strains cotransformed with centromeric plasmids containing Atg9 and the Atg9-PA fusion driven by the Atg9 native promoter were used for affinity isolation. Cells were cultured in nutrient rich medium (SMD). A strain (UNY102) expressing chromosomally tagged TAP-Atg1 and plasmid-borne Atg9-GFP was used as a control in (C) and (D). Total lysates (Total) and eluted polypeptides (Aff. Pur.) were separated by SDS-PAGE and blotted with anti-Atg9 antiserum in (C) and (D). (D) Atg9 self-interaction in nutrient-deprived conditions is independent of other Atg components. The MKO strain expressing plasmid-borne, native promoter-driven Atg9 and Atg9-PA was used for affinity isolation. Cells were subjected to rapamycin treatment for 2 h (rap) or nitrogen starvation for 3 h (SD-N). T, total lysates; IP, immunoprecipitates. DIC, differential interference contrast. Scale bar, 2 μm.

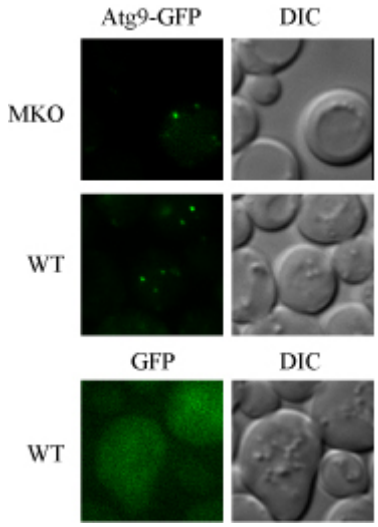

Figure 3.S1. The GFP tag does not cause observable aggregation or puncta formation. The MKO or wild-type strain expressing plasmid borne, native promoter-driven Atg9-GFP, and the wild-type strain expressing plasmid borne, *CUP1* promoter-driven GFP alone were grown in nutrient-rich medium to mid-log phase and imaged by fluorescence microscopy. DIC, differential interference contrast.

Next, we used a biochemical co-immunoprecipitation approach to test the self-interaction of Atg9. As shown in Fig. 3.1C, Atg9 was coprecipitated with Atg9-protein A (PA) in the MKO strain as well as in the wild-type strain in nutrient-rich conditions. As a negative control, we examined the ability of tandem affinity purification (TAP)-tagged Atg1 to co-immunoprecipitate Atg9-GFP; in this case, we could not examine endogenous Atg9 due to its migration at the same position as TAP-Atg1 during SDS-PAGE. In contrast to the result with Atg9-PA, Atg9-GFP was not recovered with TAP-tagged Atg1; Atg1 interacts with various other proteins including Atg13 but not Atg9, and we verified that TAP-Atg1 was able to co-immunoprecipitate Atg13 (Fig. 3.S2A). Similarly, Atg9-PA was not able to co-immunoprecipitate Atg1 (Fig. 3.S2B). Along with our previously published yeast two-hybrid results suggesting Atg9 self-interaction (168), these data

demonstrated that multiple Atg9 molecules were able to form a complex without any other known Atg proteins.

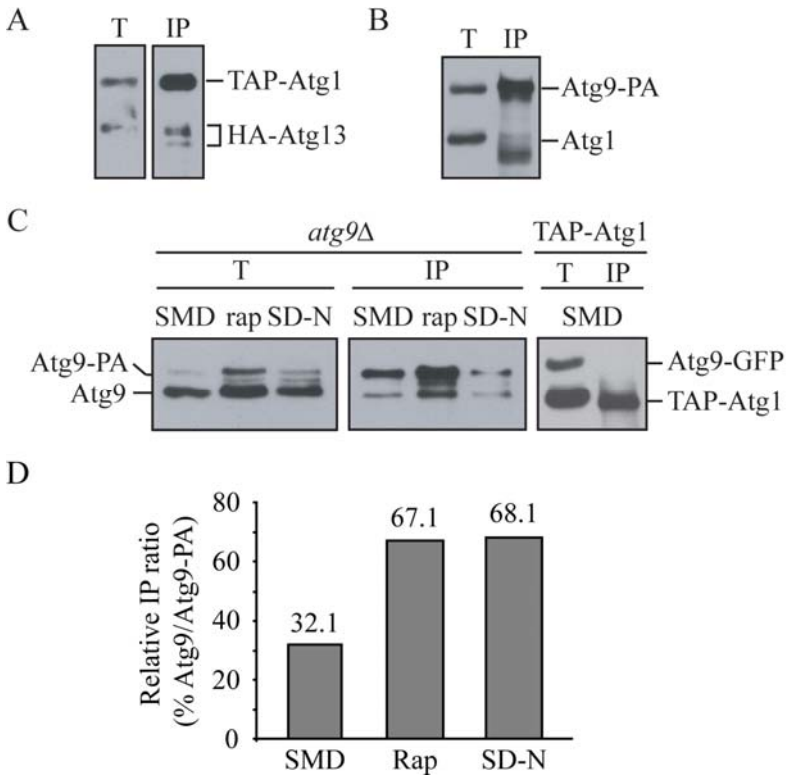

Figure 3.S2. Atg9 self-interaction is enhanced during starvation. (A) TAP-Atg1 coprecipitates HA-Atg13. The TAP-Atg1 strain (UNY102) transformed with a centromeric plasmid containing native promoter-driven HA-Atg13 was used in the affinity isolation. Total lysates and eluates were analyzed by SDS-PAGE and detected with anti-HA antibody. (B) Atg1 is not coprecipitated with Atg9-PA. The wild-type strain (SEY6210) transformed with a centromeric plasmid expressing native promoter-driven Atg9-PA was used for affinity isolation. Total lysates (T) and eluates (IP) were analyzed by SDS-PAGE and detected with anti-Atg1 antiserum. (C) Atg9 self-interacts independent of nutrient status. An *atg9*Δ strain (JKY007) expressing plasmid-borne, native promoter-driven Atg9 and Atg9-PA was used for affinity isolation. Cells were grown in nutrient-rich medium (SMD), nutrient-rich medium with rapamycin (rap), or nitrogen-starvation medium (SD-N). As a negative control, a TAP-Atg1 strain (UNY102) expressing plasmid-borne native promoter-driven Atg9-GFP was grown in nutrient-rich medium and analyzed by affinity isolation. (D) Band intensity shown in (C) was quantified using the ImageJ software (http://rsb.info.nih.gov/ij/), as percentage of Atg9 precipitated by Atg9-PA in the IP fraction.

Atg9 clustering occurs not only in nutrient-rich conditions but also during nitrogen starvation (Fig. 3.1A). To explore whether the same Atg9 complex forms during

bulk autophagy, the MKO cells were subjected to nitrogen starvation or treatment with rapamycin, a drug that partly mimics starvation conditions and induces bulk autophagy. Atg9 was coprecipitated with Atg9-PA in both conditions in the MKO strain (Fig. 3.1D). As before, Atg9-GFP was not co-isolated with TAP-tagged Atg1. Similar results were obtained using wild-type cells (Fig. 3.S2C). In addition, we found that Atg9 self-interaction is enhanced during starvation, based on quantification of the relative Atg9 amount precipitated by Atg9-PA (Fig. 3.S2D), implicating an important role of self-interaction during autophagosome formation. Collectively, we concluded that Atg9 self-interacts independent of any other known Atg proteins in both nutrient-rich and starvation conditions, which may correlate with a role for Atg9 in both selective and non-selective bulk autophagy.

An Atg9 C-terminal mutant disrupts its ability to multimerize

Next, we wanted to study the physiological function of Atg9 self-interaction in autophagy. Accordingly, we first mapped the interaction domain by the yeast two-hybrid approach. In the presence of full-length Atg9, the Atg9 C-terminal domain supported the growth of two-hybrid cells on selective plates lacking histidine as well as full-length Atg9, whereas the N terminus was not able to do so (Fig. 3.2A), indicating that Atg9 self-interaction is mediated through the C terminus. To narrow down the critical region, we further constructed a series of Atg9 C-terminal deletion mutants (Fig. 3.2B) and analyzed them using the co-immunoprecipitation assay. Atg9, Atg9Δ870-997 and Atg9Δ787-997, but not Atg9Δ766-785 or Atg9Δ766-997, were pulled-down by full-length Atg9-PA (Fig. 3.2C and unpublished data), suggesting that amino acids included in the region of 766-

786 were required for self-interaction. Atg9 and the PA vector were coexpressed as control and no detectable Atg9 was coprecipitated by PA. Based on this result, we generated four additional mutants each lacking five consecutive amino acids within the sequence of amino acids 766-786. By co-immunoprecipitation assays we determined that Atg9Δ766-770 was unable to interact with Atg9, whereas the other mutants displayed a normal interaction (Fig. 3.2D and unpublished data). We note that amino acids 766-770 are highly conserved through evolution (Fig. 3.2E).

Since Atg9 interacts with several other known Atg proteins, we further tested the ability of Atg9Δ766-770 to bind these other binding partners by yeast two-hybrid assays. Although Atg9Δ766-770 had a significantly compromised interaction with Atg9, it was still able to bind to its other binding partners, including Atg23, Atg27, Atg18 and Atg11, with apparently normal affinity (Fig. 3.2F). In addition, we verified that the interaction between Atg9Δ766-770 and Atg23 was not impaired based on co-immunoprecipitation; we used a vector expressing PA alone as a negative control (Fig. 3.2G). Therefore, the C-terminal mutant Atg9Δ766-770 specifically disrupts the self-interaction of Atg9 and was used for the following functional analyses.

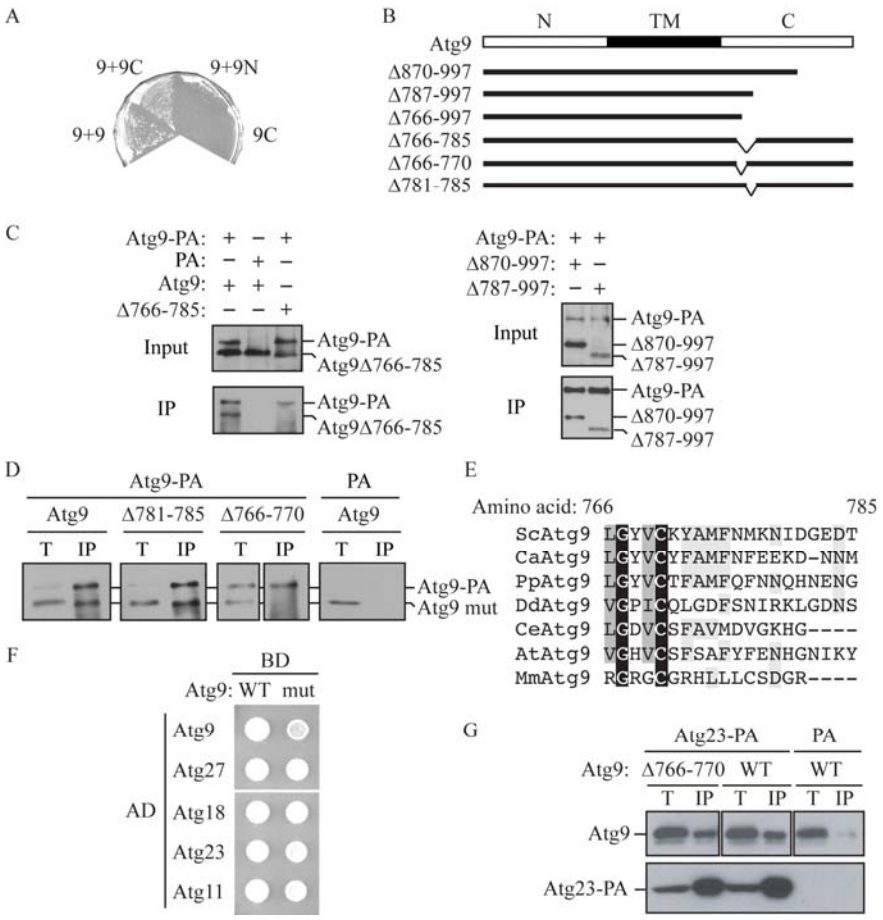

Figure 3.2. An Atg9 C-terminal mutant disrupts the ability to multimerize. (A) Atg9 self-interaction is mediated through its C terminus. Yeast two-hybrid cells (PJ69-4A) expressing full-length Atg9 with either full-length Atg9 (9+9), the Atg9 C terminus (9+9C) or the N terminus (9+9N), or expressing the Atg9 C terminus alone were grown for 6 d on plates lacking histidine. (B) Schematic representation of Atg9 truncation mutants. N, N terminus; TM, transmembrane domain; C, C terminus. (C) Atg9Δ870-997 and Atg9Δ787-997, but not Atg9Δ766-785, are coprecipitated with full-length Atg9. The MKO strain (YCY123) cotransformed with centromeric plasmids expressing native promoter-driven Atg9-PA and Atg9, Atg9Δ870-997, Atg9Δ787-997, or Atg9Δ766-785, were used for affinity isolation. Total lysates (Input) and eluted polypeptides (IP) were separated by SDS-PAGE and detected with anti-Atg9 antiserum. The MKO strain cotransformed with plasmids encoding Atg9 and PA alone was used as a control in (C) and (D). (D) An Atg9 mutant with a five-amino acid deletion (Atg9Δ766-770) loses self-interaction. MKO cells expressing plasmid-borne Atg9-PA with Atg9, Atg9Δ781-785, or Atg9Δ766-770, driven by the Atg9 native promoter, were used for affinity isolation. (E) Alignment of Atg9 amino acids 766-785. Sequences from *S. cerevisiae*, *C. albicans*, *P. pastoris*, *D. discoideum*, *C. elegans*, *A. thaliana* and *M. musculus* Atg9 were aligned using the ClustalW program. Amino acid identities, and high and low similarities are highlighted in black, dark gray and light gray, respectively. (F) Atg9Δ766-770 specifically loses self-interaction but not interactions with other Atg9 binding partners. The two-hybrid strain (PJ69-4A) was cotransformed with plasmids expressing the DNA binding domain-fused wild-type Atg9 (WT) or Atg9Δ766-770 (mut) and a series of known Atg9 binding partners fused with the activation domain. Interactions were monitored by the ability of cells to grow on plates lacking histidine for 5 d. (G) Atg9Δ766-770 interacts with Atg23 similar to wild-type Atg9. An *atg9*Δ strain expressing an integrated Atg23-PA fusion (CCH020) was transformed with a 2-micron plasmid containing wild-type Atg9-triple hemagglutinin (3HA) or Atg9Δ766-770-3HA. Total lysates (T) and eluates (IP) were separated by SDS-PAGE and detected by anti-HA or anti-PA antibody. An *atg9*Δ strain expressing plasmid-borne Atg9-3HA and PA was used as a control.

Atg9 self-interaction is required for autophagy progression

To study the function of Atg9 self-interaction in autophagy, we adopted several established assays using the Atg9Δ766-770 mutant. The processing of prApe1 into mature Ape1 results in a migration shift during SDS-PAGE and can be monitored as an indicator for selective autophagy. As shown in Fig. 3.3A, Atg9Δ766-770, which impaired the self-interaction of Atg9, blocked the maturation of prApe1; whereas the other three deletion mutants, which had no effect on Atg9 self-interaction, retained the capacity of prApe1 maturation similar to wild-type Atg9, although all of the Atg9 mutants displayed a level of stability at least equivalent to that of the wild-type protein. This indicated that the self-interaction of Atg9 is indispensable for selective autophagy.

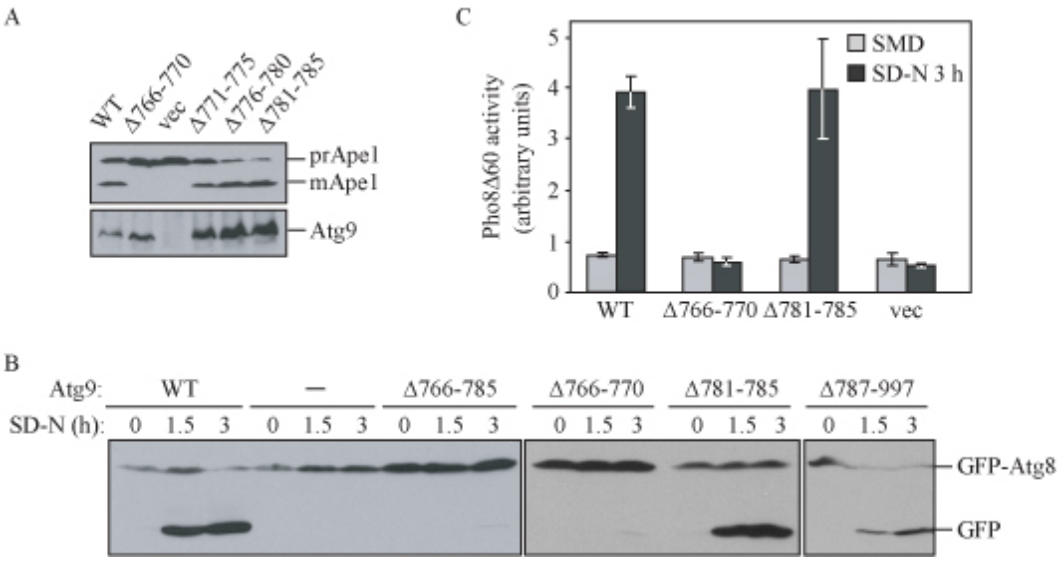

Figure 3.3. Atg9 self-interaction is required for autophagy activity in both nutrient-rich and starvation conditions. (A) Precursor Ape1 maturation is blocked in cells expressing Atg9Δ766-770. An *atg9*Δ strain (JKY007) was transformed with an empty vector, or a plasmid expressing wild-type Atg9 or a series of truncation mutants (Δ766-770, Δ771-775, Δ776-780, Δ781-785) driven by the Atg9 native promoter. Protein extracts were analyzed by western blotting using antiserum to Ape1 or Atg9. (B) GFP-Atg8 processing is impaired by deletion of residues 766-770 of Atg9. The *atg9*Δ strain (JKY007) was cotransformed with a GFP-Atg8 plasmid and an empty vector (-), or a plasmid expressing wild-type Atg9 or a series of truncation mutants (Δ766-785, Δ766-770, Δ781-785, Δ787-997). Cells were grown in nutrient rich medium to mid-log phase then shifted to nitrogen starvation conditions (SD-N). Aliquots were taken at the indicated time points and analyzed by Western blotting using anti-GFP antibody. (C) Pho8Δ60 activity is reduced in Atg9Δ766-770-expressing cells. The *atg9*Δ strain (CCH002) transformed with a plasmid expressing native promoter-driven wild-type Atg9 (WT), Atg9Δ766-770, Atg9Δ781-785, or an empty vector (vec), were grown in nutrient-rich medium (SMD) to mid-log phase then shifted to starvation medium (SD-N) for 3 h. The Pho8Δ60 activity was measured according to Materials and methods. Error bars indicate the standard deviation of three independent experiments.

We also observed that Atg9 self-interaction occurs under nitrogen starvation conditions, which suggests that a protein complex containing multiple Atg9 proteins may be involved in bulk autophagy. To test this hypothesis, we carried out two assays to measure bulk autophagy activity when Atg9 self-interaction was altered. Atg8 is conjugated to phosphatidylethanolamine (PE) and remains associated with the completed autophagosome, and thus is a marker for autophagy progression (60, 91). During autophagy, the GFP-tagged Atg8 is transported to the vacuole where Atg8 is rapidly

degraded, while the GFP moiety remains relatively stable. Thus, the accumulation of free GFP detected by western blot reflects autophagy activity (193). We assayed GFP-Atg8 processing with the mutants mentioned above, and found that only with Atg9Δ766-770 and Atg9Δ766-785, both of which affected Atg9 self-interaction (Fig. 3.2D and unpublished data), GFP-Atg8 processing was blocked. With two other mutants Atg9Δ781-785 and Atg9Δ787-997 that did not affect Atg9 self-interaction, GFP-Atg8 was processed similar to cells expressing wild-type Atg9 (Fig. 3.3B). These data demonstrated that loss of Atg9 self-interaction caused a defect in bulk autophagy. To quantitatively confirm this result, we measured the Pho8Δ60 enzymatic activity. Pho8Δ60 is a truncated form of alkaline phosphatase that can be delivered to the vacuole only via autophagy (145). Approximately four-fold induction of Pho8Δ60 activity by starvation was observed with wild-type Atg9 and Atg9Δ781-785, whereas the empty vector and Atg9Δ766-770 showed only the basal level of Pho8Δ60 activity (Fig. 3.3C). We further introduced alanine mutations at each conserved residue (Fig. 3.2E) in the region 766-770, and found that these mutations also caused defects in the Cvt pathway and bulk autophagy (Table 3.2). Thus, even point mutations in the highly conserved interaction domain interfere with Atg9 function. Taken together, these results indicate that Atg9 self-interaction is also functionally essential for bulk autophagy. Thus our data revealed a previously unknown mechanism of Atg9 shared in both selective and bulk autophagy, involving formation of a multiple Atg9-containing complex that depends on interaction between Atg9 proteins.

Table 3.2. Point mutations to alanine in Atg9 amino acids 766-770 affect autophagy.

	Cvt	Autophagy
LGYVC	+	+
L to A	-	-
G to A	-	-
V to A	-	-
C to A	-	+/-
V to A C to A	-	-

-, complete block; +/-, partial block

Self-interaction promotes anterograde transport of Atg9 and formation of intact phagophores

We decided to investigate the underlying mechanisms of the functional defects seen with the Atg9Δ766-770 mutant. In the absence of Atg9, a number of Atg proteins are not correctly localized to the PAS, including Atg2, Atg14 and Atg18 (200). Therefore it is possible that formation of a multimeric Atg9 complex is required for recruitment of these proteins to the PAS. To examine this possibility, we visualized the localization of Atg2, Atg18 and Atg14 in cells expressing wild-type Atg9 or Atg9Δ766-770. As shown in Fig. 3.4, in the presence of either wild-type Atg9 or Atg9Δ766-770, Atg2, Atg18 and Atg14 localized to a primary perivacuolar punctum, which colocalized with RFP-Ape1 and corresponded to the PAS. These data suggested that PAS recruitment of Atg proteins by Atg9Δ766-770 was not affected, and thus was not the causal factor for the autophagy deficiencies.

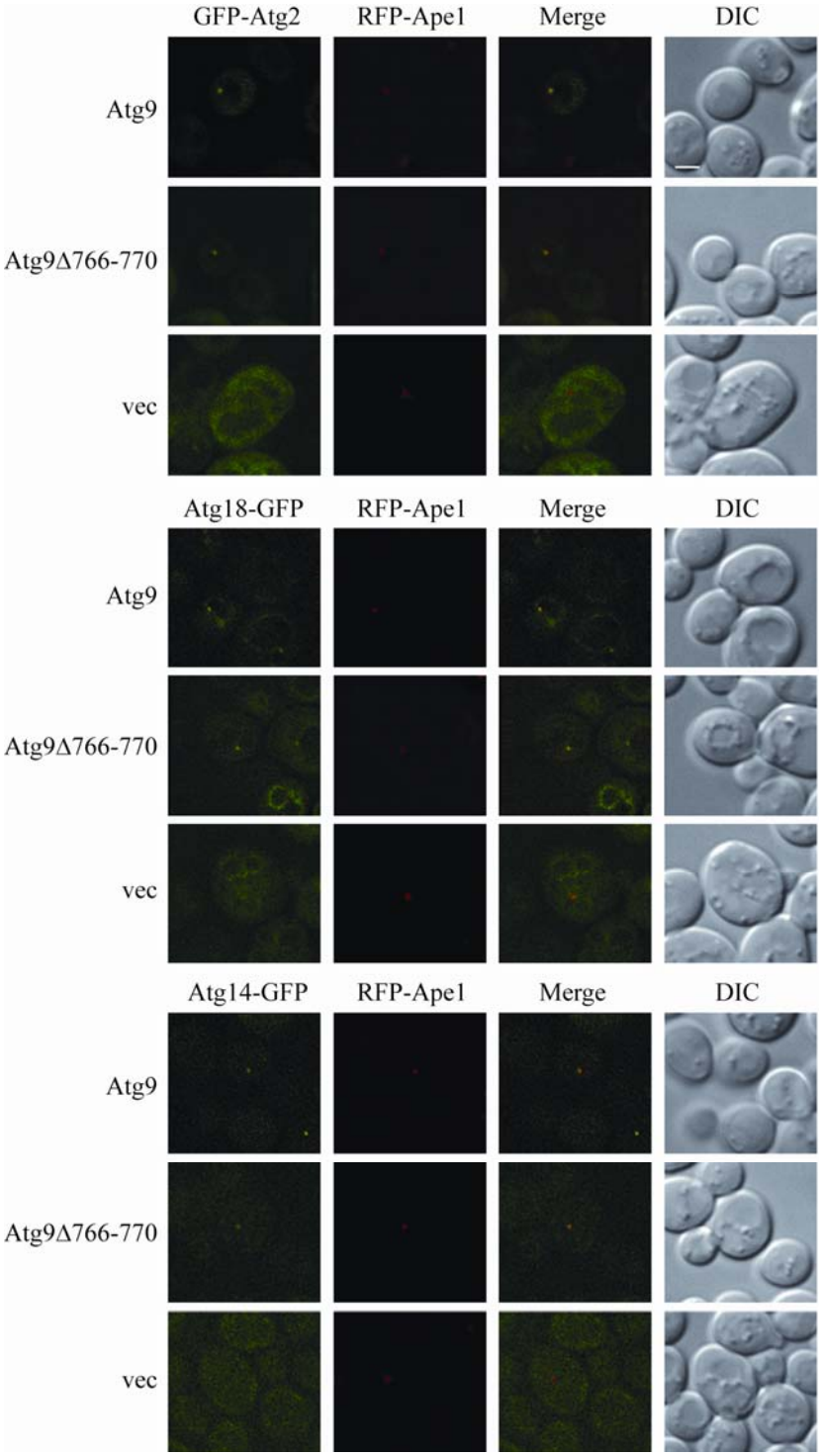

Figure 3.4. Atg9Δ766-770 is not defective in the PAS recruitment of other Atg proteins. An *atg9*Δ strain expressing integrated RFP-Ape1 (CCH025) was cotransformed with a plasmid expressing either *CUP1* promoter-driven GFP-Atg2 or native *ATG18* promoter-driven Atg18-GFP and a 2-micron plasmid expressing wild-type Atg9, Atg9Δ766-770, or an empty vector. An *atg9*Δ strain expressing chromosomally tagged Atg14-GFP and RFP-Ape1 (CCH026) was transformed with the above 2-micron plasmid expressing wild-type Atg9, Atg9Δ766-770, or an empty vector. Cells were cultured in nutrient-rich medium to mid-log phase and imaged by fluorescence microscopy. DIC, differential interference contrast. Scale bar, 2 μm.

We then hypothesized that the self-interaction may be involved in the trafficking of Atg9. According to the "cycling" model of Atg9 transport, when the retrograde transport of Atg9 is impaired, Atg9 will accumulate at the PAS as one primary punctum (169), but this accumulation was not observed with Atg9Δ766-770 in otherwise wild-type yeast cells; besides, Atg9Δ766-770 partially colocalized with mitochondria similar to wild-type Atg9 (unpublished data). Thus, Atg9 self-interaction is unlikely to be involved in the retrograde trafficking of Atg9 back to the peripheral (i.e., non-PAS) sites. Accordingly, to study whether self-interaction is involved in Atg9 anterograde transport, we used the TAKA (transport of Atg9 after knocking out *ATG1*) assay (26). Atg1 is a key regulator that activates the retrieval of Atg9 from the PAS to the peripheral sites and deleting *ATG1* restricts Atg9 to the PAS. The TAKA assay examines the epistasis of a second mutation relative to *atg1*Δ with regard to Atg9 localization at the PAS. Using fluorescence microscopy, we imaged the localization of Atg9Δ766-770-GFP and wild-type Atg9-GFP in *atg1*Δ cells in nutrient-rich and starvation conditions.

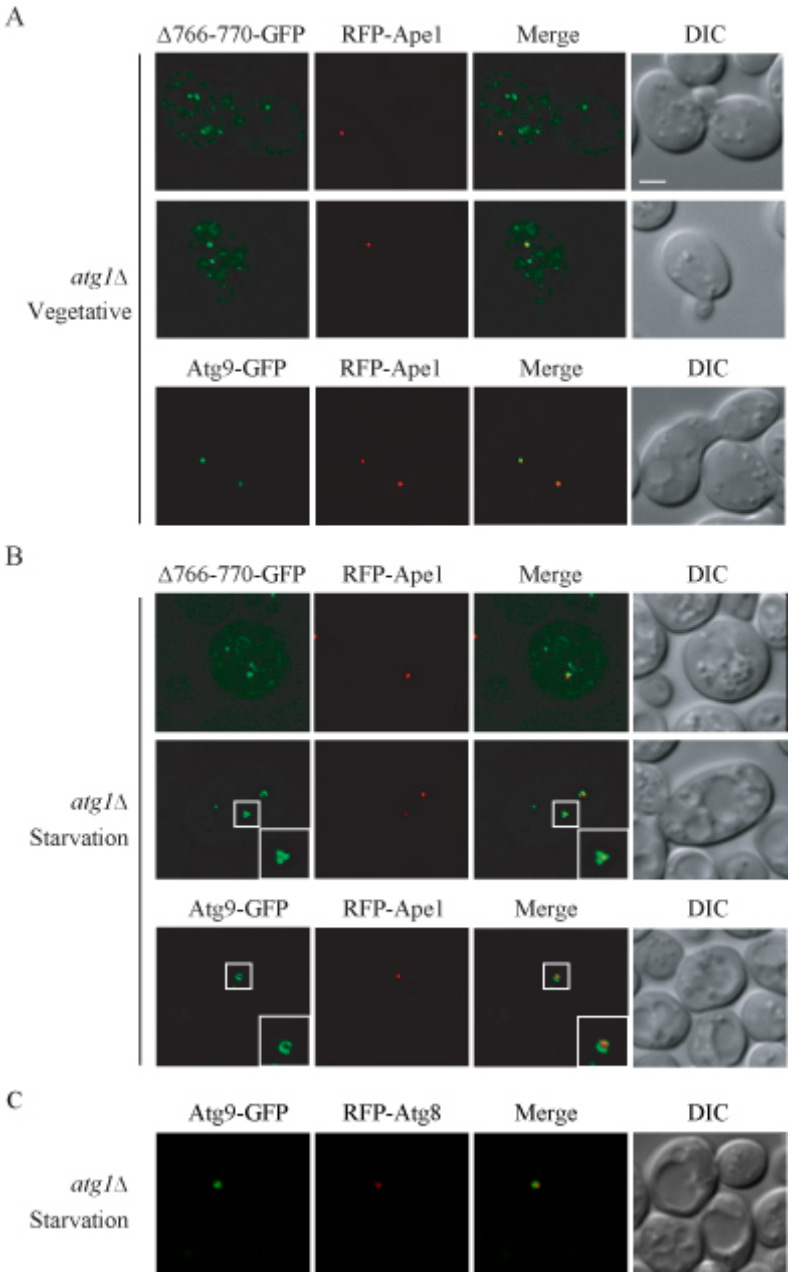

Figure 3.5. Atg9Δ766-770 is defective in PAS targeting and phagophore formation. (A) Atg9Δ766-770 has a partial defect in anterograde transport from peripheral sites to the PAS during growth. The *atg1*Δ *atg9*Δ strain (CCH001) was cotransformed with a RFP-Ape1 plasmid and a plasmid expressing wild-type Atg9-GFP or Atg9Δ766-770-GFP driven by the *CUP1* promoter. Cells were cultured in nutrient rich medium to mid-log phase and imaged by fluorescence microcopy. (B) Atg9Δ766-770 forms an abnormal fragmented phagophore. The cells in (A) were cultured to mid-log phase and subject to nitrogen starvation for 3 h before imaging by fluorescence microscopy. Lower-right panels are enlarged images of the boxed regions. (C) The phagophore is co-labeled with Atg9 and Atg8. The *atg1*Δ *atg9*Δ strain (CCH001) was cotransformed with plasmids expressing Atg9-GFP and RFP-Atg8. Cells were cultured to mid-log phase and subject to nitrogen starvation for 2 h before imaging by fluorescence microscopy. DIC, differential interference contrast. Scale bar, 2 μm.

As shown in Fig. 3.5A, in contrast to wild-type Atg9, which was restricted to the PAS (marked with RFP-Ape1) in 87% (52/60) of the cells, the Atg9Δ766-770 mutant distributed to multiple punctate or dispersed structures, in addition to the PAS location in 70% (52/74) of the cells. Such localization was observed regardless of nutrient supply (Fig. 3.5B). During nitrogen starvation, in 53% (23/43) of the *atg1*Δ cells, Atg9Δ766-770 localized to multiple puncta, compared with only 11% (12/107) of the cells displaying peripheral localization with wild-type Atg9. Thus, these results demonstrated that loss of Atg9 self-interaction partially blocked the anterograde trafficking of Atg9 to the PAS during selective and bulk autophagy. Self-interacting and forming a complex could concentrate Atg9 molecules as clusters at the peripheral compartments, which may be important for efficient trafficking of Atg9 from these sites for subsequent delivery to the PAS.

Upon nutrient deprivation, formation of continuous cup-shaped or ring-like structures by wild-type Atg9-GFP was visualized around the cargo prApe1 at the PAS and co-labeled with Atg8 by fluorescence microscopy (Fig. 3.5B and C), suggesting that they were functional rather than dead-end structures, based on previous studies showing that in *atg1* temperature-sensitive cells autophagosomes started to emerge from the Atg8-labeled PAS in 10 min and subsequently entered the vacuole after shift from nonpermissive to permissive temperature (199). These structures were approximately 500 nm in diameter, which fits within the size range of completed autophagosomes in yeast (400-900 nm) (202). Together, these data suggested that the expanding phagophore (or precursor membranes of phagophore) is an Atg9-containing intermediate. Additionally, the Atg9-containing structures were seen with various sizes and curvatures (Fig. 3.S3),

which may represent different expansion stages of the phagophore. Although, caution must be taken with this observation, as cup-shaped phagophores are not readily visualized in wild-type cells, probably due to the transient existence of phagophores and fast dissociation of Atg9 upon autophagosome completion. It is also possible that these structures may appear exaggerated under the fluorescence microscope by accumulation of fluorescent Atg9 proteins due to *ATG1* deletion.

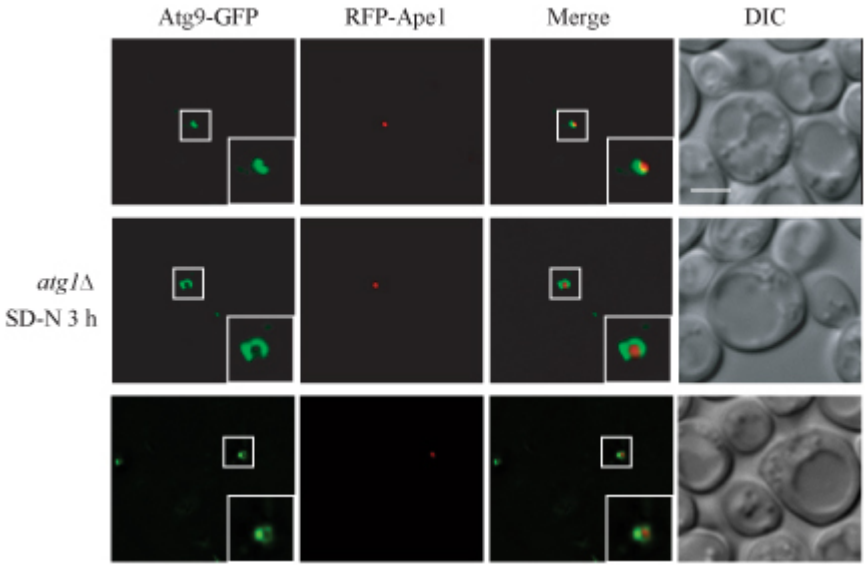

Figure 3.S3. Atg9-containing phagophores at different expansion stages. The *atg1*Δ *atg9*Δ strain (CCH001) was cotransformed with a RFP-Ape1 plasmid and a plasmid expressing *CUP1* promoter-driven wild-type Atg9-GFP. Cells were cultured in nutrient-rich medium to mid-log phase, and subject to nitrogen starvation for 3 h before imaging by fluorescence microscopy. Lower-right panels are enlarged images of the boxed regions. DIC, differential interference contrast. Scale bar, 2 μm.

Interestingly, the phagophore structure was fragmented and/or failed to elongate normally when Atg9Δ766-770-GFP replaced the wild-type Atg9-GFP (Fig. 3.5B). To further characterize the Atg9-containing structures at the PAS at a higher resolution, we applied immunoelectron microscopy (IEM). Atg9-GFP or Atg9Δ766-770-GFP was

expressed in an *atg1*Δ *atg9*Δ strain and the Atg9 protein detected with anti-GFP antibody. As previously reported (6), the Cvt complex formed by prApe1 and its receptor Atg19 was localized as a spherical electron-dense particle usually near the vacuole. Consistent with our result by fluorescence microscopy, wild-type Atg9 gold particles (arrows) were concentrated on the surface of membranous structures (arrowheads) surrounding the Cvt complex, whereas the Atg9Δ766-770 mutant that lost self-interaction appeared less clustered at the PAS (Fig. 3.6A and B). In sections prepared by freeze substitution but not immunostained, the membrane structures were more readily detected. In this case, it appeared that there were more membranes, potentially corresponding to the phagophore, surrounding the Cvt complex in wild-type cells relative to the Atg9Δ766-770 mutant. This result suggests that Atg9 self-interaction may be required to foster expansion of, or maintain the integrity of, the phagophore at the PAS.

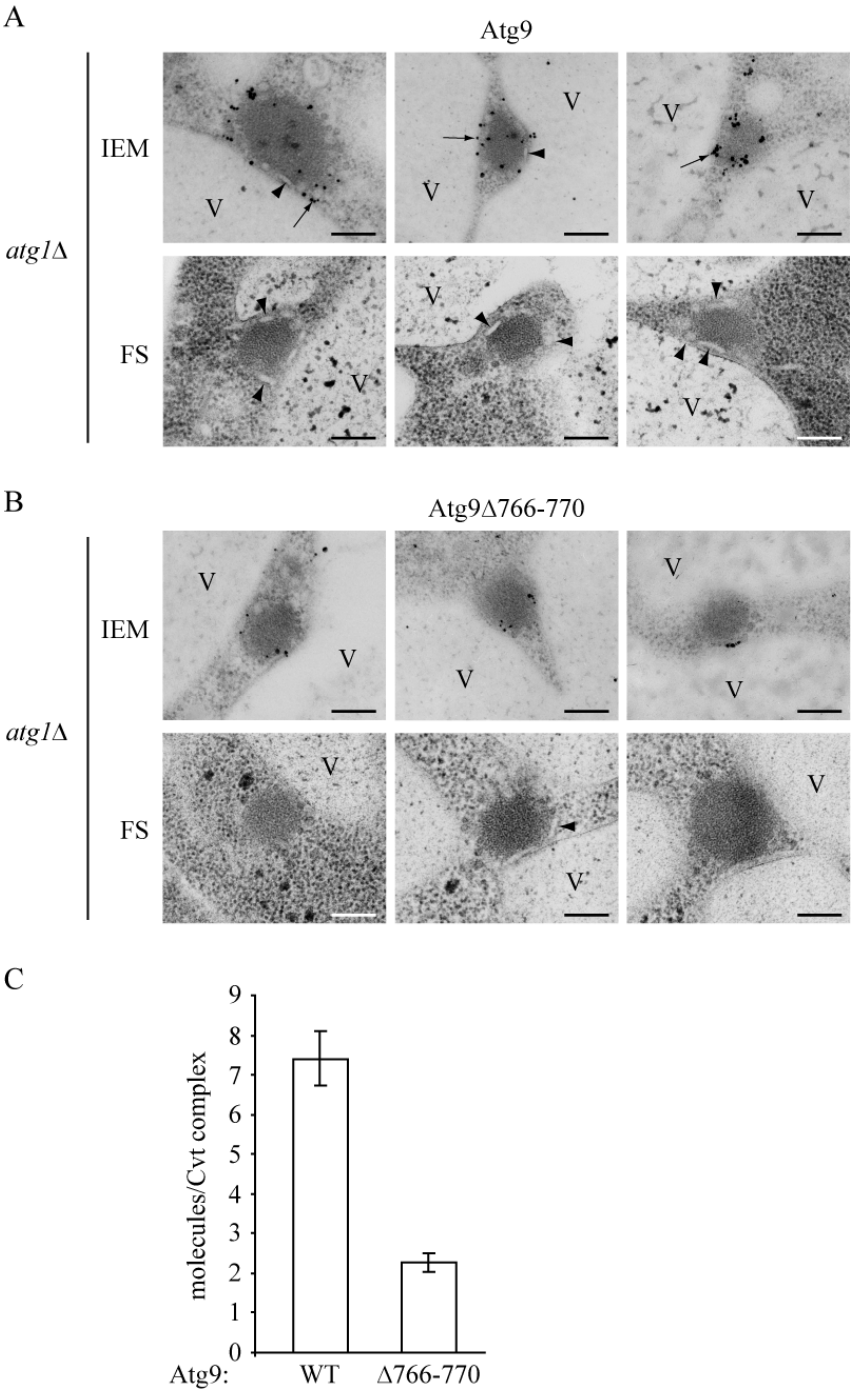

Figure 3.6. Atg9 localizes to the phagophore structure surrounding the Cvt complex. (A and B) The *atg1*Δ *atg9*Δ strain was transformed with a plasmid expressing *CUP1* promoter-driven Atg9-GFP (A) or Atg9Δ766-770-GFP (B). Cells were grown to mid-log phase, shifted to SD-N for 3 h, and prepared for electron microscopy using freeze substitution (FS) and stained with anti-GFP antibody followed by immunogold as indicated (IEM). Representative images are shown. Arrows mark Atg9 and membranous structures enwrapping the Cvt complex are indicated by arrowheads. V, vacuole. (C) The number of Atg9 or Atg9Δ766-770 molecules around Cvt complexes was quantified based on IEM images shown in (A) and (B). n=100; $P < 0.0001$. Error bars indicate s.e.m. and statistical significance was analyzed by Student's two-tailed *t* test. Scale bar, 200 nm.

To quantitatively analyze this difference, we further counted the average number of wild-type or mutant Atg9 molecules around the Cvt complex. As shown in Fig. 3.6C, the molecule number of Atg9Δ766-770 per Cvt complex was markedly reduced compared with wild-type Atg9, suggesting that Atg9 self-association is essential for efficient delivery to the PAS. Base on these data and our previous Atg9 "cycling" model, we propose that an Atg9 complex is dependent upon its self-interaction, and that the complex formation may facilitate not only the flow of membrane to the PAS but also the fusion of small membrane fragments into a continuous larger phagophore to form an autophagosome.

The ability to multimerize is required for Atg9 function at the PAS

Since Atg9Δ766-770 partially affected the anterograde trafficking of Atg9 to the PAS, it is possible that the abnormal phagophore structure we observed with Atg9Δ766-770 is due to insufficient supply of this protein to the PAS. To test this possibility, we relied on the overexpression of Atg11, which increases the anterograde transport of Atg9 to the PAS (54). We imaged the GFP-tagged Atg9 and CFP-tagged Atg11 pairs with a YFP/CFP filter set by fluorescence microscopy, and, as reported previously (78), no detectable bleed-through of the GFP signal from the CFP filter was seen. Since Atg9Δ766-770 did not affect its interaction with Atg11 (Fig. 3.2F), we were able to overcome the inefficient anterograde transport of Atg9Δ766-770 to the PAS by overexpressing Atg11 in both *atg1*Δ and wild-type cells (Fig. 3.7A and unpublished data), such that in nutrient-rich conditions the subcellular localization of Atg9Δ766-770 (68%; 36/53 cells) basically was indistinguishable from wild-type Atg9 (84%; 48/57 cells). The

transport restoration was also observed in starvation conditions (Fig. 3.7A; 73% of Atg9Δ766-770 cells (36/49) and 84% of wild-type Atg9 cells (46/55)). This phenotype indicates that the deletion of residues 766-770 did not absolutely block the ability of Atg9 to transit to the PAS and rules out accumulation in the endoplasmic reticulum due to protein misfolding as the cause of the functional defect. The increase in PAS localization of Atg9Δ766-770, however, did not result in the maturation of prApe1, indicating that this type of selective autophagy was still defective (Fig. 3.7B). The Pho8Δ60 activity assay also showed that bulk autophagy was not rescued by enhancing the anterograde flow of the mutant Atg9 (Fig. 3.7C). In either case, the overexpression of Atg11 did not interfere with the function of wild-type Atg9, indicating that this level of Atg11 did not cause a dominant negative phenotype. Therefore, these results clearly suggested that a normal multimeric state or the ability to multimerize is essential for Atg9 function after it reaches the PAS, which is a critical step during phagophore formation.

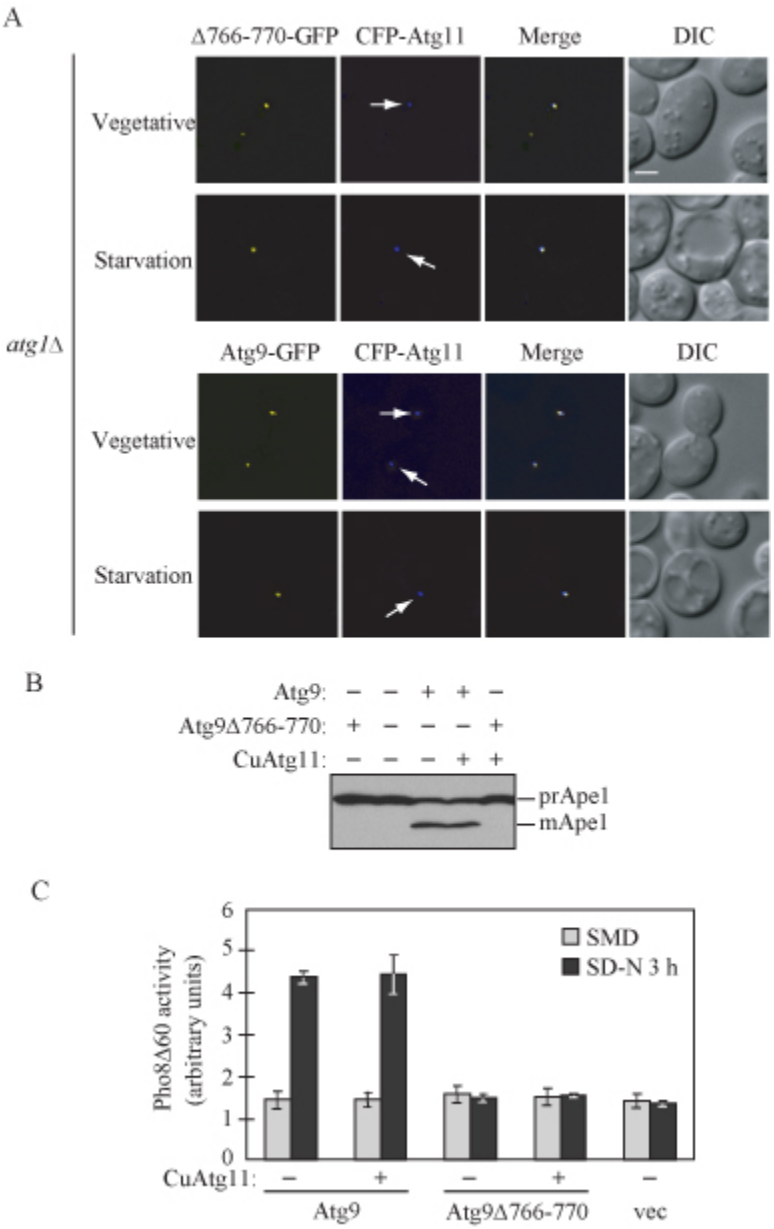

Figure 3.7. Atg9 functions in an oligomeric state at the PAS. (A) Overexpression of Atg11 rescues Atg9Δ766-770 transport to the PAS in both nutrient-rich and starvation conditions. The *atg1*Δ *atg9*Δ strain (CCH001) was cotransformed with centromeric plasmids containing *CUP1* promoter-driven CFP-Atg11 and wild-type Atg9-GFP, or Atg9Δ766-770-GFP. Cells were cultured in nutrient-rich medium to mid-log phase and imaged by fluorescence microscopy (Vegetative), or shifted to starvation medium for 3 h before microscopy imaging (Starvation). DIC, differential interference contrast. Scale bar, 2 μm. (B) Atg11 overexpression does not rescue the Cvt pathway in cells expressing Atg9Δ766-770. The *atg9*Δ strain (JKY007) expressing plasmid-borne wild-type Atg9 or Atg9Δ766-770, with or without *CUP1* promoter-driven Atg11, were grown to mid-log phase, and protein extracts were analyzed by Western blotting using anti-Ape1 antiserum. (C) Atg11 overexpression does not rescue Atg9Δ766-770 function in bulk autophagy. The *atg9*Δ strain (CCH002) expressing plasmid-borne *CUP1* promoter-driven wild-type Atg9 or Atg9Δ766-770, or an empty vector (vec), with or without *CUP1* promoter-driven Atg11, were grown in SMD to mid-log phase and shifted to SD-N for 3 h. The Pho8Δ60 activity was measured according to Materials and methods. Error bars indicate the standard deviation of three independent experiments.

To further investigate the nature of the Atg9 complex, we performed a native gel analysis using the MKO strain expressing wild-type Atg9 or the mutant. We discovered that Atg9Δ766-770 migrated faster than wild-type Atg9 in native conditions (Fig. 3.8A). As a control, we examined the dodecamer complex assembled by prApe1 (88) and found that it remained intact, suggesting that Atg9Δ766-770 was not able to form complexes as large (or as stable) as those seen with the wild-type protein. Consistent with the previous results showing that overexpression of Atg11 did not rescue the functional defect of the Atg9Δ766-770 mutant (Fig. 3.7B), overexpression of Atg11 did not rescue the defect in complex formation of Atg9Δ766-770 in native conditions (Fig. 3.8B). We further analyzed the Atg9 complex size in the wild-type background, by expressing wild-type or mutant Atg9 in the *atg9*Δ strain. As shown in Fig. 3.8C, both wild-type and mutant Atg9 displayed similar migration patterns as in the MKO cells, suggesting that the known Atg9 interaction partners among Atg proteins may be dynamically associated with Atg9, rather than stably present in the core Atg9 complex. In addition, consistent with Fig. 3.1 and 3.S2, we also detected that the Atg9 complex remained intact upon rapamycin treatment (Fig. 3.8C).

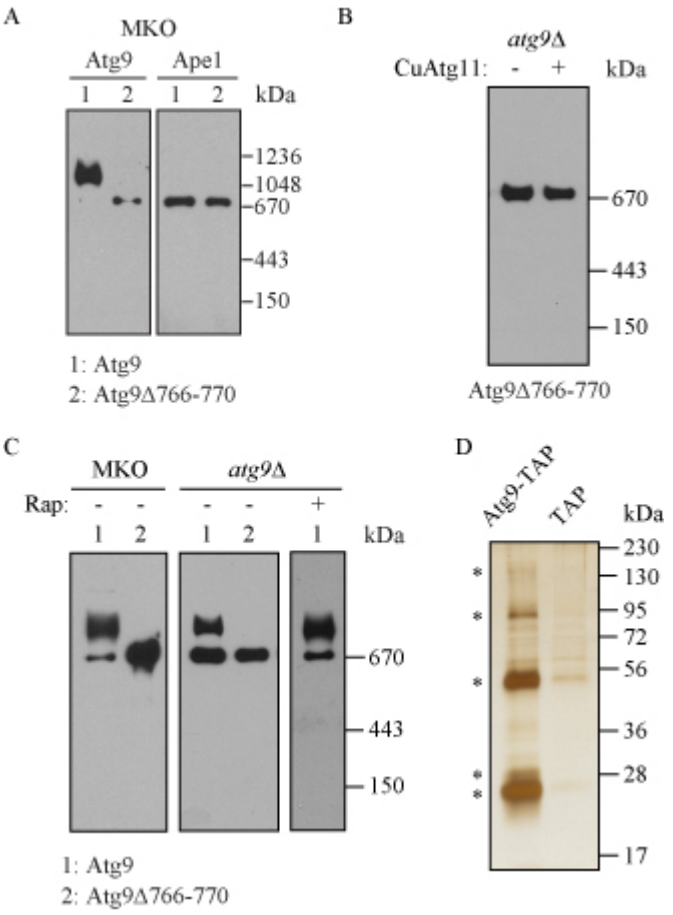

Figure 3.8. Biochemical characterization of the Atg9-containing complex. (A) Atg9Δ766-770 forms smaller complexes than wild-type Atg9 in the MKO strain. The MKO strain (YCY123) was transformed with a 2-micron plasmid expressing wild-type Atg9 or Atg9Δ766-770. Cell lysates were prepared under native conditions as described in Materials and methods and analyzed on native gels in (A), (B) and (C). (B) Atg11 overexpression does not rescue the defect in complex formation resulting from Atg9 loss of self-interaction. The *atg9*Δ strain was cotransformed with plasmids expressing *CUP1* promoter-driven HA-Atg11 and Atg9Δ766-770 as indicated. (C) Atg9 forms stable complexes in the wild-type strain during starvation. The MKO (YCY123) or *atg9*Δ (JKY007) strain was transformed with a 2-micron plasmid expressing wild-type Atg9 or Atg9Δ766-770. Cells were grown in SMD to mid-log phase, and treated with rapamycin for additional 1.5 h if indicated. Native gels are detected with antiserum to Atg9 or Ape1 in (A), and with Atg9 antiserum in (B) and (C). (D) The Atg9 complex contains five different proteins. Two strains expressing the chromosomally tagged Atg9-TAP (CCH019) or an integrated TAP tag alone driven by the *ATG9* promoter (CCH027) were used in tandem affinity purification as described in Materials and Methods. The eluates were analyzed on 10% SDS-PAGE gels and detected by silver staining. Proteins coprecipitated with Atg9 are marked by asterisks.

We noticed that Atg9Δ766-770 did not migrate as a monomer (~150 kDa on native gels, unpublished data), but ran at a position that might correspond to a tetramer.

This might reflect the fact that the mutant only partially impaired Atg9 complex formation as suggested by a compromised, but not complete loss of, interaction seen by the yeast two-hybrid assay (Fig. 3.2F), but it is also possible that the Atg9 complex contains unknown protein components as potential regulators of Atg9 function. To distinguish between these two possibilities, we performed the native purification of the Atg9 complex by the tandem affinity purification (TAP) method. We generated a strain expressing the chromosomally tagged Atg9-TAP fusion and another strain expressing the TAP tag alone integrated immediately after the *ATG9* promoter as control. The TAP tag was cleaved from Atg9-TAP following the first immunoprecipitation by IgG sepharose, and the Atg9 complex was isolated by a second immunoprecipitation with calmodulin affinity resin. The proteins precipitated by Atg9 were analyzed on SDS-PAGE gels and detected by silver strain. Besides Atg9 (at the size of ~130 kDa), four major protein bands were detected at approximately 94 kDa, 54 kDa, 28 kDa and 25 kDa, compared with control (Fig. 3.8D), suggesting that the Atg9 complex is actually composed of multiple proteins, although we cannot rule out at present that these represent degradation products. It will be helpful to further study the identity and function of these components in the Atg9 complex during phagophore formation and expansion.

Discussion

Atg9 is the only known integral membrane protein that is required in the formation of sequestering vesicles during all types of autophagy, including the Cvt pathway, pexophagy, mitophagy (80) and bulk autophagy, and it may play a key role in lipid delivery to the PAS. In addition to the PAS, Atg9 is localized at cytoplasmic punctate structures, which undergo dynamic movement revealed by time-lapse microscopy (168). Our data indicate that the clustered organization of Atg9 may be mediated by the ability to self-interact. We also found that self-interaction is important for efficient anterograde transport of Atg9 to the PAS (Fig. 3.5). It is possible that Atg9 multimerization as clusters may function in promoting membrane "budding", although the mechanism that triggers Atg9 movement from the peripheral compartments is not clear.

Our microscopy analyses revealed for the first time that Atg9 is localized on the membrane structures enwrapping the Cvt complex at the PAS, and hence Atg9 may be used as a marker for monitoring phagophore expansion, although the PAS in *atg1*Δ may represent a fairly static membrane structure, compared with the authentic growing phagophore in wild-type cells. Also, we do note that we cannot unequivocally identify the apparent membrane fragments as belonging to the phagophore because we did not carry out dual immunolabeling with anti-Atg8, which is known to localize to the PAS in the *atg1*Δ strain. We speculate that the precise regulation of Atg9 self-interaction may facilitate tethering and fusion of small membranes at the PAS. Notably, no yeast SNAREs have yet been localized to the PAS (170), implying that membrane fusion at,

and closure of, the phagophore may adopt a mechanism different from the conventional SNARE-mediated manner, although it is possible that SNAREs are present at too low a level to detect by fluorescence microscopy. Recent studies suggest that lipidated Atg8–PE mediates membrane hemifusion of liposomes in vitro (134). Yet, how Atg8 leads to membrane hemifusion in vivo and how hemifusion of lipid bilayers contributes to phagophore expansion is not clear. A recent analysis of Atg8 function suggests that Atg8 may largely determine the autophagosome size, but not the biogenesis of the initial phagophore or its completion (227). As suggested in this study, it is possible that Atg9 plays a critical role in initiating the phagophore. Furthermore, Atg9 along with Atg8–PE, and other Atg proteins, actively participate in the fusion process that expands the phagophore into the autophagosome. However, as noted above, it is not yet known whether Atg8–PE is present on the Atg9-containing membrane segments that are involved in autophagosome biogenesis.

It should be noted that the cup-shaped phagophore is formed in cells lacking Atg1 (Fig. 3.5B, 3.6A, 3.6B and 3.S3). Thus the Atg1 kinase, originally proposed to function in phagophore initiation, appears to be dispensable for this process. In addition, both Atg2 and Atg18 are absent from the PAS in *atg1*Δ cells (200). Therefore, the cup-shaped phagophore we observed around prApe1 seems to form independently of Atg1, Atg2 and Atg18. Given the previous reports showing that the absence of any of these three proteins causes accumulation of Atg9 at the PAS (169), it would be reasonable to hypothesize that Atg1, Atg2 and Atg18 function at the vesicle completion step and promote dissociation of Atg9 after vesicle sealing, and lacking any of them will arrest the phagophore as an intermediate structure. Notably, Atg1 also seems to function at a late stage and not

required for induction of micropexophagy in the methylotrophic yeast *Pichia pastoris* (132). Thus, the protein machinery responsible for autophagy induction, and the exact role of Atg1, remain to be further elucidated.

The multiple knockout (MKO) strain allowed us to investigate the formation of the Atg9 complex bypassing the complexity caused by multiple Atg9 binding partners among Atg proteins. Using Atg9 as a phagophore marker, the MKO strain will provide advantages for studying proteins required in distinct steps during autophagosome formation including nucleation, expansion and completion of the sequestering vesicle. We found that additional proteins may be stably present in the Atg9 complex (Fig. 3.8D), and it is possible that they function as regulatory units. It will be interesting to further characterize these members of the Atg9 complex for a better understanding of membrane dynamics during de novo autophagosome biogenesis.

Materials and methods

Yeast strains and media

The *S. cerevisiae* strains used in this study are listed in Table 3.1. For disruption of *ATG9*, the entire coding region was replaced by the *Kluyveromyces lactis LEU2* gene using PCR primers containing ~45 bases of identity to the regions flanking the open reading frame. For PCR-based integration of the GFP or TAP tag, pFA6a-GFP(S65T)-TRP1, or pBS1479 and pBS1539, was used as the template, respectively (113, 161). For integration of the Atg9-3GFP fusion, the integrative plasmid pATG9-3GFP(306) was linearized by digestion with StuI and integrated into the *URA3* gene locus. For integration of the Atg9-3DsRed fusion, the DNA fragment containing the *ATG9* gene and native promoter was released from pATG9-3GFP(306) and cloned into pTPIARP2-3DsRed(305) using XhoI and BamHI; the resulting integrative plasmid pAtg9-3DsRed(305) was linearized by digestion with AflII and integrated into the *LEU2* gene locus.

Yeast cells were grown in rich medium (YPD; 1% yeast extract, 2% peptone, 2% glucose) or synthetic minimal medium (SMD; 0.67% yeast nitrogen base, 2% glucose, amino acids, and vitamins as needed). Starvation experiments were conducted in synthetic medium lacking nitrogen (SD-N; 0.17% yeast nitrogen base without amino acids, 2% glucose).

Plasmids

Plasmids expressing HA-Atg13 (pHAAtg13(315) (25)), RFP-Ape1 (pRFPApe1(414) (197)), GFP-Atg8 (pGFP-AUT7(414) (2)), Atg9 (pAPG9(416);

essentially constructed the same as pAPG9(414) (144)), Atg9-GFP (pAPG9GFP(416) and pCuAPG9GFP(416) (144)), Atg9-PA (pAtg9PA(314) (54)), HA-Atg11 (pCuHA-CVT9(414) (87)), CFP-Atg11 (pCuHACFPCVT9(414) (86)), GFP-Atg2 (pCuGFPAPG2(414) (218)) and Atg18-GFP (pCVT18GFP(414) (47)) have been described previously. Yeast two-hybrid plasmids expressing Atg11 (pAD-Atg11), Atg18 (pAD-Atg18), Atg23 (pAD-Atg23), Atg27 (pAD-Atg27), Atg9 (pAD-Atg9 and pBD-Atg9), the Atg9 N terminus (pAD-Atg9N) or the C terminus (pAD-Atg9C) have been described previously (54).

The plasmids pAtg9Δ787-997(416) and pAtg9Δ870-997(416) were generated by amplifying the Atg9Δ787-997 and Atg9Δ870-997 fragments from pAPG9(416) and cloning them into the two AatII sites in pAPG9(416). To generate the plasmid expressing Atg9Δ766-997-GFP driven by the *TPI1* promoter (pS1S2(416)), the N-terminus of *ATG9* (928 bp) was amplified and cloned in the vector pPEP416 (165) digested with EcoRI/SacII. The 3' primer introduced an XbaI site and a SacII site preceded by a stop codon. The resulting pS1(416) plasmid was then cut with XbaI/SacII, and the central part of *ATG9* (1404 bp) was amplified and inserted using the same enzymes. For internal deletions of Atg9 (Atg9Δ766-785-GFP, Atg9Δ766-770-GFP, Atg9Δ771-775-GFP, Atg9Δ776-780-GFP and Atg9Δ781-785-GFP), the truncated open reading frames were amplified by PCR and cloned into NotI and BamHI sites of pAPG9GFP(416). For generation of non-tagged pAtg9Δ766-785(416), pAtg9Δ766-770(416), pAtg9Δ781-785(416), or pCuAtg9Δ766-770-GFP(416), and pAtg9Δ766-770-3HA(426), the fragment containing the indicated deletion was released from pAtg9Δ766-785-GFP(416), pAtg9Δ766-770-GFP(416), or pAtg9Δ781-785-GFP(416) by AgeI and SphI digestion

and introduced into pAPG9(416), pCuAPG9GFP(416), or pAtg9-3HA(426), respectively. Point mutations in Atg9 amino acids 766-770 were introduced by site-directed mutagenesis. To construct the two-hybrid plasmid pBD-Atg9Δ766-770, the Atg9Δ766-770 fragment was amplified from pAtg9Δ766-770GFP(416) and cloned into pGBDU-C1 using BamHI and SalI sites.

Protein A affinity isolation

Cells were grown to OD_{600} = 0.8 in SMD; for rapamycin treatment, cells were cultured with 0.2 μg/ml rapamycin at 30°C for an additional 2 h. 50 ml of cells were harvested and resuspended in lysis buffer (20 mM Tris-HCl pH 7.5, 150 mM KCl, 5 mM $MgCl_2$, 1% Triton X-100, 1 mM PMSF and protease inhibitor cocktail). The detergent extracts were incubated with IgG-sepharose beads overnight at 4°C. The beads were washed with lysis buffer 6 times and eluted in SDS-PAGE sample buffer by incubating at 37°C for 30 min. The eluates were resolved by SDS-PAGE and immunoblotted with anti-Atg9 antiserum, or anti-HA or anti-PA antibody.

Fluorescence microscopy

Fluorescence signals were visualized on an Olympus IX71 fluorescence microscope (Olympus, Mellville, NY). The images were captured by a Photometrics CoolSNAP HQ camera (Roper Scientific, Inc., Tucson, AZ) and deconvolved using DeltaVision software (Applied Precision, Issaquah, WA). When necessary, a mild fixation procedure was applied as previously described to visualize Atg9 without affecting various fluorescent proteins (54).

Native gel analysis

3-12% Bis-Tris Gels (Invitrogen, Carlsbad, CA) were used for blue native gel electrophoresis. Spheroplasts were generated from 25 ml of cells at mid-log phase as described previously (212), and cell lysates were prepared according to the Invitrogen NativePAGE Novex Bis-Tris Gel System manual.

Tandem affinity purification

400 ml cells were cultured to OD_{600} = 0.8 in YPD. Spheroplasts were prepared and TAP purification done as previously reported (161, 212). The eluates were resolved by SDS-PAGE, and silver staining of proteins in polyacrylamide gels was preformed using the SilverSNAP Stain Kit II (Thermo Scientific, Rockford, IL).

Electron microscopy

Immunoelectron microscopy (IEM) was performed according to the procedures described previously (6) with the following modifications: The blocking solution contained 0.05% Tween 20 or 0.5% cold fish gelatin (Sigma-Aldrich, St. Louis, MO), and the secondary antibody was conjugated to Ultra Small gold particles (Aurion, Wageningen, The Netherlands) and visualized with silver enhancement.

Additional assays

The GFP-Atg8 processing assay and the Pho8Δ60 activity assay were carried out as previously described (2, 193).

CHAPTER 4

Assaying autophagic activity in transgenic GFP-Lc3 and GFP-Gabarap zebrafish embryos

Abstract

Autophagy mediates the bulk turnover of cytoplasmic constituents in lysosomes. During embryonic development in animals, a dramatic degradation of yolk proteins and synthesis of zygotic proteins takes place, leading to intracellular remodeling and cellular differentiation. Zebrafish represents a unique system to study autophagy due in part to its rapid embryonic development relative to other vertebrates. The technical advantages of this organism make it uniquely suited to various studies including high throughput drug screens. To study autophagy in zebrafish, we identified two zebrafish Atg8 homologs, *lc3* and *gabarap*, and generated two transgenic zebrafish lines expressing GFP-tagged versions of the corresponding proteins. Similar to yeast Atg8 and mammalian LC3, zebrafish Lc3 undergoes post-translational modification starting at the pharyngula stage during embryonic development. We observed a high level of autophagy activity in zebrafish embryos, which can be further upregulated by the TOR inhibitor rapamycin or the calpain inhibitor calpeptin. In addition, zebrafish Gabarap accumulates within lysosomes upon autophagy induction. Thus, we established a convenient zebrafish tool to assay autophagic activity during embryogenesis in vivo.

Introduction

Autophagy is a cellular degradative pathway that delivers cytoplasmic cargo to the lysosome. There are many forms of autophagy including macroautophagy, microautophagy, and chaperone-mediated autophagy. The best studied of these processes is macroautophagy, which will be referred to as autophagy throughout the remainder of this article. During autophagy, a double-membrane vesicle called an autophagosome is formed around cargo. Autophagosomes subsequently fuse with a lysosome, allowing breakdown of the vesicle inner membrane; hydrolases then degrade the cargo, and the resulting macromolecules are released back into the cytosol for use as cellular nutrients. The study of autophagy is important because of its roles in human heath and pathology including host immune defense, antigen presentation, tumor suppression, cardiovascular disease, gastrointestinal disorders, neurodegeneration and longevity (14, 59, 121, 126, 179).

Mutant screens in *S. cerevisiae* have revealed approximately 31 genes required for autophagy (*ATG* genes) and many of these have mammalian homologs (226). Autophagy requires two highly conserved ubiquitin-like conjugation systems. The ubiquitin-like protein Atg12 is activated by the E1 enzyme (Atg7), subsequently transferred to an E2 enzyme (Atg10) and finally conjugated to its target Atg5. The second ubiquitin conjugation system promotes the C-terminal processing of the ubiquitin-like protein Atg8 and its eventual attachment to phosphatidylethanolamine (PE). Atg8 processing occurs by means of its initial cleavage by Atg4, activation by the E1 enzyme, Atg7, and transfer to the E2 enzyme Atg3, which lipidates Atg8 (44, 61). Unlike most of the other known

autophagy gene products, a population of Atg8 remains associated with the autophagosome and is degraded in the lysosome (76). This unique localization pattern of Atg8 has made it an excellent tool for monitoring the formation of autophagosomes in multiple organisms including *S. cerevisiae* (85, 96), *A. thaliana* (238), *D. melanogaster* (176), and mice (129), and also in cell culture (76).

Humans have approximately eight Atg8 homologs, including microtubule-associated protein 1 light chain 3 (LC3) isoforms A, B and C, gamma-aminobutyric acid A receptor-associated protein (GABARAP) isoforms L1, L2 and L3, Golgi-associated ATPase enhancer of 16 kDa (GATE-16) and Atg8-like protein (ATG8L) (55), and the best studied of these is LC3. LC3 is conjugated to PE in response to starvation conditions or chemical treatments that upregulate autophagy. GABARAP shows many similarities with LC3 but its conjugation is only mildly affected by starvation, and under certain conditions conjugation may be activated independent of mTOR inactivation (77, 208). GATE-16 is proposed to be involved in intra-Golgi transport and post-mitotic Golgi reassembly (178). ATG8L is the least studied homolog, and the function of GATE-16 and ATG8L in autophagy is not well understood.

Whereas the study of autophagy in multiple organisms has proceeded at a rapid pace over the last decade (94), little autophagy research has been performed in zebrafish. This paucity is likely due to the current lack of tools to monitor autophagy in this organism. To expand in vivo research of autophagy in zebrafish we have created transgenic GFP-Lc3 and GFP-Gabarap fish.

Results

Zebrafish Lc3 is converted to form II at the pharyngula stage during embryogenesis

Yeast Atg8 and its mammalian homolog LC3 specifically label the growing phagophores and completed autophagosomes (76, 91). GABARAP, a second mammalian homolog of Atg8, is another modifier in lipidation reactions mediated by Atg7, Atg3 and Atg4 in the same manner as Atg8 and LC3, and localizes to autophagosome membranes when overexpressed (77). In order to generate a marker protein for autophagosomes in zebrafish, we cloned cDNAs of two zebrafish homologs of Atg8. Both genes are predicted to encode a protein of 122 amino acids, which undergoes cleavage at the C terminus (Fig. 4.1A and B). Based on phylogenetic analysis and sequence homology, we named them Lc3 and Gabarap, with Lc3 more closely related to mammalian LC3 (91% identity) and Gabarap to mammalian GABARAP (94% identity) (Fig. 4.1C). Both proteins showed a high degree of homology to yeast Atg8 (Lc3 32%, and Gabarap 52% identity).

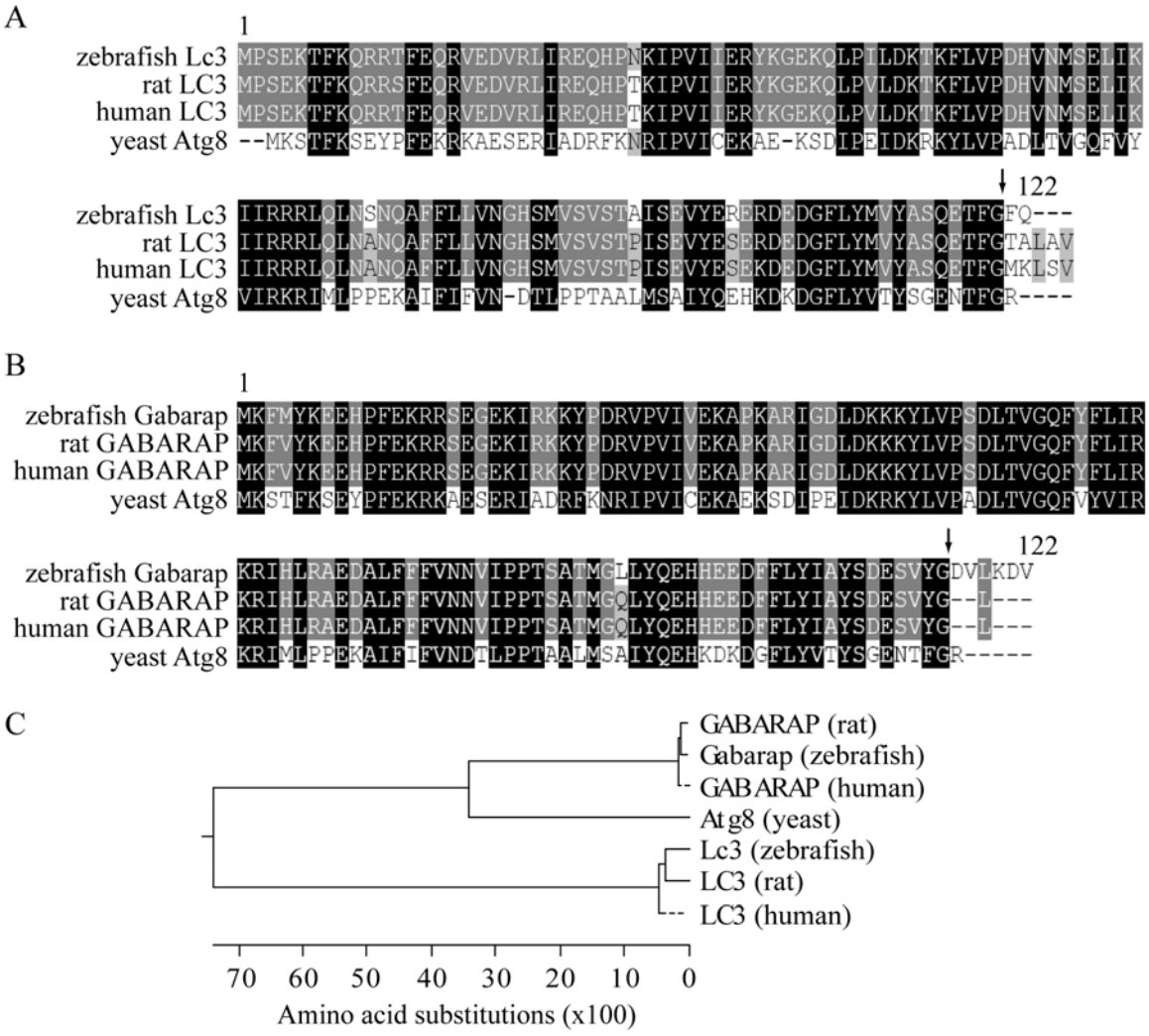

Figure 4.1. Alignment of zebrafish Lc3 (A) or Gabarap (B) with yeast and mammalian homologs. Protein sequences from *S. cerevisiae* (yeast), *D. rerio* (zebrafish), *R. norvegicus* (rat) and *H. sapiens* (human) were aligned using the ClustalW program. Amino acid identities, and high and low similarities are highlighted in black, dark gray and light gray, respectively. Arrows indicate the potential cleavage and lipidation site. (C) Phylogenetic tree of Atg8 homologs in yeast, zebrafish and mammals.

To determine when autophagy might be induced in embryos during development, we first analyzed the temporal expression pattern of Lc3 and Gabarap by RT-PCR. *lc3* and *gabarap* transcripts were detected at the early cleavage stage (1-2 cell, 0 hours post-fertilization (hpf)) (Fig. 4.2A), indicating that both *lc3* and *gabarap* mRNA are

maternally deposited, since transcription of zebrafish zygotic DNA does not start until 3 hpf (158). To investigate whether the presence of *lc3* transcripts corresponded to expression of the protein and if conjugation of Lc3 occurred, we examined the appearance of Lc3 with an anti-mammalian LC3 antibody that cross-reacts with the zebrafish homolog. We were able to detect a 16 kDa band that presumably corresponds to the Lc3-I form and a 14 kDa band that is equivalent to Lc3-II (Fig. 4.2B). In contrast to mouse embryos, in which LC3 conversion is observed even in metaphase II oocytes (214), the conversion of Lc3-I to Lc3-II was evident at 48 hpf but not at 24 hpf. In addition, the total expression level of Lc3 increased in 48 hpf embryos compared to 24 hpf. The earliest time point at which we observed conversion to the Lc3-II form was at 32 hpf (data not shown), suggesting that autophagy is upregulated in zebrafish embryos at the pharyngula period. One possible explanation for the delay in autophagy induction is that other proteins essential for autophagy are not yet produced. In support of this hypothesis we found that although *lc3* and *beclin 1* are maternally deposited, some other predicted autophagy-related genes in zebrafish start transcription at, or after, approximately 24 hpf (Fig. 4.2C). In particular, mRNA transcripts for the zebrafish homologs of *ulk1* and *atg9* were not detected at 0 hpf, indicating that they were not maternally deposited, whereas *beclin 1* transcripts were detected at 0 hpf similar to *lc3*.

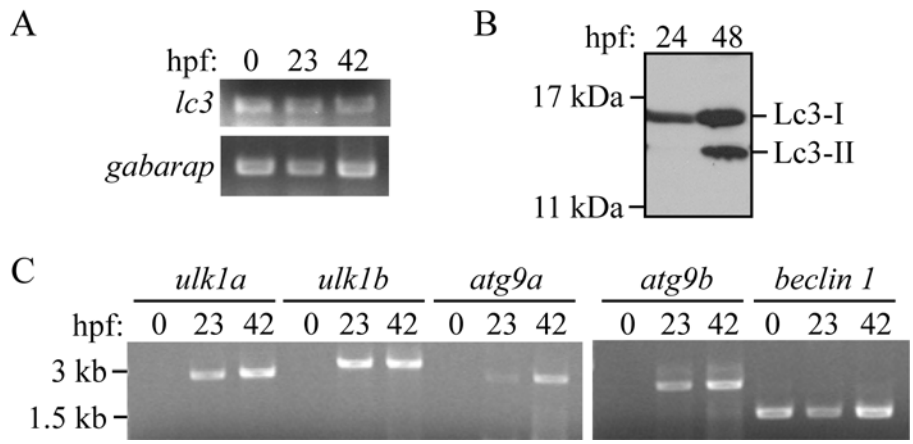

Figure 4.2. The zebrafish LC3 homolog Lc3 undergoes post-translational modification during embryonic development. (A) *lc3* and *gabarap* mRNAs are maternally deposited in zebrafish embryos. RT-PCR was performed with RNA isolated from 0, 23, and 42 hpf wild-type embryos using gene-specific primers. (B) Lc3-I converts to Lc3-II after 24 hpf. Protein extracts were isolated from 24 and 48 hpf wild-type embryos, analyzed by SDS-PAGE and detected using anti-LC3 antibody. (C) Some autophagy-related genes start transcription at or after 23 hpf. RT-PCR was performed with RNA isolated from 0, 23, and 42 hpf wild-type embryos using specific primers to the zebrafish *ulk1a*, *ulk1b*, *atg9a*, *atg9b* and *beclin 1* genes.

Lc3-I to Lc3-II conversion is enhanced in the presence of lysosomal inhibitors

Having established that the Lc3 protein is expressed and that it undergoes post-translational modification similar to its mammalian and yeast homologs during zebrafish embryonic development, we decided to study the extent of autophagy during embryogenesis by analyzing Lc3-II conversion. To evaluate the basal level of autophagy, we utilized two lysosomal protease inhibitors, pepstatin A, an inhibitor of cathepsins D and E, and E64d, an inhibitor of cathepsins B, H and L (207). At the concentration and time used in this analysis, these inhibitors imposed no readily observable effects on embryo viability when applied in the embryo water (data not shown). We treated 2 days post-fertilization (dpf) embryos with the above drugs for 24 hours, and observed the accumulation of Lc3-II (Fig. 4.3). Treatment with lysosomal protease inhibitors alone resulted in a substantial increase in the Lc3-II to Lc3-I ratio, suggesting that constitutive

autophagy occurred at a high basal level during normal embryogenesis; since Lc3-II is turned over in the lysosome, stabilization of the protein when lysosomal degradation is blocked is an indication of autophagic flux (95).

Starvation is a known inducer of autophagy, however, since the embryonic yolk is a stable nutrient supply during embryogenesis, we tested rapamycin, a TOR inhibitor that is widely used to induce autophagy in yeast and mammalian cells by mimicking starvation conditions (175). With a final concentration of 1 μM rapamycin in embryo water, which has been previously shown to inhibit the TOR signaling pathway in zebrafish embryos and larvae but not cause cell death (116), we observed no detectable change in the Lc3-II/Lc3-I ratio after 24 hours of treatment (Fig. 4.3A and B); this may be explained by the possibility that rapamycin treatment enhanced the overall autophagic flux, and Lc3-II was rapidly degraded in lysosomes under these conditions (95). Therefore, we simultaneously treated embryos with rapamycin and lysosomal protease inhibitors, and in this case observed an increase in Lc3-II levels. To determine if the change in Lc3-II level was dependent on autophagy machinery, we used 3-methyladenine (3-MA), which inhibits the class III phosphatidylinositol 3-kinase (PtdIns3K) and autophagosome formation. 3-MA treatment blocked the increase in the Lc3-II/Lc3-I ratio seen with rapamycin in the presence of lysosomal protease inhibitors, confirming that the Lc3-II upregulation was a consequence of autophagy (Fig. 4.3).

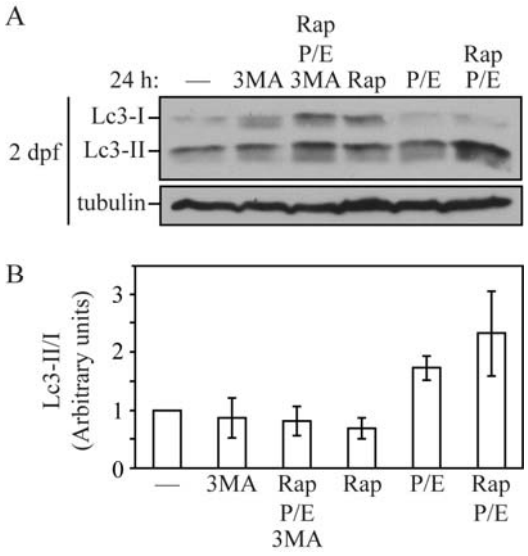

Figure 4.3. Lc3-II accumulates in response to rapamycin and lysosomal inhibitor treatment. (A) GFP-Lc3 embryos at 2 dpf were treated with the indicated chemicals or the solvent DMSO (—) for 24 h. Protein extracts were analyzed by SDS-PAGE and detected using anti-LC3, or anti-tubulin antibody as a loading control. (B) The Lc3-II to Lc3-I ratio in (A) was quantified using ImageJ software (http://rsb.info.nih.gov/ij/). The value for DMSO-treatment was set to 1.0 and other values were normalized. Error bars represent the standard deviation (s.d.) of three independent experiments. Rap, rapamycin; 3MA, 3-methyladenine; P/E, pepstatin A and E64d.

Generation of GFP-Lc3 and GFP-Gabarap transgenic zebrafish

To extend our in vivo analysis of autophagy in live embryos, we generated transgenic zebrafish lines expressing an N-terminal green fluorescent protein (GFP)-fused Lc3 (GFP-Lc3) under the control of the constitutive CMV (human cytomegalovirus) promoter (Fig. 4.4A). The transgenic line showed no developmental or adulthood abnormalities. GFP-Lc3 transgene expression was visualized from the early cleavage stage and throughout adulthood (Fig. 4.4B). The expression of GFP-Lc3 was observed in various tissues, with the highest expression in muscle, lens and spinal cord. We also generated a GFP-Gabarap transgenic line (Fig. 4.4), to study whether Gabarap participates in autophagy in vivo. The GFP-Gabarap transgene showed a similar expression pattern as GFP-Lc3.

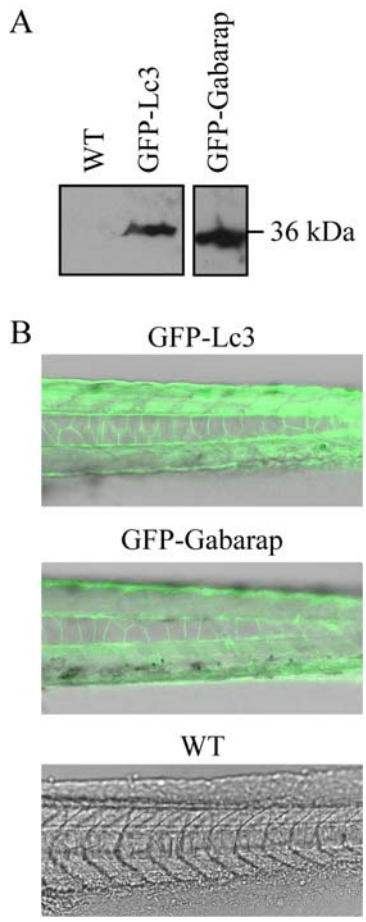

Figure 4.4. Generation of GFP-Lc3 and GFP-Gabarap transgenic zebrafish. (A) GFP-Lc3 and GFP-Gabarap transgene expression was confirmed by western blot of protein lysates from GFP-Lc3, GFP-Gabarap or non-transgenic wild-type (WT) embryos using anti-GFP antibody. (B) GFP-Lc3, GFP-Gabarap or non-tagged wild-type embryos were observed by confocal fluorescence microscopy and merged with bright-field images.

Basal autophagy in zebrafish embryos can be further upregulated by rapamycin or calpeptin

Using the GFP-Lc3 line, we examined autophagic responses in zebrafish embryos. We found that LysoTracker Red, which accumulates in acidic organelles in living cells, could successfully stain lysosomes in live embryos when supplied in water (Fig. 4.5A). Embryos at the hatching period contained a number of lysosomes, which were further induced upon rapamycin treatment. Even though basal levels of autophagy were easily

detected by western blot of Lc3 (Fig. 4.3), we observed very few GFP-Lc3 punctate dots (indicative of autophagosomes) prior to drug treatment, whereas following rapamycin treatment the GFP-Lc3 puncta increased; however, these puncta did not display extensive colocalization with LysoTracker Red. When lysosomal protease inhibitors were also added, the total number of puncta increased as did the extent of colocalization. This result suggested that although formation of GFP-Lc3 puncta could be induced by rapamycin alone, the chimeric protein was degraded within the lysosome except in the presence of lysosomal protease inhibitors, again indicating the occurrence of autophagic flux. The colocalization of GFP-Lc3 puncta with lysosomes was also dramatically increased when embryos were treated with pepstatin A and E64d alone, supporting the idea that basal autophagic flux is high in embryos. In addition, 3-MA suppressed the accumulation of Lc3-positive puncta in the presence of lysosomal inhibitors and rapamycin, whereas lysosomes in embryos seemed not affected by 3-MA (Fig. 4.5A). We further quantified the colocalization of Lc3 puncta with lysosomes (Fig. 4.5B), and the results suggest that formation of GFP-Lc3 puncta correlates with conversion of endogenous Lc3-I to Lc3-II (Fig. 4.3).

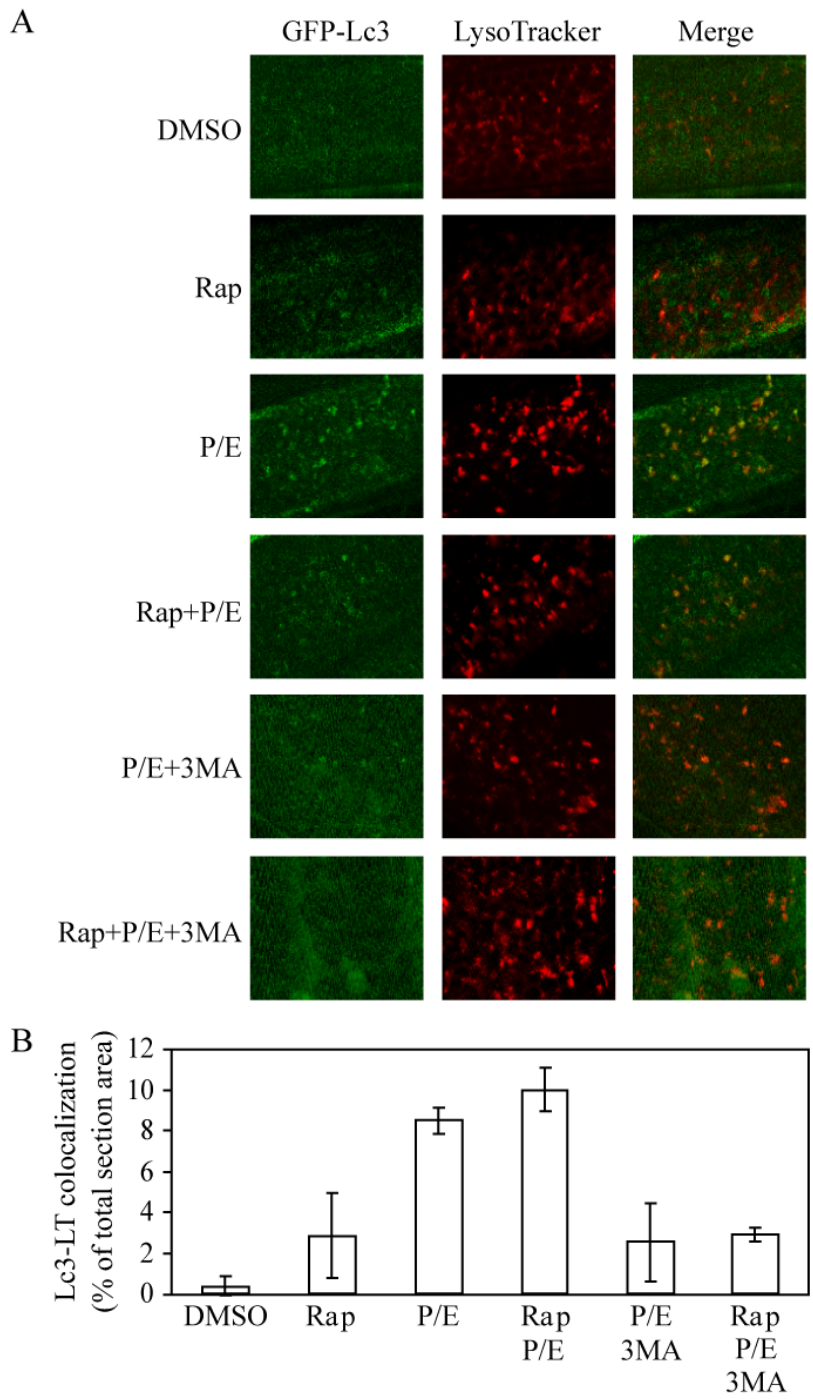

Figure 4.5. GFP-Lc3 puncta formation and lysosome colocalization are induced by rapamycin and lysosomal inhibitors. (A) GFP-Lc3 embryos at 3 dpf were treated with the indicated chemicals or DMSO for 24 h, and then stained with LysoTracker Red for 1 h before imaging by confocal fluorescence microscopy. (B) Colocalization of GFP-Lc3 puncta with LysoTracker Red (LT) in (A) was quantified using Leica Simulator SP5 software. Rap, rapamycin; 3MA, 3-methyladenine; P/E, pepstatin A and E64d.

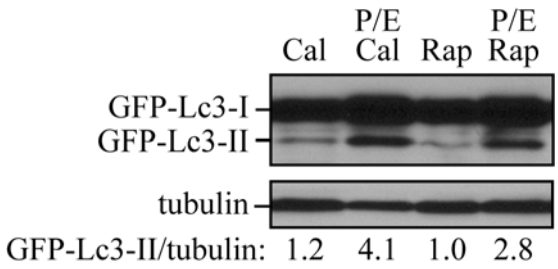

Figure 4.S1. Calpeptin or rapamycin enhance autophagic flux. GFP-Lc3 embryos at 2 dpf were treated with the indicated chemicals for 24 h. Protein extracts were analyzed by SDS-PAGE and detected using anti-LC3, or anti-tubulin antibody as a loading control. The ratio of GFP-Lc3-II versus tubulin was quantified using ImageJ software (http://rsb.info.nih.gov/ij/) and indicated below each lane. The value for rapamycin treatment was set to 1.0 and other values were normalized. Cal, calpeptin; Rap, rapamycin; P/E, pepstatin A and E64d.

A recent study revealed a TOR-independent pathway that can enhance autophagy (223). In this case, adenylyl cyclase produces cyclic AMP, which locally increases intracellular Ca^{2+} levels and calpain activity. This further results in cleavage and activation of the small G protein $G_{s\alpha}$, which in turn activates adenylyl cyclase, causing a loop that inhibits autophagy. Various chemicals have been tested to target different steps in this pathway to induce autophagy, including 2'5'-ddA (adenylyl cyclase inhibitor), verapamil (L-type Ca+ channel antagonist), calpeptin (calpain inhibitor) and clonidine (G_i protein activator). We decided to examine the effects of these chemical inducers on autophagy in zebrafish embryos. The calpain inhibitor calpeptin appeared to be very potent for inducing formation of Lc3-positive puncta and autolysosomes, as judged by the colocalization of GFP-Lc3 and LysoTracker Red (Fig. 4.6A and B). Conversion of endogenous Lc3 was also upregulated by calpeptin (Fig. 4.6C). The other treatments had less dramatic (2'5'-ddA and verapamil) or essentially no effect (clonidine) on autophagy at the concentrations and times used in this analysis. We also confirmed the conversion of the GFP-Lc3 fusion protein by examining embryos treated with rapamycin or calpeptin, although GFP-Lc3 was overexpressed and largely present as the unconjugated form (Fig.

4.6D). However, the level of GFP-Lc3-II was dramatically increased when rapamycin or calpeptin were added in the presence of lysosomal protease inhibitors (Fig. 4.S1), in agreement with our previous results examining Lc3-II levels (Fig. 4.3). Finally, compared with the no treatment control, the concentrations and time used in the chemical treatments did not induce apparent apoptotic cell death, as assessed by staining with the vital dye acridine orange (Fig. 4.S2). Thus, we established two pharmacological strategies to effectively upregulate autophagy in zebrafish embryos, that is, targeting either TOR or the TOR-independent autophagy pathway by rapamycin or calpeptin, respectively.

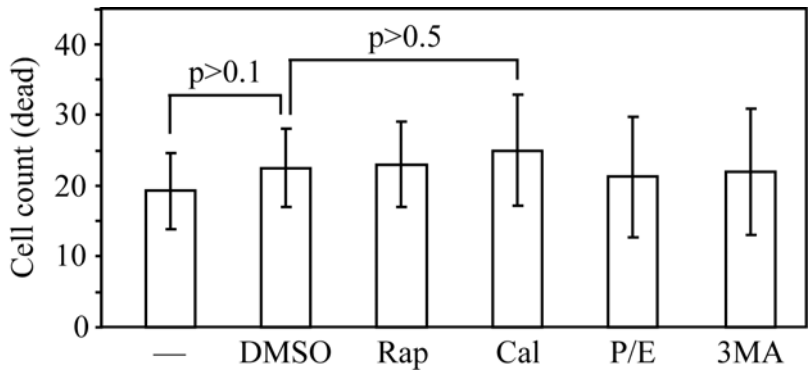

Figure 4.S2. Quantification of cell death by acridine orange staining. 2 dpf non-transgenic wild-type embryos were raised in the embryo water with or without the indicated solvent (DMSO) or chemicals (at the concentrations mentioned in Materials and Methods) for 24 h and stained with acridine orange. Images of each embryo from the cloaca to the two-thirds distance towards the tail tip were taken by fluorescence microscopy. The number of acridine orange-stained cells was counted manually and represented as mean ± s.d. of four embryos. Significance was calculated by a non-paired samples *t*-test. Rap, rapamycin; Cal, calpeptin; P/E, pepstatin A and E64d; 3MA, 3-methyladenine.

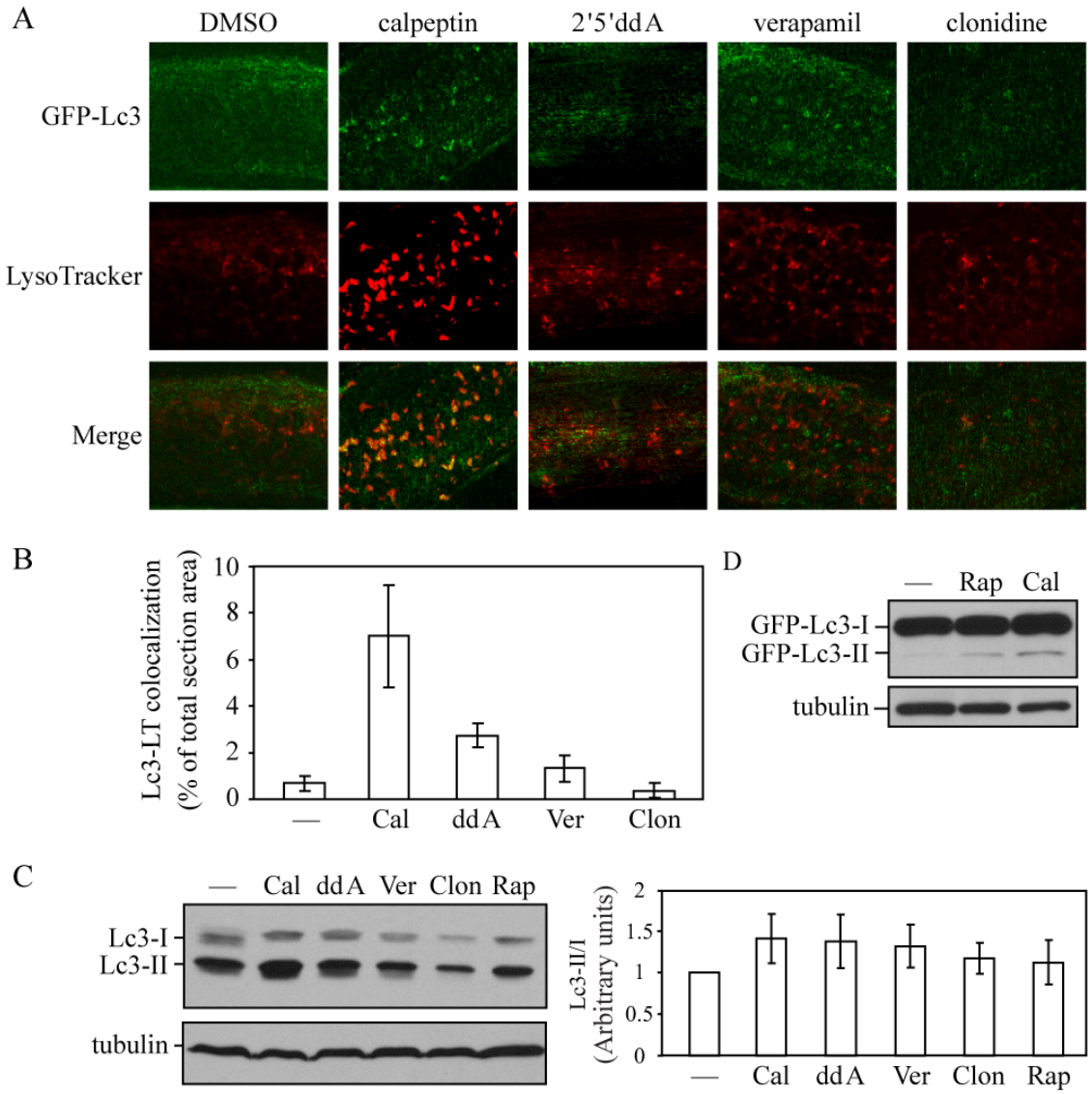

Figure 4.6. Autophagy is upregulated in response to chemical inducers functioning independently of the TOR pathway. (A) GFP-Lc3 embryos at 3 dpf were treated with the indicated drugs or DMSO for 24 h, and then stained with LysoTracker Red for 1 h before imaging by confocal fluorescence microscopy. (B) Colocalization of GFP-Lc3 dots with LysoTracker Red (LT) in (A) was quantified using Leica Simulator SP5 software. (C and D) Wild-type (C) or GFP-Lc3 (D) embryos at 2 dpf were treated with the indicated chemicals or the solvent DMSO (—) for 24 h. Protein extracts were analyzed by SDS-PAGE and detected by western blot using anti-LC3, or anti-tubulin antibody as a loading control. (C, right) The relative increase of the Lc3-II/Lc3-I ratio induced by chemicals was quantified by ImageJ software (http://rsb.info.nih.gov/ij/) and represented as mean ± s.d. of three independent experiments. The value of Lc3-II/Lc3-I from the DMSO-treated sample was set to 1.0 and other values were normalized. Rap, rapamycin; Cal, calpeptin.

Gabarap accumulates within lysosomes under autophagy-inducing conditions

Whether another mammalian Atg8 homolog, GABARAP, is involved in autophagy is controversial. Previously, one paper shows that overexpressed mammalian GABARAP is subject to lipidation by the same machinery as LC3 and localizes to autophagosome membranes under starvation conditions (77), whereas another group reports that puncta formation and lysosomal turnover of endogenous GABARAP is not activated during starvation-induced autophagy (208). Notably, different cell culture lines were used in these reports.

In order to address this discrepancy in vivo, we analyzed the localization of Gabarap under autophagy-inducing conditions using the GFP-Gabarap transgenic embryos. We treated 3 dpf embryos with rapamycin and lysosomal inhibitors for 24 h, and stained them with LysoTracker Red. Rapamycin triggered GFP-fused Gabarap puncta formation and translocation to lysosomes, which were enhanced in the presence of lysosomal protease inhibitors (Fig. 4.7A and B). However, puncta formation of Gabarap was not as significant as that of Lc3, although colocalization with LysoTracker Red was similar, indicating that Gabarap may localize to a lesser degree than Lc3 on autophagosomal membranes (Fig. 4.5B versus 4.7B). In addition, western blotting showed that the GFP-Gabarap fusion protein possessed two forms, and the conversion from form I to II was also induced by calpeptin (Fig. 4.7C). We found that there was evidence for a low level of autophagic flux based on treatment with lysosomal protease inhibitors, suggesting that the overall rate of turnover was quite low. Therefore, in zebrafish embryos, Gabarap was likely turned over constitutively, but at a low level, within lysosomes, and during autophagy induction its lysosomal accumulation increased.

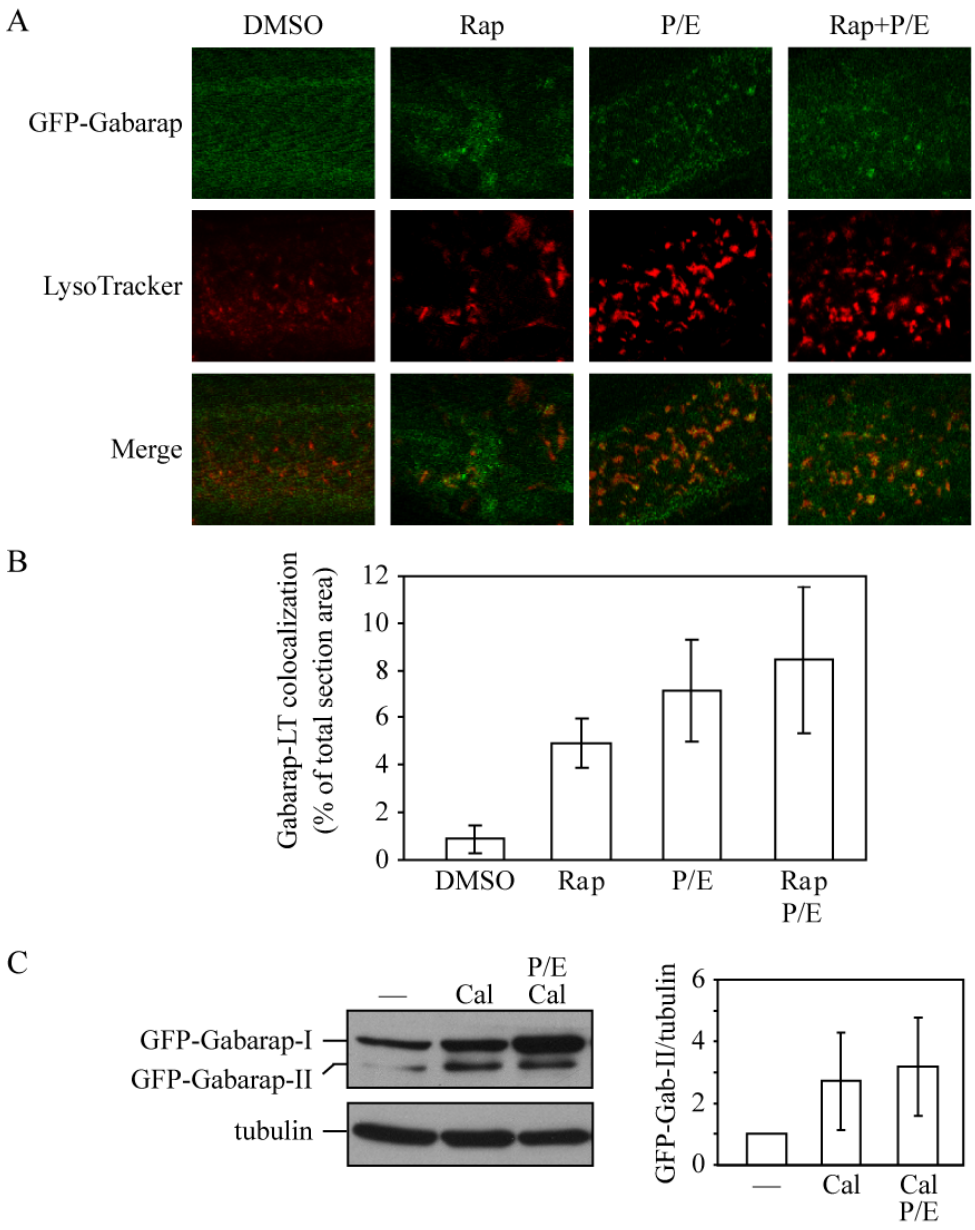

Figure 4.7. Gabarap accumulates within lysosomes after treatment with rapamycin and lysosomal inhibitors. (A) GFP-Gabarap embryos at 3 dpf were treated with the indicated chemicals or DMSO for 24 h, and then stained with LysoTracker Red for 1 h before imaging by confocal fluorescence microscopy. (B) Colocalization of GFP-Gabarap puncta with LysoTracker Red (LT) in (A) was quantified using Leica Simulator SP5 software. (C, left) GFP-Gabarap embryos at 2 dpf were treated with the indicated chemicals or the solvent DMSO (—) for 24 h. Protein extracts were analyzed by SDS-PAGE and detected using anti-GABARAP, or anti-tubulin antibody as a loading control. (C, right) The relative increase of the GFP-Gabarap-II/tubulin ratio induced by chemicals was quantified by ImageJ software (http://rsb.info.nih.gov/ij/). The value of GFP-Gabarap-II versus tubulin from the DMSO-treated sample was set to 1.0 and other values were normalized. Error bars represent the s.d. of three independent experiments. Rap, rapamycin; Cal, calpeptin; P/E, pepstatin A and E64d.

Discussion

Due to its optical clarity and short development time, zebrafish are ideal for studying development. Through a BLAST search, we found that homologs of multiple autophagy-related genes, including *ulk1*/*atg1*, *atg2*, *atg3*, *atg4*, *atg5*, *beclin 1*/*atg6*, *atg7*, *lc3*/*atg8*, *atg9*, *atg12* and *atg16* are present in the zebrafish genome, which suggests that this organism may be useful as a model system for studying the function and mechanism of autophagy. It has recently been reported that autophagy is required in mice for preimplantation embryonic development; autophagosomes are observed in GFP-LC3 mouse embryos at the one- to four-cell stage, and autophagy-defective embryos fail to develop beyond the four- and eight-cell stage (214). In contrast to zebrafish development that proceeds quickly after fertilization, mammalian development progresses relatively slowly. It is unknown if autophagy is required during the one- to four-cell stage in non-mammalian vertebrates such as fish, amphibians, or birds; however, it is unlikely that zebrafish undergo autophagy during the 1-4 cell stages as *ulk1a*, *ulk1b*, *atg9a*, and *atg9b* (genes that are presumably required for autophagy as they are in other organisms) were not expressed in 0 hpf embryos (Fig. 4.2C). However, by 24 hpf *ulk1a*, *ulk1b*, *atg9b*, and to a lesser extent *atg9*a transcripts were easily detected. PE-conjugated Lc3 was not seen in 24 hpf embryos, but Lc3-II was clearly observed by 48 hpf. The appearance of transcripts for genes necessary for autophagy by 24 hpf, the subsequent appearance of PE-conjugated Lc3 by 48 hpf, and the high basal level of autophagy by the 48 hpf time point opens the possibility that autophagy may play a role in zebrafish development during later developmental stages.

In recent years autophagy has been shown to play multiple important roles in human health and pathology (59, 120, 126). Therefore, it is likely that chemical screens for compounds that regulate autophagy, and subsequent dissection of the mechanisms involved, will become an important area of research. Indeed a screen using a panel of 253 compounds was recently performed to identify drugs that induce autophagy (223). As a secondary screen these researchers used a zebrafish Huntington disease model to determine if these drugs caused clearance of aggregate-prone proteins, but they did not directly show autophagy induction in zebrafish (223). Here, we have shown for the first time that aqueous administration of rapamycin, calpeptin and 2'5'-ddA, and to a lesser extent verapamil, induce autophagy (Fig. 4.3 and 4.6). Our findings not only provide the first instance of monitoring chemical upregulation of autophagy in zebrafish, but also corroborate the hypothesis that these drugs induce autophagy in this system. Because drug administration can be achieved simply by aqueous exposure, zebrafish would be an ideal organism for primary or secondary in vivo small molecule screens for compounds that regulate autophagy (7, 164).

The optical transparency of zebrafish combined with their external development make them an ideal organism for in vivo microscopy analysis, especially during the developmental period. We therefore have created transgenic GFP-Lc3 and GFP-Gabarap zebrafish lines. Both GFP-Lc3 and GFP-Gabarap accumulate in lysosomes in response to drug treatment, suggesting these GFP-tagged Atg8 homologs are incorporated into autophagosomes as found in other organisms. These fish will provide an essential tool for the study of autophagy in zebrafish by allowing monitoring of autophagosome formation in this model system as has been done in other organisms.

Materials and methods

Zebrafish strains and maintenance

The AB and local strains of wild-type fish were used in this study. Embryos were collected from pairwise matings of adults and raised at 28.5°C. Larvae were staged according to morphological features previously described (90).

Cloning and RT-PCR

Total RNA was extracted from zebrafish embryos using Trizol (Invitrogen, USA). Reverse transcription was performed using oligo-dT and SuperScript II (Invitrogen, USA), and PCR reactions using the Phusion High Fidelity DNA polymerase (New England Biolabs, USA). Zebrafish *lc3*, *gabarap*, *ulk1a*, *ulk1b*, *atg9a*, *atg9b* and *beclin 1* were identified by a BLAST search of the zebrafish genomic database with mammalian homologs of autophagy genes. RT-PCR primers were designed based on the BLAST search results and the products were sequenced to confirm the homology. Primer sequences are available upon request.

Generation of transgenic zebrafish

gabarap was cloned into the pEGFP-C1 vector (Clontech, USA) using EcoRI and KpnI. The fragment containing the CMV promoter, GFP-Gabarap and the polyA sequence was then released using AseI and MluI, blunted by the Klenow enzyme and ligated into the pminiTol2 vector linearized by EcoRV, resulting in pminiTol2-GFP-

Gabarap. For construction of pminiTol2-GFP-Lc3, the *gabarap* gene was replaced by *lc3* introduced into the vector using XhoI and XmaI.

pT3TS-Tol2 was linearized by XbaI and transcribed with T3 RNA polymerase using the Ambion mMESSAGE mMACHINE® kit (Ambion, USA) to produce Tol2 transposase mRNA. Approximately 25 ng of plasmid DNA (pminiTol2-GFP-Lc3 or pminiTol2-GFP-Gabarap) and 100 ng of Tol2 mRNA were coinjected into newly fertilized embryos at the one-cell stage to produce transgenic fish. Injected embryos were raised to adulthood and out-crossed to wild-type fish to identify transgenic founders.

Immunoblotting

Embryos were dechorionated, deyolked, and homogenized in SDS loading buffer. After being boiled at 95ºC for 5 min, embryo lysates were resolved on 10% or 15% gels and probed by western blot with anti-LC3 (NB100-2331, Novus Biologicals, USA), anti-GABARAP (206) or anti-tubulin (Sigma, USA) antibodies. The specificity of the LC3 antibody NB100-2331 to Lc3 was confirmed by detecting GFP-Lc3 with both NB100-2331 and an anti-GFP antibody.

Drug treatment

Drug treatment was performed in 24-well plates. The following chemicals dissolved in DMSO were added to the embryo water at the final concentrations indicated in parentheses: rapamycin (1 μM), calpeptin (50 μM), 2'5'-dideoxyadenosine (2'5'-ddA; 100 μM), verapamil (3 μM), clonidine (3 μM), pepstatin A (10 μg/ml) and E64d (5

μg/ml). 3-methyladenine was dissolved in water as a 0.33 M stock and used at a final concentration of 10 mM.

LysoTracker assay

Embryos were incubated for 1 h in embryo water with 10 μM LysoTracker Red (Invitrogen, USA), and rinsed several times with fresh water before imaging by confocal microscopy.

Acridine orange staining assay

Post-fertilization embryos at 2 days were subject to 24 h-chemical treatment and stained with acridine orange as previously reported (215). Four embryos from each treatment were collected, washed three times with fresh water and imaged on an Olympus IX71 fluorescence microscope using the GFP filter at a magnification of 20X.

Confocal fluorescence microscopy

Embryos were transferred into 0.003% (w/v) 1-phenyl-2-thiourea prior to 24 hours post-fertilization to prevent pigmentation. They were mounted live in water containing 0.16 mg/ml tricaine (Sigma, USA) for imaging. Images were taken using the Leica SP5 confocal system under a 40X water immersion lens.

Quantitative analyses of colocalization of GFP-Lc3 or GFP-Gabarap with LysoTracker Red signals were performed with images using the Leica Simulator SP5 software. Since GFP-Lc3 and GFP-Gabarap showed both a uniform cytosolic signal and more intense spots, threshold values were set to reduce the cytosolic signal and identify

the more intense dots. The same threshold value was applied for all samples in an indicated experiment. The amount of colocalization between LysoTracker Red signals and GFP-Lc3 or GFP-Gabarap dots was quantified in three independent visual fields from three independent embryos. The Y-axis represents the percentage of the colocalization area per visual field. All values are represented as mean ± standard deviation (s.d.).

CHAPTER 5

Summary and perspectives

Yeast autophagy and Atg9

Autophagy is a so-called "self-eating" process in eukaryotic cells induced by stress, for example, starvation, hypoxia and infection. Macromolecules from autophagic degradation are released from the vacuole and used for the synthesis of critical proteins and the maintenance of vital cellular functions during starvation. Under other stress conditions, such as those resulting in damaged or dysfunctional organelles, autophagy may protect cells from further damage by sequestering these compartments from the remainder of the cytoplasm.

Autophagosome biogenesis is considered a de novo process, in which small membranes are sequentially added onto the phagophore, the initial sequestering structure, leading to expansion and ultimately the formation of a completed autophagosome (128). In budding yeast, this process occurs at a distinct perivacuolar site, known as the preautophagosomal structure or phagophore assembly site (PAS).

How the rapid membrane remodeling that is characteristic of autophagosome biogenesis is achieved remains a fundamental open question. To elucidate the molecular mechanism, I focus on the autophagy-related (Atg) protein Atg9. Atg9 is unique among

the current 31 characterized Atg proteins, in that it is the only transmembrane protein required for autophagosome formation, and displays a relatively distinct subcellular localization pattern. Atg9 is present both at the PAS and at multiple peripheral structures; Atg9 partially localizes at mitochondria and possibly at the Golgi complex, both of which may provide membranes to the forming autophagosome (72, 168, 239). In Chapter 2, I proposed a cycling model in which Atg9 shuttles between the peripheral sites and the PAS, supported by live imaging studies showing Atg9 movement in the cytoplasm and by the finding of several Atg factors that play a role in Atg9 delivery to and retrieval from the PAS (54, 130, 169). The anterograde transport of Atg9 from the peripheral sites to the PAS may function in delivering lipid and proteins to the site of vesicle formation, and retrieval of Atg9 from the PAS may recycle the protein back to the membrane origin for the next round of delivery.

Atg9 transport to the PAS is mediated by Atg11

Several components have been shown to be required in Atg9 retrieval from the PAS, including the Atg1-Atg13 complex, Atg2, Atg18, and the phosphatidylinositol 3-kinase complex (93). An intriguing question is what factors regulate the anterograde transport of Atg9 to the site of vesicle formation. For this purpose, we performed a yeast two-hybrid screen among all identified Atg proteins and found several Atg9 interacting partners, including Atg11, Atg23 and Atg27. I found that anterograde transport of Atg9 to the PAS is blocked in *atg11*Δ or *atg1*Δ *atg11*Δ yeast mutants (54). Through random mutagenesis experiments, I obtained a point mutation H192L in the Atg9 N-terminal domain that disrupts its interaction with Atg11, but maintains Atg9 interaction with

Atg23 or Atg27 (data not shown). Identification of the specific mutation is important for functional studies, because data from our lab have suggested that Atg23 and Atg27 are also involved in Atg9 transport from mitochondria to the PAS (105, 232). The H192L mutation is located within the minimal sufficient region for Atg9-Atg11 interaction (amino acids 159-255, which map to the central part of the Atg9 N-terminal arm), assayed by yeast two-hybrid analysis. H192L also locates to the minimal required region for interaction (amino acids 154-201) reported in a parallel paper (19).

Using the $Atg9^{H192L}$ mutant, I found that the Atg9-Atg11 interaction is necessary for the recruitment of Atg9 to the PAS and normal progression of selective autophagy (the Cvt pathway) during vegetative growth, but is not required in bulk autophagy under starvation conditions or with rapamycin treatment (a drug that mimics starvation conditions and induces bulk autophagy). This finding suggests that different mechanisms may be involved in these two fundamental processes, which is consistent with our previous finding that Atg11 is specific for selective autophagy (87). In addition, we demonstrate that the integrity of the actin cytoskeleton is essential for correct targeting of Atg11 to the PAS. We previously reported that actin is also required for proper Atg9 transport to the PAS (167). In the *atg9*Δ mutant, Atg11 localizes to the PAS as in wild-type cells; in contrast, Atg9 is retained on its peripheral compartments in the absence of Atg11, suggesting that Atg11 localization to the PAS is not dependent upon the Atg9-Atg11 interaction, whereas Atg9 localization requires interaction with Atg11. Taken together, I concluded that Atg11 mediates the movement of Atg9 to the PAS, but not vice versa.

Accordingly, I proposed that the anterograde transport of Atg9 may serve as a membrane shuttle for vesicle assembly during selective autophagic pathways and that movement from the peripheral compartments to the PAS is facilitated by Atg11, Atg23 and Atg27 along the actin cytoskeleton (Fig. 2.9) (54).

Atg11: A scaffold protein

Atg11 is a peripheral membrane protein, predicted to contain four coiled-coil domains that support interactions with multiple Atg proteins (234). I found that Atg9-Atg11 interaction is mediated through the Atg9 N-terminal cytosolic domain and the second coiled-coil domain of Atg11. In addition to Atg9, Atg11 also independently interacts with the prApe1 and Ams1 receptor Atg19, and with the Atg1-Atg13 complex that is involved in vesicle formation. This finding suggests that there may be multiple pools of Atg11 in the cell, recruiting cargos and membrane components to the vesicle forming machinery at the PAS.

In collaboration with Dr. Iryna Monastyrska in our lab, I found that several mutants defective in the Arp (actin-related protein) 2/3 complex, which nucleates branching of actin filaments, block Atg9 trafficking and autophagy activity, by screening a temperature-sensitive yeast library (130). Using the $Atg9^{H192L}$ mutant, we showed that the interaction between Atg9 and Atg11 is essential for Atg9 binding Arp2 and Atg9 movement. Thus, these data proposed that the Arp2/3 complex may serve a function of determining the direction of Atg9-Atg11 traveling along the cytoskeletal network.

Non-mitochondrial peripheral pools of Atg9

So far, the membrane source of autophagosomes is not clear. The finding in Chapter 2 raises the hypothesis that mitochondria act as a membrane source in autophagy. Certain morphological observations support this possibility. For example, during macropexophagy in the methylotrophic yeast *Hansenula polymorpha* (82), or upon invasion of the bacterium *Legionella pneumophila* into macrophages (211), sequestering membranes or phagosomes are surrounded by and closely associated with mitochondria. It should be noted that the mitochondrial pool of Atg9 only counts for approximately 40% of the total cellular Atg9. The identity of the other peripheral compartments where Atg9 resides is not known. It is possible that Atg9 is sorted through the secretory pathway and directed to multiple organelles or membranous structures. In wild-type yeast under steady state conditions, Atg9 does not reside in the ER, endosomes, peroxisomes, vacuole, or plasma membrane (86, 168); however, it is possible that localization to the ER is only transient.

Other data from our lab suggests that Atg9 partially cofractionates with a Golgi marker protein by density gradient analysis (232). In addition, Atg27, an Atg9 binding partner that recruits Atg9 to the PAS, localizes to the PAS, mitochondria, and mostly to the Golgi complex. Thus, it is tempting to speculate that Atg9 and Atg27 may colocalize in part at this latter site. A study in mammalian cells suggests that mammalian Atg9 traffics between the *trans*-Golgi network (TGN) and endosomes (239). Based on the conservation between mammalian and yeast Atg9, the Golgi complex would be the best candidate as another non-PAS compartment in which Atg9 localizes.

Membrane delivery during pexophagy

Another specific type of autophagy is pexophagy. During yeast pexophagy, excess peroxisomes induced by oleic acid as the sole carbon source are selectively degraded through autophagy in the vacuole, after cells are shifted back to glucose medium. Compared with bulk autophagy and the Cvt pathway, pexophagy is less characterized in *S. cerevisiae*. Both micro- and macropexophagy have been identified in the methylotrophic yeasts (49, 82). During micropexophagy, peroxisomes targeted for destruction are engulfed by projections extended directly from the vacuolar membrane; while in macropexophagy, peroxisomes are sequestered by membranes that are of a non-vacuole origin and subsequently released into the vacuole, similar to the process in autophagy. It is not clear which mechanism(s) *S. cerevisiae* uses for degradation of peroxisomes.

I found that with the $Atg9^{H192L}$ mutant, pexophagy proceeds normally (Fig. 5.1), which is consistent with the finding from a report that examined a truncated Atg9 mutant lacking N-terminal amino acids 154-201 that loses interaction with Atg11 (19). My finding suggests that although Atg9 and Atg11 are both required for pexophagy in *S. cerevisiae*, the interaction between the two proteins does not seem essential for the process in this organism. The result supports a hypothesis that peroxisome uptake may occur through a micropexophagic mode in *S. cerevisiae* because the membrane source for sequestration would primarily be the vacuole, and dependence of pexophagy on Atg9 transport would be minimal.

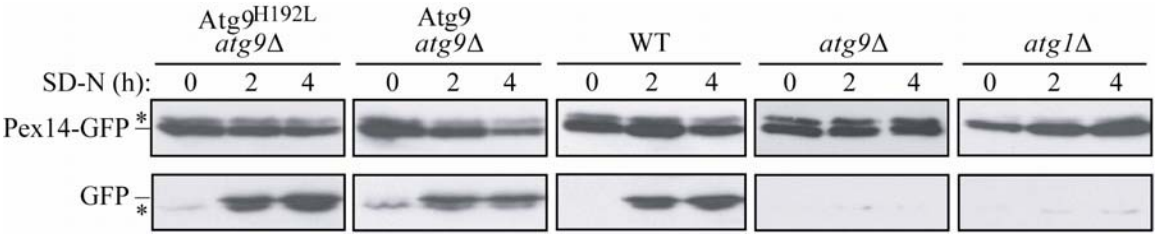

Figure 5.1. Pexophagy is not disrupted by loss of Atg9-Atg11 interaction. An *atg9*Δ strain expressing an integrated Pex14-GFP fusion was transformed with a plasmid encoding either wild-type Atg9 or Atg9^{H192L}. Cells were grown in medium containing oleic acid as the sole carbon source and shifted to glucose-rich, nitrogen-limiting conditions (SD-N). At the indicated time points, aliquots were taken, and protein extracts were analyzed by western blot using anti-GFP antibody. Cleavage of Pex14-GFP to generate free GFP is a measure of vacuole-dependent peroxisome degradation. The positions of Pex14-GFP and free GFP are indicated. Wild-type, *atg1*Δ and *atg9*Δ strains expressing the integrated Pex14-GFP fusion were used as controls. The asterisks mark nonspecific bands.

Atg9 self-interaction is essential for autophagosome formation

During my study of Atg9 trafficking, I noticed that fluorescent-tagged Atg9 is organized in large clusters, suggesting that the protein might self-interact. In addition, I found that two different fusion chimeras, Atg9-GFP and Atg9-DsRed, largely colocalize. In Chapter 3, I confirmed the self-interaction by yeast two-hybrid analysis and coimmunoprecipitation, and further mapped the interaction site to the C terminus of Atg9. Autophagy was blocked when I mutated this site by deleting conserved five amino acids (Atg9Δ766-770) (52).

Similar to wild-type Atg9, this loss-of-self-interaction mutant partially localizes to mitochondria (data not shown), but its delivery to the PAS is less efficient (52). What is the possible cause of this transport defect? On the mitochondrial surface, the wild-type Atg9 clusters undergo highly dynamic movement (168), which is reminiscent of lipid rafts that form in the membrane of the TGN: selected membrane protein cargos accumulate in the rafts, and then bud from the TGN into transport vesicles. Raft-like microdomains have also been suggested to form on the mitochondrial outer-membrane,

playing a role in signal transduction (41, 122). Given the recent discovery of mitochondria-derived vesicles (138), I speculate that Atg9 molecules are concentrated into clusters that are organized by self-association at the membrane sources, and this process may be essential for efficient trafficking of the protein (similar to the budding events in the secretory pathway and at the plasma membrane; Fig. 5.2). Future studies are important to analyze the underlying mechanism that triggers such movement.

Data in Chapter 2 showed that Atg9 delivery to the PAS is mediated by Atg11 (54). I found that overexpressing Atg11 enhanced the trafficking of the loss-of-self-interaction Atg9 mutant to the PAS. However, autophagy activity was still defective, which suggests that there must be a second function for Atg9 self-interaction at the phagophore assembly site. By fluorescence microscopy, I observed a cup-shaped structure formed by wild-type Atg9 around the cargo RFP-Ape1, in *atg1*Δ cells. This structure was presumably the growing phagophore, which is unable to complete the autophagosome formation process due to loss of Atg1. Although resolution by fluorescence microscopy is limited, it appeared that the phagophore structure was abnormal in cells expressing the Atg9 self-interaction mutant. To gain additional insight, we examined the phagophore in *atg1*Δ cells by immunoelectron microscopy. The phagophore membranes associated with Atg9Δ776-770 appeared to be more fragmented, and less total membrane was present at the presumed PAS. These results suggest that Atg9 self-interaction has a direct role in phagophore formation. Membrane tethering and fusion usually require the function of SNAREs and Rab family proteins, but no one has yet demonstrated the direct involvement of these factors in autophagosome formation. Here, I proposed a membrane-supplying and tethering mechanism involving Atg9 during

autophagy, possibly in cooperation with several other autophagy-related proteins that associate with lipids, such as Atg8, and in mammalian cells, Bif-1 (134, 201). On the other hand, the ability to form cup-shaped phagophores in *atg1*Δ cells indicates that Atg1 (and its kinase activity) may be dispensable for autophagy induction; together with our finding that Atg1 kinase-defective mutants block the retrieval of Atg9 from the PAS (our unpublished results), the kinase activity of Atg1 seems to have a function at a later step(s) of autophagosome formation.

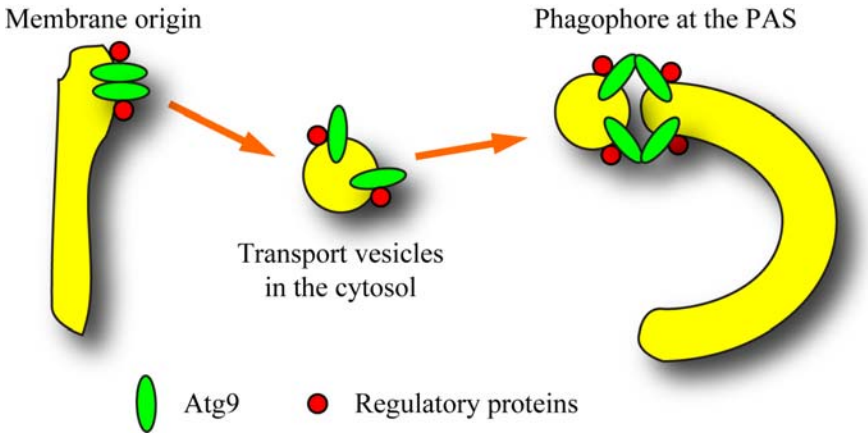

Figure 5.2. Possible roles of Atg9 self-association during autophagosome formation. Atg9 forms clusters on the surface of membrane sources through self-interaction, which promotes its trafficking to the PAS. Regulation of assembly and disassembly of the Atg9 complex by additional components allows the Atg9-containing vesicles to fuse with the existing phagophore membrane, which leads to phagophore expansion.

Identification of components in the Atg9 complex

The loss-of-self-interaction mutant Atg9 did not migrate as a monomer under native conditions, suggesting that other binding proteins may be present in the Atg9 complex. To test this hypothesis, I purified the Atg9 complex by tandem affinity purification and resolved it by SDS-PAGE. Four major protein bands were detected in

our system besides Atg9, migrating at the sizes of 94, 50, 28 and 25 kDa. In the future, it would be interesting to characterize these components and their roles in regulating Atg9 self-interaction during autophagosome formation. Notably, from the reported large-scale proteomic studies in yeast, three non-Atg proteins have been identified to co-purify with Atg9, Ccr4 (94.7 kD), Cdc39 (240 kD) and Tif5 (45.3 kD) (42, 43). Among them, Ccr4 and Cdc39 are components of the CCR4-NOT transcriptional complex involved in regulating transcription and destabilizing mRNAs by deadenylation, and Tif5 is the translation initiation factor eIF-5 with a function as a GTPase-activating protein (GAP) for GTP hydrolysis (27). It is essentially unknown in what manner the transcription and translation complexes may function together with Atg9, but the role of Tif5 as a GAP is intriguing because it may provide a hint to study the energy supply for membrane assembly. Therefore, based on these data, I propose dual roles of Atg9 self-interaction: to promote the flow of membrane from peripheral origins to the PAS and to mediate tethering of small membranes to the forming phagophore, possibly with the help of other regulatory factors (Fig. 5.2). Mass spectrometry, together with in vitro tethering and fusion experiments with the Atg9 C terminus anchored on liposomes, will be helpful to further solve the conundrum of phagophore assembly.

ATG gene homologs in zebrafish

Autophagy occurs during developmental processes in which massive cell clearance is prominent. The zebrafish model provides the advantages of in vivo analyses of autophagy during vertebrate embryogenesis. In Chapter 4, to assay autophagy activity in zebrafish, I identified two zebrafish Atg8 (an autophagosome marker) homologs, *lc3*

and *gabarap*, and generated two transgenic zebrafish lines expressing GFP-tagged versions of the corresponding proteins. Yeast Atg8 or its mammalian homolog LC3 is processed into a cytosolic form, and upon autophagy it is conjugated to PE, which is specifically associated with autophagosomal membranes. Similarly, I found that zebrafish Lc3 undergoes post-translational modification (which represents autophagy induction) starting at an early embryonic developmental stage between 24 hpf and 48 hpf, and observed a high level of basal autophagy activity in zebrafish embryos. Moreover, I developed a small-scale chemical screen for autophagy inducers using zebrafish embryos, and found that basal autophagy can be further upregulated by the TOR inhibitor rapamycin or the calpain inhibitor calpeptin (53). Thus, it is promising to use the zebrafish assay for future large-scale drug screens of in vivo autophagy modulators.

In addition, I cloned several other autophagy genes in zebrafish, *beclin 1*/*ATG6*, two zebrafish *ATG9* homologs (namely *atg9a* and *atg9b*) and two *ATG1* homologs (*ulk1a* and *ulk1b*). I examined temporal and spatial expression patterns of these genes by RT-PCR (Fig. 4.2C) and in situ hybridization (data not shown). *beclin 1*, *atg9a* and *atg9b* are mostly expressed ubiquitously, whereas *ulk1a* mainly expresses in heart, skeletal muscle, branchial arch and cells surrounding the ears, and *ulk1b* expresses highly in the central nervous system, lens and liver. I also performed morpholino knockdown of *ulk1a*, which leads to defective somite and trunk development, pericardial edema and deformed eyes at 24 hpf and 48 hpf (data not shown), consistent with a high expression of *ulk1a* in these tissues. It suggests that autophagy may play an essential role during zebrafish embryogenesis. Future work will focus on more detailed morphological and histological characterization of these defects. Finally, I constructed plasmids overexpressing *ulk1*s,

which could be injected into embryos and be used to study functions of the Ulk1 kinase during development.

REFERENCES

1. Abeliovich H, Darsow T, Emr SD. 1999. Cytoplasm to vacuole trafficking of aminopeptidase I requires a t-SNARE-Sec1p complex composed of Tlg2p and Vps45p. *EMBO J* 18: 6005-16
2. Abeliovich H, Zhang C, Dunn WA, Jr., Shokat KM, Klionsky DJ. 2003. Chemical genetic analysis of Apg1 reveals a non-kinase role in the induction of autophagy. *Mol Biol Cell* 14: 477-90
3. Alessi DR, James SR, Downes CP, Holmes AB, Gaffney PR, et al. 1997. Characterization of a 3-phosphoinositide-dependent protein kinase which phosphorylates and activates protein kinase Bα. *Curr Biol* 7: 261-9
4. Arico S, Petiot A, Bauvy C, Dubbelhuis PF, Meijer AJ, et al. 2001. The tumor suppressor PTEN positively regulates macroautophagy by inhibiting the phosphatidylinositol 3-kinase/protein kinase B pathway. *J Biol Chem* 276: 35243-6
5. Azad MB, Chen Y, Henson ES, Cizeau J, McMillan-Ward E, et al. 2008. Hypoxia induces autophagic cell death in apoptosis-competent cells through a mechanism involving BNIP3. *Autophagy* 4: 195-204
6. Baba M, Osumi M, Scott SV, Klionsky DJ, Ohsumi Y. 1997. Two distinct pathways for targeting proteins from the cytoplasm to the vacuole/lysosome. *J Cell Biol* 139: 1687-95
7. Berger J, Currie P. 2007. The role of zebrafish in chemical genetics. *Curr Med Chem* 14: 2413-20
8. Bernales S, McDonald KL, Walter P. 2006. Autophagy counterbalances endoplasmic reticulum expansion during the unfolded protein response. *PLoS Biol* 4: e423
9. Bjorkoy G, Lamark T, Brech A, Outzen H, Perander M, et al. 2005. p62/SQSTM1 forms protein aggregates degraded by autophagy and has a protective effect on huntingtin-induced cell death. *J Cell Biol* 171: 603-14
10. Brugarolas J, Lei K, Hurley RL, Manning BD, Reiling JH, et al. 2004. Regulation of mTOR function in response to hypoxia by REDD1 and the TSC1/TSC2 tumor suppressor complex. *Genes Dev* 18: 2893-904
11. Budovskaya YV, Stephan JS, Deminoff SJ, Herman PK. 2005. An evolutionary proteomics approach identifies substrates of the cAMP-dependent protein kinase. *Proc Natl Acad Sci U S A* 102: 13933-8
12. Budovskaya YV, Stephan JS, Reggiori F, Klionsky DJ, Herman PK. 2004. The Ras/cAMP-dependent protein kinase signaling pathway regulates an early step of the autophagy process in *Saccharomyces cerevisiae*. *J Biol Chem* 279: 20663-71

13. Byfield MP, Murray JT, Backer JM. 2005. hVps34 is a nutrient-regulated lipid kinase required for activation of p70 S6 kinase. *J Biol Chem* 280: 33076-82
14. Cadwell K, Liu JY, Brown SL, Miyoshi H, Loh J, et al. 2008. A key role for autophagy and the autophagy gene Atg16l1 in mouse and human intestinal Paneth cells. *Nature* 456: 259-63
15. Cao Q, Yu C, Xue R, Hsueh W, Pan P, et al. 2008. Autophagy induced by suberoylanilide hydroxamic acid in Hela S3 cells involves inhibition of protein kinase B and up-regulation of Beclin 1. *Int J Biochem Cell Biol* 40: 272-83
16. Cao Y, Cheong H, Song H, Klionsky DJ. 2008. In vivo reconstitution of autophagy in *Saccharomyces cerevisiae*. *J Cell Biol* 182: 703-13
17. Carew JS, Nawrocki ST, Kahue CN, Zhang H, Yang C, et al. 2007. Targeting autophagy augments the anticancer activity of the histone deacetylase inhibitor SAHA to overcome Bcr-Abl-mediated drug resistance. *Blood* 110: 313-22
18. Chan EYW, Longatti A, McKnight NC, Tooze SA. 2009. Kinase-inactivated ULK proteins inhibit autophagy via their conserved C-terminal domains using an Atg13-independent mechanism. *Mol Cell Biol* 29: 157-71
19. Chang C-Y, Huang W-P. 2007. Atg19 mediates a dual interaction cargo sorting mechanism in selective autophagy. *Mol Biol Cell* 18: 919-29
20. Chang Y-Y, Neufeld TP. 2009. An Atg1/Atg13 complex with multiple roles in TOR-mediated autophagy regulation. *Mol Biol Cell* (In press)
21. Chen JL, Lin HH, Kim KJ, Lin A, Forman HJ, Ann DK. 2008. Novel roles for protein kinase Cδ-dependent signaling pathways in acute hypoxic stress-induced autophagy. *J Biol Chem* 283: 34432-44
22. Chen Y, McMillan-Ward E, Kong J, Israels SJ, Gibson SB. 2007. Mitochondrial electron-transport-chain inhibitors of complexes I and II induce autophagic cell death mediated by reactive oxygen species. *J Cell Sci* 120: 4155-66
23. Chen Y, McMillan-Ward E, Kong J, Israels SJ, Gibson SB. 2008. Oxidative stress induces autophagic cell death independent of apoptosis in transformed and cancer cells. *Cell Death Differ* 15: 171-82
24. Chen ZH, Kim HP, Sciurba FC, Lee SJ, Feghali-Bostwick C, et al. 2008. Egr-1 regulates autophagy in cigarette smoke-induced chronic obstructive pulmonary disease. *PLoS ONE* 3: e3316
25. Cheong H, Nair U, Geng J, Klionsky DJ. 2008. The Atg1 kinase complex is involved in the regulation of protein recruitment to initiate sequestering vesicle formation for nonspecific autophagy in *Saccharomyces cerevisiae*. *Mol Biol Cell* 19: 668-81
26. Cheong H, Yorimitsu T, Reggiori F, Legakis JE, Wang C-W, Klionsky DJ. 2005. Atg17 regulates the magnitude of the autophagic response. *Mol Biol Cell* 16: 3438-53
27. Das S, Ghosh R, Maitra U. 2001. Eukaryotic translation initiation factor 5 functions as a GTPase-activating protein. *J Biol Chem* 276: 6720-6
28. Delgado MA, Elmaoued RA, Davis AS, Kyei G, Deretic V. 2008. Toll-like receptors control autophagy. *EMBO J* 27: 1110-21
29. Ding WX, Ni HM, Gao W, Hou YF, Melan MA, et al. 2007. Differential effects of endoplasmic reticulum stress-induced autophagy on cell survival. *J Biol Chem* 282: 4702-10

30. Ding WX, Ni HM, Gao W, Yoshimori T, Stolz DB, et al. 2007. Linking of autophagy to ubiquitin-proteasome system is important for the regulation of endoplasmic reticulum stress and cell viability. *Am J Pathol* 171: 513-24
31. Drubin DG, Jones HD, Wertman KF. 1993. Actin structure and function: roles in mitochondrial organization and morphogenesis in budding yeast and identification of the phalloidin-binding site. *Mol Biol Cell* 4: 1277-94
32. Dunn WA, Jr., Cregg JM, Kiel JA, van der Klei IJ, Oku M, et al. 2005. Pexophagy: the selective autophagy of peroxisomes. *Autophagy* 1: 75-83
33. Epple UD, Suriapranata I, Eskelinen EL, Thumm M. 2001. Aut5/Cvt17p, a putative lipase essential for disintegration of autophagic bodies inside the vacuole. *J Bacteriol* 183: 5942-55
34. Fader CM, Sanchez D, Furlan M, Colombo MI. 2008. Induction of autophagy promotes fusion of multivesicular bodies with autophagic vacuoles in k562 cells. *Traffic* 9: 230-50
35. Farre JC, Manjithaya R, Mathewson RD, Subramani S. 2008. PpAtg30 tags peroxisomes for turnover by selective autophagy. *Dev Cell* 14: 365-76
36. Fass E, Shvets E, Degani I, Hirschberg K, Elazar Z. 2006. Microtubules support production of starvation-induced autophagosomes but not their targeting and fusion with lysosomes. *J Biol Chem* 281: 36303-16
37. Filimonenko M, Stuffers S, Raiborg C, Yamamoto A, Malerod L, et al. 2007. Functional multivesicular bodies are required for autophagic clearance of protein aggregates associated with neurodegenerative disease. *J Cell Biol* 179: 485-500
38. Fujita E, Kouroku Y, Isoai A, Kumagai H, Misutani A, et al. 2007. Two endoplasmic reticulum-associated degradation (ERAD) systems for the novel variant of the mutant dysferlin: ubiquitin/proteasome ERAD(I) and autophagy/lysosome ERAD(II). *Hum Mol Genet* 16: 618-29
39. Fujita N, Itoh T, Omori H, Fukuda M, Noda T, Yoshimori T. 2008. The Atg16L complex specifies the site of LC3 lipidation for membrane biogenesis in autophagy. *Mol Biol Cell* 19: 2092-100
40. Furuta S, Hidaka E, Ogata A, Yokota S, Kamata T. 2004. Ras is involved in the negative control of autophagy through the class I PI3-kinase. *Oncogene* 23: 3898-904
41. Garofalo T, Giammarioli AM, Misasi R, Tinari A, Manganelli V, et al. 2005. Lipid microdomains contribute to apoptosis-associated modifications of mitochondria in T cells. *Cell Death Differ* 12: 1378-89
42. Gavin AC, Aloy P, Grandi P, Krause R, Boesche M, et al. 2006. Proteome survey reveals modularity of the yeast cell machinery. *Nature* 440: 631-6
43. Gavin AC, Bosche M, Krause R, Grandi P, Marzioch M, et al. 2002. Functional organization of the yeast proteome by systematic analysis of protein complexes. *Nature* 415: 141-7
44. Geng J, Klionsky DJ. 2008. The Atg8 and Atg12 ubiquitin-like conjugation systems in macroautophagy. 'Protein modifications: beyond the usual suspects' review series. *EMBO Rep* 9: 859-64
45. Gerhardt B, Kordas TJ, Thompson CM, Patel P, Vida T. 1998. The vesicle transport protein Vps33p is an ATP-binding protein that localizes to the cytosol in an energy-dependent manner. *J Biol Chem* 273: 15818-29

46. Gozuacik D, Bialik S, Raveh T, Mitou G, Shohat G, et al. 2008. DAP-kinase is a mediator of endoplasmic reticulum stress-induced caspase activation and autophagic cell death. *Cell Death Differ* 15: 1875-86
47. Guan J, Stromhaug PE, George MD, Habibzadegah-Tari P, Bevan A, et al. 2001. Cvt18/Gsa12 is required for cytoplasm-to-vacuole transport, pexophagy, and autophagy in Saccharomyces cerevisiae and Pichia pastoris. *Mol Biol Cell* 12: 3821-38
48. Gutierrez MG, Master SS, Singh SB, Taylor GA, Colombo MI, Deretic V. 2004. Autophagy is a defense mechanism inhibiting BCG and Mycobacterium tuberculosis survival in infected macrophages. *Cell* 119: 753-66
49. Habibzadegah-Tari P, Dunn WA, Jr. 2004. Glucose-induced pexophagy in Pichia pastoris. In *Autophagy*, ed. DJ Klionsky, pp. pp.126-37. Georgetown, Texas: Landes Bioscience
50. Hanada T, Noda NN, Satomi Y, Ichimura Y, Fujioka Y, et al. 2007. The Atg12-Atg5 conjugate has a novel E3-like activity for protein lipidation in autophagy. *J Biol Chem* 282: 37298-302
51. Hara T, Takamura A, Kishi C, Iemura S, Natsume T, et al. 2008. FIP200, a ULK-interacting protein, is required for autophagosome formation in mammalian cells. *J Cell Biol* 181: 497-510
52. He C, Baba M, Cao Y, Klionsky DJ. 2008. Self-interaction is critical for Atg9 transport and function at the phagophore assembly site during autophagy. *Mol Biol Cell* 19: 5506-16
53. He C, Bartholomew CR, Zhou W, Klionsky DJ. 2009. Assaying autophagic activity in transgenic GFP-Lc3 and GFP-Gabarap zebrafish embryos. *Autophagy* (In press)
54. He C, Song H, Yorimitsu T, Monastyrska I, Yen W-L, et al. 2006. Recruitment of Atg9 to the preautophagosomal structure by Atg11 is essential for selective autophagy in budding yeast. *J Cell Biol* 175: 925-35
55. Hemelaar J, Lelyveld VS, Kessler BM, Ploegh HL. 2003. A single protease, Apg4B, is specific for the autophagy-related ubiquitin-like proteins GATE-16, MAP1-LC3, GABARAP, and Apg8L. *J Biol Chem* 278: 51841-50
56. Hosokawa N, Hara T, Kaizuka T, Kishi C, Takamura A, et al. 2009. Nutrient-dependent mTORC1 association with the ULK1-Atg13-FIP200 complex required for autophagy. *Mol Biol Cell* (In press)
57. Hoyer-Hansen M, Bastholm L, Szyniarowski P, Campanella M, Szabadkai G, et al. 2007. Control of macroautophagy by calcium, calmodulin-dependent kinase kinase-β, and Bcl-2. *Mol Cell* 25: 193-205
58. Hrzenjak A, Kremser ML, Strohmeier B, Moinfar F, Zatloukal K, Denk H. 2008. SAHA induces caspase-independent, autophagic cell death of endometrial stromal sarcoma cells by influencing the mTOR pathway. *J Pathol* 216: 495-504
59. Huang J, Klionsky DJ. 2007. Autophagy and human disease. *Cell Cycle* 6: 1837-49
60. Huang W-P, Scott SV, Kim J, Klionsky DJ. 2000. The itinerary of a vesicle component, Aut7p/Cvt5p, terminates in the yeast vacuole via the autophagy/Cvt pathways. *J Biol Chem* 275: 5845-51

61. Ichimura Y, Kirisako T, Takao T, Satomi Y, Shimonishi Y, et al. 2000. A ubiquitin-like system mediates protein lipidation. *Nature* 408: 488-92
62. Inoki K, Li Y, Xu T, Guan KL. 2003. Rheb GTPase is a direct target of TSC2 GAP activity and regulates mTOR signaling. *Genes Dev* 17: 1829-34
63. Inoki K, Zhu T, Guan KL. 2003. TSC2 mediates cellular energy response to control cell growth and survival. *Cell* 115: 577-90
64. Ishihara N, Hamasaki M, Yokota S, Suzuki K, Kamada Y, et al. 2001. Autophagosome requires specific early Sec proteins for its formation and NSF/SNARE for vacuolar fusion. *Mol Biol Cell* 12: 3690-702
65. Itakura E, Kishi C, Inoue K, Mizushima N. 2008. Beclin 1 forms two distinct phosphatidylinositol 3-kinase complexes with mammalian Atg14 and UVRAG. *Mol Biol Cell* 19: 5360-72
66. Itoh T, Fujita N, Kanno E, Yamamoto A, Yoshimori T, Fukuda M. 2008. Golgi-resident small GTPase Rab33B interacts with Atg16L and modulates autophagosome formation. *Mol Biol Cell* 19: 2916-25
67. Iwata A, Riley BE, Johnston JA, Kopito RR. 2005. HDAC6 and microtubules are required for autophagic degradation of aggregated huntingtin. *J Biol Chem* 280: 40282-92
68. Jager S, Bucci C, Tanida I, Ueno T, Kominami E, et al. 2004. Role for Rab7 in maturation of late autophagic vacuoles. *J Cell Sci* 117: 4837-48
69. Jahreiss L, Menzies FM, Rubinsztein DC. 2008. The itinerary of autophagosomes: from peripheral formation to kiss-and-run fusion with lysosomes. *Traffic* 9: 574-87
70. James P, Halladay J, Craig EA. 1996. Genomic libraries and a host strain designed for highly efficient two-hybrid selection in yeast. *Genetics* 144: 1425-36
71. Juhasz G, Hill JH, Yan Y, Sass M, Baehrecke EH, et al. 2008. The class III PI(3)K Vps34 promotes autophagy and endocytosis but not TOR signaling in Drosophila. *J Cell Biol* 181: 655-66
72. Juhasz G, Neufeld TP. 2006. Autophagy: a forty-year search for a missing membrane source. *PLoS Biol* 4: e36
73. Juhasz G, Puskas LG, Komonyi O, Erdi B, Maroy P, et al. 2007. Gene expression profiling identifies FKBP39 as an inhibitor of autophagy in larval Drosophila fat body. *Cell Death Differ* 14: 1181-90
74. Jung CH, Jun CB, Ro SH, Kim YM, Otto NM, et al. 2009. ULK-Atg13-FIP200 complexes mediate mTOR signaling to the autophagy machinery. *Mol Biol Cell* (In press)
75. Kabeya Y, Kamada Y, Baba M, Takikawa H, Sasaki M, Ohsumi Y. 2005. Atg17 functions in cooperation with Atg1 and Atg13 in yeast autophagy. *Mol Biol Cell* 16: 2544-53
76. Kabeya Y, Mizushima N, Ueno T, Yamamoto A, Kirisako T, et al. 2000. LC3, a mammalian homologue of yeast Apg8p, is localized in autophagosome membranes after processing. *EMBO J* 19: 5720-8
77. Kabeya Y, Mizushima N, Yamamoto A, Oshitani-Okamoto S, Ohsumi Y, Yoshimori T. 2004. LC3, GABARAP and GATE16 localize to autophagosomal membrane depending on form-II formation. *J Cell Sci* 117: 2805-12

78. Kaksonen M, Sun Y, Drubin DG. 2003. A pathway for association of receptors, adaptors, and actin during endocytic internalization. *Cell* 115: 475-87
79. Kamada Y, Funakoshi T, Shintani T, Nagano K, Ohsumi M, Ohsumi Y. 2000. Tor-mediated induction of autophagy via an Apg1 protein kinase complex. *J Cell Biol* 150: 1507-13
80. Kanki T, Klionsky DJ. 2008. Mitophagy in yeast occurs through a selective mechanism. *J Biol Chem* 283: 32386-93
81. Kawamata T, Kamada Y, Kabeya Y, Sekito T, Ohsumi Y. 2008. Organization of the pre-autophagosomal structure responsible for autophagosome formation. *Mol Biol Cell* 19: 2039-50
82. Kiel JAKW, Veenhuis M. 2004. Selective degradation of peroxisomes in the methylotrophic yeast Hansenula polymorpha. In *Autophagy*, ed. DJ Klionsky, pp. pp.140-53. Georgetown, Texas: Landes Bioscience
83. Kihara A, Noda T, Ishihara N, Ohsumi Y. 2001. Two distinct Vps34 phosphatidylinositol 3-kinase complexes function in autophagy and carboxypeptidase Y sorting in *Saccharomyces cerevisiae*. *J Cell Biol* 152: 519-30
84. Kim I, Rodriguez-Enriquez S, Lemasters JJ. 2007. Selective degradation of mitochondria by mitophagy. *Arch Biochem Biophys* 462: 245-53
85. Kim J, Huang W-P, Klionsky DJ. 2001. Membrane recruitment of Aut7p in the autophagy and cytoplasm to vacuole targeting pathways requires Aut1p, Aut2p, and the autophagy conjugation complex. *J Cell Biol* 152: 51-64
86. Kim J, Huang W-P, Stromhaug PE, Klionsky DJ. 2002. Convergence of multiple autophagy and cytoplasm to vacuole targeting components to a perivacuolar membrane compartment prior to de novo vesicle formation. *J Biol Chem* 277: 763-73
87. Kim J, Kamada Y, Stromhaug PE, Guan J, Hefner-Gravink A, et al. 2001. Cvt9/Gsa9 functions in sequestering selective cytosolic cargo destined for the vacuole. *J Cell Biol* 153: 381-96
88. Kim J, Scott SV, Oda MN, Klionsky DJ. 1997. Transport of a large oligomeric protein by the cytoplasm to vacuole protein targeting pathway. *J Cell Biol* 137: 609-18
89. Kim PK, Hailey DW, Mullen RT, Lippincott-Schwartz J. 2008. Ubiquitin signals autophagic degradation of cytosolic proteins and peroxisomes. *Proc Natl Acad Sci U S A* 105: 20567-74
90. Kimmel CB, Ballard WW, Kimmel SR, Ullmann B, Schilling TF. 1995. Stages of embryonic development of the zebrafish. *Dev Dyn* 203: 253-310
91. Kirisako T, Baba M, Ishihara N, Miyazawa K, Ohsumi M, et al. 1999. Formation process of autophagosome is traced with Apg8/Aut7p in yeast. *J Cell Biol* 147: 435-46
92. Kirisako T, Ichimura Y, Okada H, Kabeya Y, Mizushima N, et al. 2000. The reversible modification regulates the membrane-binding state of Apg8/Aut7 essential for autophagy and the cytoplasm to vacuole targeting pathway. *J Cell Biol* 151: 263-76
93. Klionsky DJ. 2005. The molecular machinery of autophagy: unanswered questions. *J Cell Sci* 118: 7-18

94. Klionsky DJ. 2007. Autophagy: from phenomenology to molecular understanding in less than a decade. *Nat Rev Mol Cell Biol* 8: 931-7
95. Klionsky DJ, Abeliovich H, Agostinis P, Agrawal DK, Aliev G, et al. 2008. Guidelines for the use and interpretation of assays for monitoring autophagy in higher eukaryotes. *Autophagy* 4: 151-75
96. Klionsky DJ, Cuervo AM, Seglen PO. 2007. Methods for monitoring autophagy from yeast to human. *Autophagy* 3: 181-206
97. Klionsky DJ, Emr SD. 2000. Autophagy as a regulated pathway of cellular degradation. *Science* 290: 1717-21
98. Kochl R, Hu XW, Chan EY, Tooze SA. 2006. Microtubules facilitate autophagosome formation and fusion of autophagosomes with endosomes. *Traffic* 7: 129-45
99. Kouroku Y, Fujita E, Tanida I, Ueno T, Isoai A, et al. 2007. ER stress (PERK/eIF2α phosphorylation) mediates the polyglutamine-induced LC3 conversion, an essential step for autophagy formation. *Cell Death Differ* 14: 230-9
100. Kraft C, Deplazes A, Sohrmann M, Peter M. 2008. Mature ribosomes are selectively degraded upon starvation by an autophagy pathway requiring the Ubp3p/Bre5p ubiquitin protease. *Nat Cell Biol* 10: 602-10
101. Kubota H, Obata T, Ota K, Sasaki T, Ito T. 2003. Rapamycin-induced translational derepression of GCN4 mRNA involves a novel mechanism for activation of the eIF2α kinase GCN2. *J Biol Chem* 278: 20457-60
102. Lee IH, Cao L, Mostoslavsky R, Lombard DB, Liu J, et al. 2008. A role for the NAD-dependent deacetylase Sirt1 in the regulation of autophagy. *Proc Natl Acad Sci U S A* 105: 3374-9
103. Lee IH, Finkel T. 2009. Regulation of autophagy by the p300 acetyltransferase. *J Biol Chem* (In press)
104. Lee SB, Kim S, Lee J, Park J, Lee G, et al. 2007. ATG1, an autophagy regulator, inhibits cell growth by negatively regulating S6 kinase. *EMBO Rep* 8: 360-5
105. Legakis JE, Yen W-L, Klionsky DJ. 2007. A cycling protein complex required for selective autophagy. *Autophagy* 3: 422-32
106. Levine B, Klionsky DJ. 2004. Development by self-digestion: molecular mechanisms and biological functions of autophagy. *Dev Cell* 6: 463-77
107. Li J, Ni M, Lee B, Barron E, Hinton DR, Lee AS. 2008. The unfolded protein response regulator GRP78/BiP is required for endoplasmic reticulum integrity and stress-induced autophagy in mammalian cells. *Cell Death Differ* 15: 1460-71
108. Liang J, Shao SH, Xu ZX, Hennessy B, Ding Z, et al. 2007. The energy sensing LKB1-AMPK pathway regulates $p27^{kip1}$ phosphorylation mediating the decision to enter autophagy or apoptosis. *Nat Cell Biol* 9: 218-24
109. Liang XH, Jackson S, Seaman M, Brown K, Kempkes B, et al. 1999. Induction of autophagy and inhibition of tumorigenesis by beclin 1. *Nature* 402: 672-6
110. Long J, Zhao J, Yan Z, Liu Z, Wang N. 2009. Antitumor effects of a novel sulfur-containing hydroxamate histone deacetylase inhibitor H40. *Int J Cancer* 124: 1235-44
111. Long X, Lin Y, Ortiz-Vega S, Yonezawa K, Avruch J. 2005. Rheb binds and regulates the mTOR kinase. *Curr Biol* 15: 702-13

112. Long X, Ortiz-Vega S, Lin Y, Avruch J. 2005. Rheb binding to mammalian target of rapamycin (mTOR) is regulated by amino acid sufficiency. *J Biol Chem* 280: 23433-6
113. Longtine MS, McKenzie A, 3rd, Demarini DJ, Shah NG, Wach A, et al. 1998. Additional modules for versatile and economical PCR-based gene deletion and modification in Saccharomyces cerevisiae. *Yeast* 14: 953-61
114. Lum JJ, Bauer DE, Kong M, Harris MH, Li C, et al. 2005. Growth factor regulation of autophagy and cell survival in the absence of apoptosis. *Cell* 120: 237-48
115. Ma Y, Hendershot LM. 2001. The unfolding tale of the unfolded protein response. *Cell* 107: 827-30
116. Makky K, Tekiela J, Mayer AN. 2007. Target of rapamycin (TOR) signaling controls epithelial morphogenesis in the vertebrate intestine. *Dev Biol* 303: 501-13
117. Mammucari C, Milan G, Romanello V, Masiero E, Rudolf R, et al. 2007. FoxO3 controls autophagy in skeletal muscle in vivo. *Cell Metab* 6: 458-71
118. Manning BD, Tee AR, Logsdon MN, Blenis J, Cantley LC. 2002. Identification of the tuberous sclerosis complex-2 tumor suppressor gene product tuberin as a target of the phosphoinositide 3-kinase/akt pathway. *Mol Cell* 10: 151-62
119. Marks PA, Richon VM, Miller T, Kelly WK. 2004. Histone deacetylase inhibitors. *Adv Cancer Res* 91: 137-68
120. Martinet W, Knaapen MW, Kockx MM, De Meyer GR. 2007. Autophagy in cardiovascular disease. *Trends in molecular medicine* 13: 482-91
121. Martinet W, Knaapen MW, Kockx MM, De Meyer GR. 2007. Autophagy in cardiovascular disease. *Trends Mol Med* 13: 482-91
122. McBride HM, Neuspiel M, Wasiak S. 2006. Mitochondria: more than just a powerhouse. *Curr Biol* 16: R551-60
123. Meiling-Wesse K, Epple UD, Krick R, Barth H, Appelles A, et al. 2005. Trs85 (Gsg1), a component of the TRAPP complexes, is required for the organization of the preautophagosomal structure during selective autophagy via the Cvt pathway. *J Biol Chem* 280: 33669-78
124. Mercer CA, Kaliappan A, Dennis PB. 2009. A novel, human Atg13 binding protein, Atg101, interacts with ULK1 and is essential for macroautophagy. *Autophagy* (In press)
125. Mizushima N, Kuma A, Kobayashi Y, Yamamoto A, Matsubae M, et al. 2003. Mouse Apg16L, a novel WD-repeat protein, targets to the autophagic isolation membrane with the Apg12-Apg5 conjugate. *J Cell Sci* 116: 1679-88
126. Mizushima N, Levine B, Cuervo AM, Klionsky DJ. 2008. Autophagy fights disease through cellular self-digestion. *Nature* 451: 1069-75
127. Mizushima N, Noda T, Ohsumi Y. 1999. Apg16p is required for the function of the Apg12p-Apg5p conjugate in the yeast autophagy pathway. *EMBO J* 18: 3888-96
128. Mizushima N, Yamamoto A, Hatano M, Kobayashi Y, Kabeya Y, et al. 2001. Dissection of autophagosome formation using Apg5-deficient mouse embryonic stem cells. *J Cell Biol* 152: 657-68

129. Mizushima N, Yamamoto A, Matsui M, Yoshimori T, Ohsumi Y. 2004. In vivo analysis of autophagy in response to nutrient starvation using transgenic mice expressing a fluorescent autophagosome marker. *Mol Biol Cell* 15: 1101-11
130. Monastyrska I, He C, Geng J, Hoppe AD, Li Z, Klionsky DJ. 2008. Arp2 links autophagic machinery with the actin cytoskeleton. *Mol Biol Cell* 19: 1962-75
131. Monastyrska I, Shintani T, Klionsky DJ, Reggiori F. 2006. Atg11 directs autophagosome cargoes to the PAS along actin cables. *Autophagy* 2: 119-21
132. Mukaiyama H, Oku M, Baba M, Samizo T, Hammond AT, et al. 2002. Paz2 and 13 other PAZ gene products regulate vacuolar engulfment of peroxisomes during micropexophagy. *Genes Cells* 7: 75-90
133. Nair U, Klionsky DJ. 2005. Molecular mechanisms and regulation of specific and nonspecific autophagy pathways in yeast. *J Biol Chem* 280: 41785-8
134. Nakatogawa H, Ichimura Y, Ohsumi Y. 2007. Atg8, a ubiquitin-like protein required for autophagosome formation, mediates membrane tethering and hemifusion. *Cell* 130: 165-78
135. Narendra D, Tanaka A, Suen DF, Youle RJ. 2008. Parkin is recruited selectively to impaired mitochondria and promotes their autophagy. *J Cell Biol* 183: 795-803
136. Natarajan K, Meyer MR, Jackson BM, Slade D, Roberts C, et al. 2001. Transcriptional profiling shows that Gcn4p is a master regulator of gene expression during amino acid starvation in yeast. *Mol Cell Biol* 21: 4347-68
137. Nazarko TY, Huang J, Nicaud JM, Klionsky DJ, Sibirny AA. 2005. Trs85 is required for macroautophagy, pexophagy and cytoplasm to vacuole targeting in *Yarrowia lipolytica* and *Saccharomyces cerevisiae*. *Autophagy* 1: 37-45
138. Neuspiel M, Schauss AC, Braschi E, Zunino R, Rippstein P, et al. 2008. Cargo-selected transport from the mitochondria to peroxisomes is mediated by vesicular carriers. *Curr Biol* 18: 102-8
139. Nezis IP, Simonsen A, Sagona AP, Finley K, Gaumer S, et al. 2008. Ref(2)P, the Drosophila melanogaster homologue of mammalian p62, is required for the formation of protein aggregates in adult brain. *J Cell Biol* 180: 1065-71
140. Nice DC, Sato TK, Stromhaug PE, Emr SD, Klionsky DJ. 2002. Cooperative binding of the cytoplasm to vacuole targeting pathway proteins, Cvt13 and Cvt20, to phosphatidylinositol 3-phosphate at the pre-autophagosomal structure is required for selective autophagy. *J Biol Chem* 277: 30198-207
141. Nicklin P, Bergman P, Zhang B, Triantafellow E, Wang H, et al. 2009. Bidirectional transport of amino acids regulates mTOR and autophagy. *Cell* 136: 521-34
142. Nobukuni T, Joaquin M, Roccio M, Dann SG, Kim SY, et al. 2005. Amino acids mediate mTOR/raptor signaling through activation of class 3 phosphatidylinositol 3OH-kinase. *Proc Natl Acad Sci U S A* 102: 14238-43
143. Noda NN, Kumeta H, Nakatogawa H, Satoo K, Adachi W, et al. 2008. Structural basis of target recognition by Atg8/LC3 during selective autophagy. *Genes Cells* 13: 1211-8
144. Noda T, Kim J, Huang W-P, Baba M, Tokunaga C, et al. 2000. Apg9p/Cvt7p is an integral membrane protein required for transport vesicle formation in the Cvt and autophagy pathways. *J Cell Biol* 148: 465-80

145. Noda T, Matsuura A, Wada Y, Ohsumi Y. 1995. Novel system for monitoring autophagy in the yeast *Saccharomyces cerevisiae*. *Biochem Biophys Res Commun* 210: 126-32
146. Noda T, Ohsumi Y. 1998. Tor, a phosphatidylinositol kinase homologue, controls autophagy in yeast. *J Biol Chem* 273: 3963-6
147. Noda T, Suzuki K, Ohsumi Y. 2002. Yeast autophagosomes: de novo formation of a membrane structure. *Trends Cell Biol* 12: 231-5
148. Obara K, Sekito T, Niimi K, Ohsumi Y. 2008. The Atg18-Atg2 complex is recruited to autophagic membranes via phosphatidylinositol 3-phosphate and exerts an essential function. *J Biol Chem* 283: 23972-80
149. Oda MN, Scott SV, Hefner-Gravink A, Caffarelli AD, Klionsky DJ. 1996. Identification of a cytoplasm to vacuole targeting determinant in aminopeptidase I. *J Cell Biol* 132: 999-1010
150. Ogata M, Hino S, Saito A, Morikawa K, Kondo S, et al. 2006. Autophagy is activated for cell survival after endoplasmic reticulum stress. *Mol Cell Biol* 26: 9220-31
151. Oh M, Choi IK, Kwon HJ. 2008. Inhibition of histone deacetylase1 induces autophagy. *Biochem Biophys Res Commun* 369: 1179-83
152. Orvedahl A, Alexander D, Talloczy Z, Sun Q, Wei Y, et al. 2007. HSV-1 ICP34.5 confers neurovirulence by targeting the Beclin 1 autophagy protein. *Cell Host Microbe* 1: 23-35
153. Pandey UB, Nie Z, Batlevi Y, McCray BA, Ritson GP, et al. 2007. HDAC6 rescues neurodegeneration and provides an essential link between autophagy and the UPS. *Nature* 447: 859-63
154. Pankiv S, Clausen TH, Lamark T, Brech A, Bruun JA, et al. 2007. p62/SQSTM1 binds directly to Atg8/LC3 to facilitate degradation of ubiquitinated protein aggregates by autophagy. *J Biol Chem* 282: 24131-45
155. Papandreou I, Lim AL, Laderoute K, Denko NC. 2008. Hypoxia signals autophagy in tumor cells via AMPK activity, independent of HIF-1, BNIP3, and BNIP3L. *Cell Death Differ* 15: 1572-81
156. Pattingre S, Bauvy C, Carpentier S, Levade T, Levine B, Codogno P. 2009. Role of JNK1-dependent Bcl-2 Phosphorylation in Ceramide-induced Macroautophagy. *J Biol Chem* 284: 2719-28
157. Pattingre S, Bauvy C, Codogno P. 2003. Amino acids interfere with the ERK1/2-dependent control of macroautophagy by controlling the activation of Raf-1 in human colon cancer HT-29 cells. *J Biol Chem* 278: 16667-74
158. Pelegri F. 2003. Maternal factors in zebrafish development. *Dev Dyn* 228: 535-54
159. Pohl C, Jentsch S. 2009. Midbody ring disposal by autophagy is a post-abscission event of cytokinesis. *Nat Cell Biol* 11: 65-70
160. Priault M, Salin B, Schaeffer J, Vallette FM, di Rago JP, Martinou JC. 2005. Impairing the bioenergetic status and the biogenesis of mitochondria triggers mitophagy in yeast. *Cell Death Differ* 12: 1613-21
161. Puig O, Caspary F, Rigaut G, Rutz B, Bouveret E, et al. 2001. The tandem affinity purification (TAP) method: a general procedure of protein complex purification. *Methods* 24: 218-29

162. Ramirez-Valle F, Braunstein S, Zavadil J, Formenti SC, Schneider RJ. 2008. eIF4GI links nutrient sensing by mTOR to cell proliferation and inhibition of autophagy. *J Cell Biol* 181: 293-307
163. Ravikumar B, Acevedo-Arozena A, Imarisio S, Berger Z, Vacher C, et al. 2005. Dynein mutations impair autophagic clearance of aggregate-prone proteins. *Nat Genet* 37: 771-6
164. Redfern WS, Waldron G, Winter MJ, Butler P, Holbrook M, et al. 2008. Zebrafish assays as early safety pharmacology screens: Paradigm shift or red herring? *Journal of pharmacological and toxicological methods*
165. Reggiori F, Black MW, Pelham HR. 2000. Polar transmembrane domains target proteins to the interior of the yeast vacuole. *Mol Biol Cell* 11: 3737-49
166. Reggiori F, Klionsky DJ. 2005. Autophagosomes: biogenesis from scratch? *Curr Opin Cell Biol* 17: 415-22
167. Reggiori F, Monastyrska I, Shintani T, Klionsky DJ. 2005. The actin cytoskeleton is required for selective types of autophagy, but not nonspecific autophagy, in the yeast Saccharomyces cerevisiae. *Mol Biol Cell* 16: 5843-56
168. Reggiori F, Shintani T, Nair U, Klionsky DJ. 2005. Atg9 cycles between mitochondria and the pre-autophagosomal structure in yeasts. *Autophagy* 1: 101-9
169. Reggiori F, Tucker KA, Stromhaug PE, Klionsky DJ. 2004. The Atg1-Atg13 complex regulates Atg9 and Atg23 retrieval transport from the pre-autophagosomal structure. *Dev Cell* 6: 79-90
170. Reggiori F, Wang C-W, Nair U, Shintani T, Abeliovich H, Klionsky DJ. 2004. Early stages of the secretory pathway, but not endosomes, are required for Cvt vesicle and autophagosome assembly in *Saccharomyces cerevisiae*. *Mol Biol Cell* 15: 2189-204
171. Reggiori F, Wang C-W, Stromhaug PE, Shintani T, Klionsky DJ. 2003. Vps51 is part of the yeast Vps fifty-three tethering complex essential for retrograde traffic from the early endosome and Cvt vesicle completion. *J Biol Chem* 278: 5009-20
172. Reiling JH, Hafen E. 2004. The hypoxia-induced paralogs Scylla and Charybdis inhibit growth by down-regulating S6K activity upstream of TSC in Drosophila. *Genes Dev* 18: 2879-92
173. Robinson JS, Klionsky DJ, Banta LM, Emr SD. 1988. Protein sorting in Saccharomyces cerevisiae: isolation of mutants defective in the delivery and processing of multiple vacuolar hydrolases. *Mol Cell Biol* 8: 4936-48
174. Rodriguez-Hernandez A, Cordero MD, Salviati L, Artuch R, Pineda M, et al. 2009. Coenzyme Q deficiency triggers mitochondria degradation by mitophagy. *Autophagy* 5: 19-32
175. Rubinsztein DC, Gestwicki JE, Murphy LO, Klionsky DJ. 2007. Potential therapeutic applications of autophagy. *Nat Rev Drug Discov* 6: 304-12
176. Rusten TE, Lindmo K, Juhász G, Sass M, Seglen PO, et al. 2004. Programmed autophagy in the Drosophila fat body is induced by ecdysone through regulation of the PI3K pathway. *Dev Cell* 7: 179-92
177. Rusten TE, Vaccari T, Lindmo K, Rodahl LM, Nezis IP, et al. 2007. ESCRTs and Fab1 regulate distinct steps of autophagy. *Curr Biol* 17: 1817-25

178. Sagiv Y, Legesse-Miller A, Porat A, Elazar Z. 2000. GATE-16, a membrane transport modulator, interacts with NSF and the Golgi v-SNARE GOS-28. *EMBO J* 19: 1494-504
179. Saitoh T, Fujita N, Jang MH, Uematsu S, Yang BG, et al. 2008. Loss of the autophagy protein Atg16L1 enhances endotoxin-induced IL-1β production. *Nature* 456: 264-8
180. Sakaki K, Wu J, Kaufman RJ. 2008. Protein kinase Cθ is required for autophagy in response to stress in the endoplasmic reticulum. *J Biol Chem* 283: 15370-80
181. Sancak Y, Peterson TR, Shaul YD, Lindquist RA, Thoreen CC, et al. 2008. The Rag GTPases bind raptor and mediate amino acid signaling to mTORC1. *Science* 320: 1496-501
182. Sandoval H, Thiagarajan P, Dasgupta SK, Schumacher A, Prchal JT, et al. 2008. Essential role for Nix in autophagic maturation of erythroid cells. *Nature* 454: 232-5
183. Sanjuan MA, Dillon CP, Tait SW, Moshiach S, Dorsey F, et al. 2007. Toll-like receptor signalling in macrophages links the autophagy pathway to phagocytosis. *Nature* 450: 1253-7
184. Scherz-Shouval R, Shvets E, Fass E, Shorer H, Gil L, Elazar Z. 2007. Reactive oxygen species are essential for autophagy and specifically regulate the activity of Atg4. *EMBO J* 26: 1749-60
185. Schmelzle T, Beck T, Martin DE, Hall MN. 2004. Activation of the RAS/cyclic AMP pathway suppresses a TOR deficiency in yeast. *Mol Cell Biol* 24: 338-51
186. Schweers RL, Zhang J, Randall MS, Loyd MR, Li W, et al. 2007. NIX is required for programmed mitochondrial clearance during reticulocyte maturation. *Proc Natl Acad Sci U S A* 104: 19500-5
187. Scott RC, Juhasz G, Neufeld TP. 2007. Direct induction of autophagy by Atg1 inhibits cell growth and induces apoptotic cell death. *Curr Biol* 17: 1-11
188. Scott SV, Guan J, Hutchins MU, Kim J, Klionsky DJ. 2001. Cvt19 is a receptor for the cytoplasm-to-vacuole targeting pathway. *Mol Cell* 7: 1131-41
189. Shao Y, Gao Z, Marks PA, Jiang X. 2004. Apoptotic and autophagic cell death induced by histone deacetylase inhibitors. *Proc Natl Acad Sci U S A* 101: 18030-5
190. Shi CS, Kehrl JH. 2008. MyD88 and Trif target Beclin 1 to trigger autophagy in macrophages. *J Biol Chem* 283: 33175-82
191. Shintani T, Huang W-P, Stromhaug PE, Klionsky DJ. 2002. Mechanism of cargo selection in the cytoplasm to vacuole targeting pathway. *Dev Cell* 3: 825-37
192. Shintani T, Klionsky DJ. 2004. Autophagy in health and disease: a double-edged sword. *Science* 306: 990-5
193. Shintani T, Klionsky DJ. 2004. Cargo proteins facilitate the formation of transport vesicles in the cytoplasm to vacuole targeting pathway. *J Biol Chem* 279: 29889-94
194. Singh SB, Davis AS, Taylor GA, Deretic V. 2006. Human IRGM induces autophagy to eliminate intracellular mycobacteria. *Science* 313: 1438-41
195. Sir D, Chen WL, Choi J, Wakita T, Yen TS, Ou JH. 2008. Induction of incomplete autophagic response by hepatitis C virus via the unfolded protein response. *Hepatology* 48: 1054-61

196. Stokoe D, Stephens LR, Copeland T, Gaffney PR, Reese CB, et al. 1997. Dual role of phosphatidylinositol-3,4,5-trisphosphate in the activation of protein kinase B. *Science* 277: 567-70
197. Stromhaug PE, Reggiori F, Guan J, Wang C-W, Klionsky DJ. 2004. Atg21 is a phosphoinositide binding protein required for efficient lipidation and localization of Atg8 during uptake of aminopeptidase I by selective autophagy. *Mol Biol Cell* 15: 3553-66
198. Sun Q, Fan W, Chen K, Ding X, Chen S, Zhong Q. 2008. Identification of Barkor as a mammalian autophagy-specific factor for Beclin 1 and class III phosphatidylinositol 3-kinase. *Proc Natl Acad Sci U S A* 105: 19211-6
199. Suzuki K, Kirisako T, Kamada Y, Mizushima N, Noda T, Ohsumi Y. 2001. The pre-autophagosomal structure organized by concerted functions of *APG* genes is essential for autophagosome formation. *EMBO J* 20: 5971-81
200. Suzuki K, Kubota Y, Sekito T, Ohsumi Y. 2007. Hierarchy of Atg proteins in pre-autophagosomal structure organization. *Genes Cells* 12: 209-18
201. Takahashi Y, Coppola D, Matsushita N, Cualing HD, Sun M, et al. 2007. Bif-1 interacts with Beclin 1 through UVRAG and regulates autophagy and tumorigenesis. *Nat Cell Biol* 9: 1142-51
202. Takeshige K, Baba M, Tsuboi S, Noda T, Ohsumi Y. 1992. Autophagy in yeast demonstrated with proteinase-deficient mutants and conditions for its induction. *J Cell Biol* 119: 301-11
203. Talloczy Z, Jiang W, Virgin HW, IV, Leib DA, Scheuner D, et al. 2002. Regulation of starvation- and virus-induced autophagy by the eIF2α kinase signaling pathway. *Proc Natl Acad Sci U S A* 99: 190-5
204. Talloczy Z, Virgin HW, IV, Levine B. 2006. PKR-dependent autophagic degradation of herpes simplex virus type 1. *Autophagy* 2: 24-9
205. Tanaka Y, Guhde G, Suter A, Eskelinen EL, Hartmann D, et al. 2000. Accumulation of autophagic vacuoles and cardiomyopathy in LAMP-2-deficient mice. *Nature* 406: 902-6
206. Tanida I, Komatsu M, Ueno T, Kominami E. 2003. GATE-16 and GABARAP are authentic modifiers mediated by Apg7 and Apg3. *Biochem Biophys Res Commun* 300: 637-44
207. Tanida I, Minematsu-Ikeguchi N, Ueno T, Kominami E. 2005. Lysosomal turnover, but not a cellular level, of endogenous LC3 is a marker for autophagy. *Autophagy* 1: 84-91
208. Tanida I, Wakabayashi M, Kanematsu T, Minematsu-Ikeguchi N, Sou YS, et al. 2006. Lysosomal turnover of GABARAP-phospholipid conjugate is activated during differentiation of C2C12 cells to myotubes without inactivation of the mTor kinase-signaling pathway. *Autophagy* 2: 264-71
209. Tasdemir E, Maiuri MC, Tajeddine N, Vitale I, Criollo A, et al. 2007. Cell cycle-dependent induction of autophagy, mitophagy and reticulophagy. *Cell Cycle* 6: 2263-7
210. Teter SA, Eggerton KP, Scott SV, Kim J, Fischer AM, Klionsky DJ. 2001. Degradation of lipid vesicles in the yeast vacuole requires function of Cvt17, a putative lipase. *J Biol Chem* 276: 2083-7

211. Tilney LG, Harb OS, Connelly PS, Robinson CG, Roy CR. 2001. How the parasitic bacterium *Legionella pneumophila* modifies its phagosome and transforms it into rough ER: implications for conversion of plasma membrane to the ER membrane. *J Cell Sci* 114: 4637-50
212. Tomashek JJ, Sonnenburg JL, Artimovich JM, Klionsky DJ. 1996. Resolution of subunit interactions and cytoplasmic subcomplexes of the yeast vacuolar proton-translocating ATPase. *J Biol Chem* 271: 10397-404
213. Tracy K, Dibling BC, Spike BT, Knabb JR, Schumacker P, Macleod KF. 2007. BNIP3 is an RB/E2F target gene required for hypoxia-induced autophagy. *Mol Cell Biol* 27: 6229-42
214. Tsukamoto S, Kuma A, Murakami M, Kishi C, Yamamoto A, Mizushima N. 2008. Autophagy is essential for preimplantation development of mouse embryos. *Science* 321: 117-20
215. Tucker B, Lardelli M. 2007. A rapid apoptosis assay measuring relative acridine orange fluorescence in zebrafish embryos. *Zebrafish* 4: 113-6
216. Tucker KA, Reggiori F, Dunn WA, Jr., Klionsky DJ. 2003. Atg23 is essential for the cytoplasm to vacuole targeting pathway and efficient autophagy but not pexophagy. *J Biol Chem* 278: 48445-52
217. Twig G, Elorza A, Molina AJ, Mohamed H, Wikstrom JD, et al. 2008. Fission and selective fusion govern mitochondrial segregation and elimination by autophagy. *EMBO J* 27: 433-46
218. Wang C-W, Kim J, Huang W-P, Abeliovich H, Stromhaug PE, et al. 2001. Apg2 is a novel protein required for the cytoplasm to vacuole targeting, autophagy, and pexophagy pathways. *J Biol Chem* 276: 30442-51
219. Wang Y, Weiss LM, Orlofsky A. 2009. Host cell autophagy is induced by *Toxoplasma gondii* and contributes to parasite growth. *J Biol Chem* 284: 1694-701
220. Wang Z, Wilson WA, Fujino MA, Roach PJ. 2001. Antagonistic controls of autophagy and glycogen accumulation by Snf1p, the yeast homolog of AMP-activated protein kinase, and the cyclin-dependent kinase Pho85p. *Mol Cell Biol* 21: 5742-52
221. Watanabe M, Adachi S, Matsubara H, Imai T, Yui Y, et al. 2009. Induction of autophagy in malignant rhabdoid tumor cells by the histone deacetylase inhibitor FK228 through AIF translocation. *Int J Cancer* 124: 55-67
222. Wei Y, Pattingre S, Sinha S, Bassik M, Levine B. 2008. JNK1-mediated phosphorylation of Bcl-2 regulates starvation-induced autophagy. *Mol Cell* 30: 678-88
223. Williams A, Sarkar S, Cuddon P, Ttofi EK, Saiki S, et al. 2008. Novel targets for Huntington's disease in an mTOR-independent autophagy pathway. *Nat Chem Biol* 4: 295-305
224. Williams RM, Primig M, Washburn BK, Winzeler EA, Bellis M, et al. 2002. The Ume6 regulon coordinates metabolic and meiotic gene expression in yeast. *Proc Natl Acad Sci U S A* 99: 13431-6
225. Wu H, Yang JM, Jin S, Zhang H, Hait WN. 2006. Elongation factor-2 kinase regulates autophagy in human glioblastoma cells. *Cancer Res* 66: 3015-23

226. Xie Z, Klionsky DJ. 2007. Autophagosome formation: core machinery and adaptations. *Nat Cell Biol* 9: 1102-9
227. Xie Z, Nair U, Klionsky DJ. 2008. Atg8 controls phagophore expansion during autophagosome formation. *Mol Biol Cell* 19: 3290-8
228. Xu Y, Jagannath C, Liu XD, Sharafkhaneh A, Kolodziejska KE, Eissa NT. 2007. Toll-like receptor 4 is a sensor for autophagy associated with innate immunity. *Immunity* 27: 135-44
229. Yang Z, Huang J, Geng J, Nair U, Klionsky DJ. 2006. Atg22 recycles amino acids to link the degradative and recycling functions of autophagy. *Mol Biol Cell* 17: 5094-104
230. Yano T, Mita S, Ohmori H, Oshima Y, Fujimoto Y, et al. 2008. Autophagic control of listeria through intracellular innate immune recognition in drosophila. *Nat Immunol* 9: 908-16
231. Yen W-L, Klionsky DJ. 2008. How to live long and prosper: autophagy, mitochondria, and aging. *Physiology (Bethesda)* 23: 248-62
232. Yen W-L, Legakis JE, Nair U, Klionsky DJ. 2007. Atg27 is required for autophagy-dependent cycling of Atg9. *Mol Biol Cell* 18: 581-93
233. Yorimitsu T, He C, Wang K, Klionsky DJ. 2009. Tap42-associated protein phosphatase type 2A negatively regulates induction of autophagy. *Autophagy* (In press)
234. Yorimitsu T, Klionsky DJ. 2005. Atg11 links cargo to the vesicle-forming machinery in the cytoplasm to vacuole targeting pathway. *Mol Biol Cell* 16: 1593-605
235. Yorimitsu T, Klionsky DJ. 2005. Autophagy: molecular machinery for self-eating. *Cell Death Differ* 12 Suppl 2: 1542-52
236. Yorimitsu T, Nair U, Yang Z, Klionsky DJ. 2006. Endoplasmic reticulum stress triggers autophagy. *J Biol Chem* 281: 30299-304
237. Yorimitsu T, Zaman S, Broach JR, Klionsky DJ. 2007. Protein kinase A and Sch9 cooperatively regulate induction of autophagy in *Saccharomyces cerevisiae*. *Mol Biol Cell* 18: 4180-9
238. Yoshimoto K, Hanaoka H, Sato S, Kato T, Tabata S, et al. 2004. Processing of ATG8s, ubiquitin-like proteins, and their deconjugation by ATG4s are essential for plant autophagy. *Plant Cell* 16: 2967-83
239. Young ARJ, Chan EYW, Hu XW, Kochl R, Crawshaw SG, et al. 2006. Starvation and ULK1-dependent cycling of mammalian Atg9 between the TGN and endosomes. *J Cell Sci* 119: 3888-900
240. Zalckvar E, Berissi H, Mizrachy L, Idelchuk Y, Koren I, et al. 2009. DAP-kinase-mediated phosphorylation on the BH3 domain of beclin 1 promotes dissociation of beclin 1 from Bcl-X(L) and induction of autophagy. *EMBO Rep* (In press)
241. Zaman S, Lippman SI, Zhao X, Broach JR. 2008. How *Saccharomyces* responds to nutrients. *Annu Rev Genet* 42: 27-81
242. Zhang H, Bosch-Marce M, Shimoda LA, Tan YS, Baek JH, et al. 2008. Mitochondrial autophagy is an HIF-1-dependent adaptive metabolic response to hypoxia. *J Biol Chem* 283: 10892-903

243. Zhang Y, Gao X, Saucedo LJ, Ru B, Edgar BA, Pan D. 2003. Rheb is a direct target of the tuberous sclerosis tumour suppressor proteins. *Nat Cell Biol* 5: 578-81
244. Zhang Y, Yan L, Zhou Z, Yang P, Tian E, et al. 2009. SEPA-1 mediates the specific recognition and degradation of P granule components by autophagy in *C. elegans*. *Cell* 136: 308-21
245. Zhao J, Brault JJ, Schild A, Cao P, Sandri M, et al. 2007. FoxO3 coordinately activates protein degradation by the autophagic/lysosomal and proteasomal pathways in atrophying muscle cells. *Cell Metab* 6: 472-83